Colocated MIMO Radar Using Compressive Sensing

A Thesis

Submitted to the Faculty

of

Drexel University

by

Yao Yu

in partial fulfillment of the

requirements for the degree

of

Doctor of Philosophy

in Electrical and Computer Engineering

October 2010

Dedications

To my husband, my parents and my parents-in-law

Acknowledgments

First of all, I would like to express my deepest gratitude to my advisors, Dr. Athina P. Petropulu and Dr. Youngmoo E. Kim. Dr. Petropulu has been spending her tremendous time and efforts in leading, supporting and helping me in the last three years. It would be impossible for me to finish this work without her constant encouragement and invaluable guidance throughout my Ph.D. study. I will always look up to her as an inspiration to my professional career. I would like to sincerely thank Dr. Kim for his support in the past three years, especially in the last quarter of my stay at Drexel. Without his support this dissertation would not have been possible.

I am also deeply indebted to Professor H. Vincent Poor at Princeton University and Dr. Rabinder N. Madan at ONR for their valuable guidance and suggestions during our collaborative research.

I would express my gratitude to the members of my Ph.D. thesis committee, Professors Steven Weber, John M. Walsh and Kapil R. Dandekar for their precious time and their valuable suggestions.

Many thanks to my colleagues in the Communications and Signal Processing Laboratory (CSPL): Lun Dong, Jiangyuan Li, Xin Liu, Yupeng Liu, Hana Godrich, Sagar Shah, Shuangyu Luo and Tingshan Huang for their many forms of help and their friendship during the time we spent together.

I also would like to express my special thanks to my husband Kai Guo, my parents and my parents-in-law for their continuous understanding, supporting and encouraging in my research and life.

Last but not least, I would like to thank God for giving me this wonderful life and the path to truth.

Table of Contents

List of Tables

List of Figures

Abstract

Colocated MIMO Radar Using Compressive Sensing

Yao Yu

Advisor: Dr. Athina P. Petropulu and Dr. Youngmoo E. Kim

We propose the use of compressive sensing (CS) in the context of a multi-input multi-output (MIMO) radar system that is implemented by a small scale network. Each receive node compressively samples the incoming signal, and forwards a small number of samples to a fusion center. At the fusion center, all received data are jointly processed to extract information on the potential targets via the CS approach. Since CS-based MIMO radar would require many fewer measurements than conventional MIMO radar for reliable target detection, there would be power savings during the data transmission to the fusion center, which would prolong the life of the wireless network. First, we propose a direction of arrival (DOA)-Doppler estimation approach. Assuming that the targets are sparsely located in the DOA-Doppler space, based on the samples forwarded by the receive nodes, the fusion center formulates an ℓ_1-optimization problem, the solution of which yields the target DOA-Doppler information. The proposed approach achieves the superior resolution of MIMO radar with far fewer samples than required by conventional approaches. Second, we propose the use of step frequency to CS-based MIMO radar, which enables high range resolution, while transmitting narrowband pulses. For slowly moving targets, a novel approach is proposed that achieves significant complexity reduction by successively estimating angle-range and Doppler in a decoupled fashion and by employing initial estimates to further reduce the search space. Numerical results show that the achieved complexity reduction does not hurt resolution. Finally, we investigate optimal designs for the measurement matrix that is used to linearly compress the received signal. One optimality criterion amounts to decorrelating the bases that span the sparse space of the incoming signal and simultaneously enhancing signal-to-interference ratio (SIR). Another criterion targets SIR improvement only. It is shown via simulations that, in certain cases, the measurement matrices obtained based on the aforementioned criteria can improve detection accuracy as compared to the typically used Gaussian random measurement matrix.

1. Introduction

In this chapter, we provide some background on multi-input multi-output (MIMO) radio detection and ranging (radar) and the theory of compressive sensing (CS). Then, the contributions of this dissertation are described. Finally, we provide the outline of this dissertation.

1.1 Background Review

In this section we introduce the basic concepts of radar, MIMO radar and the theory of CS.

1.1.1 Radar Basics

A radar [1]-[3] is an target detection system that uses electromagnetic waves to detect the presence of a target and also extract information about the target, e.g., range, direction of arrival (DOA), or speed. The targets of interest can be aircraft, ships, motor vehicles, people, weather formations, and terrain. A transmitter emits electromagnetic waves in the space. When hitting an object, these waves are scattered in all directions. The signal is thus partly reflected back to receivers with a certain time delay as compared to the transmission time, as shown in Fig.1.1. At the receivers the received target echoes are processed to identify a target. Note that here radar engineers use the term *range* to denote the distance between the radar and the target.

From the perspective of transmit waveforms, the radar systems can be categorized into continuous waveform radar and pulse radar [3]. Pulse Radar (PR) sends out signals in short (few millionths of a second) bursts or pulses. PR is capable of not only detecting target range or DOA but also measuring its radial velocity. A continuous-Wave Radar (CWR)

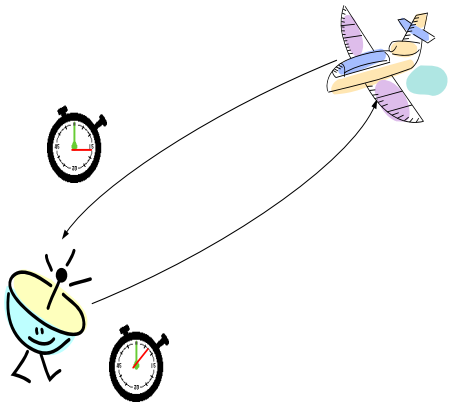

Figure 1.1: Radar System

that transmits a continuous signal utilizes the Doppler effect to detect targets. Therefore, CWR fails to detect stationary targets. We consider PR throughout this thesis.

Let us consider a monostatic radar in which the transmitter and receiver are collocated. The received signal can be approximated as an attenuated and time-delayed version of transmit signal. In particular, let the transmitted signal be $x(t)\exp(j2\pi ft)$, where $x(t)$ is a narrowband waveform and f is carrier frequency. As seen in Fig. 1.2, the target return at the receiver is given by

$$y(t) = \beta x(t-\tau)\exp(j2\pi f(t-\tau)) + n(t) \tag{1.1}$$

where β is the target reflectivity or the target response, $n(t)$ is additive white noise and τ is the time delay.

The time delay τ is of vital importance for a radar system. We can access to all the target information via knowledge of τ.

- *Range* [1]. Let us see a simple case in which the radar is equipped with a single

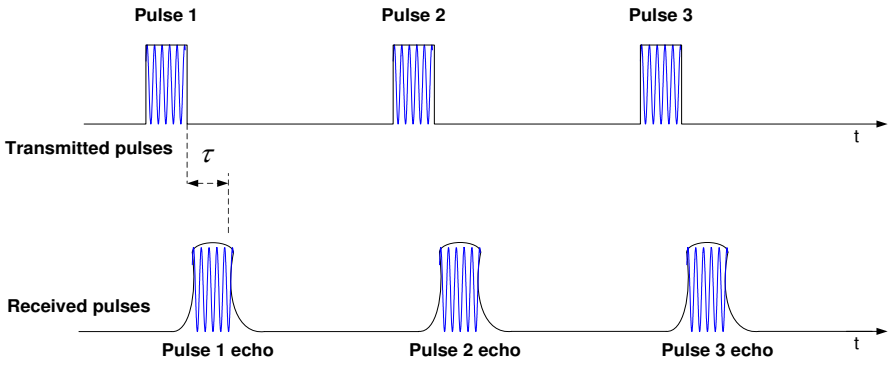

Figure 1.2: Transmitted and received signals

antenna and the target is assumed to be stationary. The radio wave is emitted by an antenna at t_0 and returns this antenna at t. The distance between the target and this antenna, i.e., the range R, is equal to

$$R = \frac{t - t_0}{2c} = \frac{\tau}{2c} \tag{1.2}$$

where c is the speed of light.

- *Doppler* [1]. The moving targets can induce a Doppler shift in the carrier frequency. The speed of targets is obtained by measuring the Doppler shift. The speed information is beneficial in that the radar systems can detect the desired target echoes in the midst of large clutter. *Clutter* encompasses the echoes reflected by the natural environment, e.g., land, sea and clouds. In most of cases, the clutter echoes can be many orders of magnitude larger than the desired target echoes. Since the clutter

objects are usually stationary or move slowly, one can take advantage of the Doppler effect to distinguish them from fast moving targets.

Suppose that a target is moving towards the radar at velocity v. Recall that the Doppler shift is given by

$$f_d \approx \frac{2v}{c} f \tag{1.3}$$

The received signal, after demodulation, can be represented by

$$y(t) = \beta x(t - 2R_0/c + vt/c) \exp(j2\pi((f + f_d)t - 2fR_0/c)) + n(t) \tag{1.4}$$

where R_0 is the target range at the reference time t_0. Under the assumption of narrowband signal, (1.4) is approximated as

$$y(t) = \beta x(t - 2R_0/c) \exp(j2\pi((f + f_d)t - 2fR_0/c)) + n(t) \tag{1.5}$$

Since the Doppler shift f_d is small as compared to the carrier frequency f, the extraction of the Doppler information requires the PR to transmit multiple pulses. The simplest way to obtain Doppler information is to perform IDFT on the samples of the pulse train.

- *DOA* [1]. Unlike the range and Doppler estimation, multiple antennas are indispensable for the DOA estimation. Let us consider a colocated antenna array of N antennas in which each antenna serves as a tranceiver. As shown in Fig. 1.3, the spacing of antennas is denoted by d and we assume that a stationary target is located at R_0 from the first antenna for simplicity. For a phased-array radar, all the antennas transmit the same waveforms $x(t)$. The received signal of the i-th antenna after demodulation is

given by

$$y_i(t) = \beta x(t - 2R_0/c)e^{j2\pi f \frac{(i-1)d\sin\theta + R_0}{c}} + n(t) \tag{1.6}$$

One can see from (1.6) that the DOA information, θ, can be extracted by performing IDFT on the samples of the antenna array that are obtained at time t.

The DOA estimation techniques fall into two categories, namely spectral-based and parametric approaches. Spectral-based methods, e.g., Capon beamformer and multiple signal classification (MUSIC) methods, form a spectrum-like function of DOA. The peak locations of this function provide DOA estimates. Unlike spectral-based approaches, parametric techniques directly yield an estimate of DOA without search, e.g., maximum likelihood (ML) approaches, ESPRIT methods and weighted subspace fitting (WSF) methods. The latter class of approaches can produce more accurate estimates than the former at the expense of computational efficiency.

1.1.2 MIMO Radar

It is well known that MIMO systems that are equipped with multiple antennas can offer significant increase in data throughput and improve link reliability (combat fading) [6]. Benefiting from the idea of MIMO communication systems, MIMO radar systems have received considerable attention in recent years. Unlike a phased-array radar [4][5] in which the transmit nodes send out the scaled versions of a single waveform, a MIMO radar transmits multiple independent waveforms from its antennas. The waveforms bearing with the target information can be extracted by a band of matched filters at the receive end. A MIMO radar system is advantageous in two different scenarios, i.e., widely separated MIMO radar [7]-[11] and colocated MIMO radar [12]-[14].

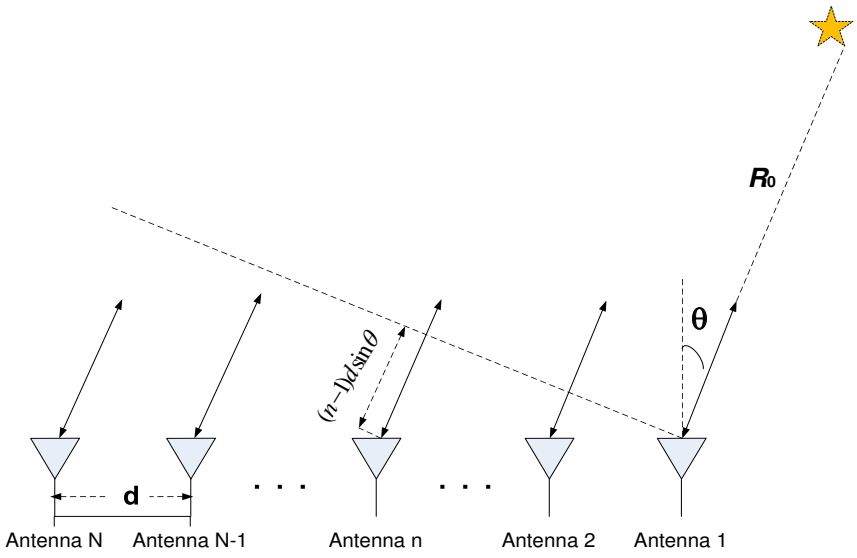

Figure 1.3: The illustration of phased array radar

Widely separated MIMO radar

In this scenario, the transmit antennas are located far apart from each other relative to their distance to the target [7]-[11]. This enables the radar to view the target from different directions simultaneously. The MIMO radar system transmits independent probing signals from decorrelated transmitters through different paths, and thus each target return carries independent information about the target. Combining these independent target returns results in a diversity gain, the MIMO radar system is capable of reducing target radar cross section (RCS) scintillations and achieving high target resolution.

The approaches to process observations can be classified as either non-coherent or coherent. The non-coherent method utilizes the information in the signal envelope only and thus merely requires time synchronization between the transmit and receive antennas. The coherent method considers the phase information of the received signal in addition to the

envelope. This requires the need for both time and phase synchronization.

Colocated MIMO radar

For a colocated MIMO radar [12]-[14], the antennas are close to each other, so that the RCS does not vary between the different paths. Let the number of transmit and receive antennas be M_t and N_r, respectively. In this scenario, the phase differences induced by transmit and receive antennas can be exploited to form a long virtual array with M_tN_r elements. This enables the MIMO radar system to achieve superior spatial resolution as compared to a traditional radar system. MIMO radar can achieve a desired beampattern by transmitting correlated waveforms [15]-[17]. This is useful in cases where the radar system wishes to avoid certain directions because they either correspond to eavesdroppers, or are known to be of no interest. In this dissertation we consider closely spaced transmit and receive antennas and uncorrelated transmit waveforms. We will elaborate on the rationale behind colocated MIMO radar below.

Assume that the transmit array of M_t antennas and the receive array of N_r antennas are colocated. The spacing of transmit antennas and receivers is d_t and d_r, respectively. The transmit antennas emit orthogonal waveforms. Let $x_i(t)e^{j2\pi ft}$ be the continuous waveforms transmitted by the *i*th transmit antenna. At each receive antenna, the M_t orthogonal waveforms can be extracted by M_t match filters. Therefore, N_r receive antennas can obtain a total of M_tN_r waveforms. The *l*th receive antenna receives from the *i*th transmit antenna:

$$y_{il}(t) = x_i(t - \tau_{il})e^{j2\pi f(t-\tau_{il})} + n_{il}(t) \tag{1.7}$$

where $\tau_{il} = \tau_{00} + \frac{((i-1)d_t+(l-1)d_r)\sin\theta}{c}$ and τ_{00} is the time delay of the reference antenna; Under

the assumption of narrowband signal, the baseband received signal is

$$\begin{aligned} y_{il}(t) &= x_i(t)e^{-j\frac{2\pi f}{c}((i-1)d_t+(l-1)d_r)\sin\theta} \\ &= x_i(t)e^{-j\frac{2\pi f d_r \sin\theta}{c}(\frac{d_t}{d_r}(i-1)+(l-1))} \end{aligned} \tag{1.8}$$

Letting $\frac{d_t}{d_r} = N_r$, then set $\{\frac{d_t}{d_r}(i-1)+(l-1)\} = \{0,1,\ldots,M_tN_r-1\}$. Therefore, the M_tN_r waveforms can be considered as the waveforms received by a virtual array of length M_tN_r that is formed by $M_r + N_r$ elements. In this way, colocated MIMO radar is capable of achieving super angular resolution as compared to phased-array radar with the same number of elements. It is worth noting that beamforming is impossible for the case of $\frac{d_t}{d_r} = N_r$. This is because the sampling rate in the spatial domain is too low to prevent aliasing.

1.1.3 Compressive sensing

Compressive sensing (CS), also known as compressed sensing or compressive sampling, is a technique for reconstructing a signal that it is sparse in some space. CS has received considerable attention recently [18]-[20], and has been applied successfully in diverse fields, e.g., image processing [21] and wireless communications [22][23].

A K-sparse signal $\mathbf{x}$ of length N can be represented by

$$\mathbf{x} = \mathbf{\Psi s} \tag{1.9}$$

where $\mathbf{\Psi}$ denotes the $N \times N$ basis matrix that spans this sparse space and $\mathbf{s}$ is the coefficient vector. $\mathbf{s}$ contains only K large elements and the remaining elements are negligible or zeros. If $K \ll N$, the signal $\mathbf{x}$ is compressible.

We consider a general problem of recovering $\mathbf{x} \in \mathbb{R}^N$ from the linear measurements

$$\mathbf{y} = \mathbf{\Phi x} = \mathbf{\Theta s} \tag{1.10}$$

where $\mathbf{\Phi}$ is an $M \times N$ matrix and $\mathbf{\Theta} = \mathbf{\Phi\Psi}$. $\mathbf{\Phi}$ and $\mathbf{\Theta}$ are referred to as the measurement matrix and the sensing matrix in the CS society, respectively.

For the case of $M \ll N$, the recovery of $\mathbf{x}$ requires to solve an underdetermined linear system. This seems hopeless in that the number of equations is less than the number of the unknowns. However, the theory of CS states that $\mathbf{x}$ of length N can be recovered exactly with high probability from much fewer measurements than N.

Recovery algorithms

- *Matching Pursuit (MP)*: These methods iteratively find the sparse vector $\mathbf{s}$. At each step, a locally optimal estimate of $\mathbf{s}$ is obtained. The well-known algorithms in this category include orthogonal MP (OMP) [24], regularized OMP (ROMP) [25][26] and acrostic compressive sampling MP (CoSaMP) [27].

- *Convex relaxation or Basis pursuit (BP)* [28]: These methods solve a convex problem that minimizes the support of $\mathbf{s}$. The mathematical insight into MP methods is provided in this section. Let us consider the recovery of a K-sparse signal $\mathbf{x}$ of length N from the measurement vector $\mathbf{y}$ of length M where $K \ll N$ and $M \ll N$. To find the sparsest solution of $\mathbf{x}$, a optimization problem is formulated as

$$\begin{aligned} &\min_{\mathbf{s}} \|\mathbf{s}\|_0 \\ &\text{s.t. } \mathbf{y} = \mathbf{\Theta s} \end{aligned} \tag{1.11}$$

  where $\|\cdot\|_0$ denotes ℓ_0 norm which counts the number of nonzero elements of the argument. Note that the solution of the problem (1.11) is the coefficient vector $\mathbf{s}$ instead of the signal $\mathbf{x}$.

  The problem of ℓ_0 norm is intractable since it is NP-hard and the solution is not unique in general. Fortunately, the ℓ_1 norm provides a natural convex relaxation of

the ℓ_0 norm:

$$\min_{\mathbf{s}} \|\mathbf{s}\|_1$$
$$\text{s.t. } \mathbf{y} = \mathbf{\Theta s} \tag{1.12}$$

where $\|\cdot\|_1$ is ℓ_1 norm tha is equal to the sum of absolute value of all the elements in the argument.

Eq. (1.12) can be recast as a linear program (LP), or second order cone program (SOCP) [29][30]. This is can be efficiently solved by a standard science software. It has been shown in [18] and [31] that the optimization problem of (1.12) succeeds in recovering a K-sparse signal with high probability using only $M \geq cK\log(N/K)$ independent identically distributed (i.i.d.) Gaussian measurements, where c is a constant.

The BP algorithms require fewer measurements than the MP algorithms but are more demanding than the MP algorithms. In our work, we apply a BP algorithm to target detection for MIMO radar.

Uniform uncertainty principle

In [32], the notion of uniform uncertainty principle (UUP) was introduced to understand the exact recovery of the sparse signal. Let $\mathbf{\Theta_T}$, $T \subset \{1, \ldots, N\}$ be the $N \times |T|$ submatrix of $\mathbf{\Theta}$ that contains the columns corresponding to the indices in T. The S-restricted isometry constant δ_S of $\mathbf{\Theta}$ is the smallest quantity for all subsets T with $|T| \leq S$ satisfying

$$(1-\delta_S)\|\mathbf{c}\|_2^2 \leq \|\mathbf{\Theta_T c}\|_2^2 \leq (1+\delta_S)\|\mathbf{c}\|_2^2 \tag{1.13}$$

where $\mathbf{c}$ is an arbitrary coefficient vector of length $|T|$.

It was shown in [33] that if S obeys

$$\delta_S + \delta_{2S} + \delta_{3S} < 1 \tag{1.14}$$

then any sparse signal of support less than S can be recovered by solving (1.12). The theorem essentially indicates that if every set of columns with cardinality less than the sparsity of the signal of interest of the sensing matrix are approximately orthogonal, then the sparse signal can be exactly recovered with high probability. In practice, however, it would involve prohibitively high complexity to check (1.14) for a large size sensing matrix.

1.2 Contributions of the Dissertation

In a MIMO radar system that is implemented by a small scale network, each node is equipped with one antenna, and the nodes are distributed at random on a disk of a small radius. A group of nodes transmit radar waveforms and another group of nodes receive target echoes. The received data by each receive node (RX) is subsequently forwarded to a fusion center at which all the data are jointly processed to detect targets and extract their information. Without any fixed infrastructure, the antennas scattered in this small network render such MIMO radar more flexible than a fixed antenna array since we can choose the nodes freely. However, the transmission of received data to the fusion center consumes a great amount of energy. This would shorten the life of the battery-operated wireless network. In this dissertation, we propose to apply CS to a MIMO radar system that is implemented by a small scale network. The CS approach enables a significant reduction in the number of measurements required by the fusion center to reliably detect targets as compared to conventional methods. The obtained power savings of transmission would significantly prolong the life of the wireless network.

1.2.1 DOA and Doppler estimation for MIMO radar using CS

We propose a novel DOA-Doppler estimation approach for MIMO radar using CS. Assuming that the targets are sparsely located in the angle-Doppler space, based on the samples forwarded by the receive nodes the fusion center formulates an ℓ_1-optimization problem, the solution of which yields target angle and Doppler information. The proposed approach achieves the superior resolution of MIMO radar with far fewer samples than required by conventional approaches. This implies power savings during the communication phase between the receive nodes and the fusion center. We provide analytical expressions for the average signal-to-jammer ratio (SJR) and propose a modified measurement matrix that improves the SJR.

This part of work has been published in:

- Y. Yu, A.P. Petropulu and H.V. Poor, "MIMO radar using compressive sampling," *IEEE Journal of Selected Topics in Signal Process.*, vol. 4, no. 1, pp. 146-163, Feb. 2010.

- Y. Yu, A. P. Petropulu and H. V. Poor, "Compressive sensing for MIMO Radar," in *Proc. IEEE International Conference on Acoustics Speech and Signal Process.*, pp. 3017-3020, Taipei, Taiwan, Apr., 2009.

- A.P. Petropulu, Y. Yu and H.V. Poor, "Distributed MIMO radar using compressive sampling," in *Proc. 42nd Asilomar Conf. Signals, Syst. Comput.*, Pacific Grove, CA, pp. 203-207, Nov. 2008.

1.2.2 CSSF MIMO Radar: Low-complexity compressive sensing based MIMO radar that uses step frequency

We propose CSSF MIMO radar, a novel approach that applies step frequency to CS-based MIMO radar. The proposed approach enables substantial range resolution improve-

ment for CS-based MIMO radar. The aforementioned work assumes that the targets are located in a small range bin and the sampling is synchronized with the first target return. Such assumptions do not allow for range estimation. We consider the case in which targets can be located across several range bins for the proposed CSSF MIMO radar. Two types of CSSF MIMO radar systems are considered, i.e., linear step-frequency radar (LSFR), and random step-frequency radar (RSFR), and their effects on the CS approach are studied. The joint angle-Doppler-range estimation entails high complexity, as it employs a basis matrix whose construction requires discretization of the angle-Doppler-range space. For the case of slowly moving targets, a novel approach is proposed that achieves significant complexity reduction by successively estimating angle-range and Doppler in a decoupled fashion and by employing initial estimates obtained via matched filtering to further reduce the space that needs to be digitized.

This part of work is included in:

- Y. Yu, A.P. Petropulu and H.V. Poor, "CSSF MIMO Radar: Low-complexity compressive sensing based MIMO radar that uses step frequency," submitted to *IEEE Trans. Aerospace and Electronic Systs.* in 2010.

- Sagar Shah, Y. Yu and A.P. Petropulu, "Step-frequency radar with compressive sampling (SFR-CS)," in *Proc. IEEE International Conference on Acoustics Speech and Signal Process.*, Dallas, TX, Mar. 2010.

- Y. Yu, A.P. Petropulu and H.V. Poor, "Reduced complexity angle-Doppler-range estimation for MIMO radar that employs compressive sensing," in *IEEE Proc. 43rd Asilomar Conf. Signals, Syst. Comput.*, Pacific Grove, CA, pp. 1196-1200, Nov. 2009.

  Y. Yu, A.P. Petropulu and H.V. Poor, "MIMO radar based on reduced complexity compressive sampling," in Proc *IEEE Radio and Wireless Symposium 2010,* pp. 21-

24, New Orleans, LA, Jan. 2010.

- Y. Yu, A.P. Petropulu and H.V. Poor, "Range estimation for MIMO step-frequency radar with compressive sensing," in *Proc. 4th International Symposium on Communications, Control and Signal Process.*, Limassol, Cyprus, pp. 1-5, Mar. 2010.

1.2.3 Measurement matrix design

We propose two novel measurement matrix designs. The first one aims at reducing the coherence of the sensing matrix (CSM) and at the same time enhancing SIR. The second one focuses on improving SIR in order to reduce complexity while keeping the CSM comparable to that of the Gaussian random measurement matrix. Reduced complexity suboptimal constructions for the two measurement matrices are also proposed. To the best of our knowledge, this is the first work on optimum matrix design; previous approaches used a Gaussian random matrix as the measurement matrix. It is shown via simulations that the two proposed measurement matrices in certain cases can improve detection accuracy as compared to the typically used Gaussian random measurement matrix.

This part of work is included in:

- Y. Yu, A.P. Petropulu and H.V. Poor, "Robust target estimation in compressive sensing based colocated MIMO radar," in *Proc. IEEE Military Commun. Conf.*, San Jose, CA, Nov. 2010, to appear.

1.3 Outline of the Dissertation

This dissertation is organized as follows.

In Chapter 2, we present the proposed approach for angle-Doppler estimation. We derive the average SJR for the proposed approach and also discuss a modification of the random measurement matrix that can improve the SJR.

In Chapter 3, we propose a CSSF MIMO radar system that enables high-resolution target detection. A decoupled scheme for CSSF MIMO radar is also described for the case of slowly moving targets. This scheme can significantly alleviate computational burden without sacrificing performance.

In Chapter 4, we propose two measurement matrices to improve detection accuracy.

Chapter 5 contains concluding remarks and possible directions for future work.

2. DOA and Doppler Estimation for MIMO Radar Using CS

This chapter exploits DOA and Doppler estimation for MIMO radar for the scenario in which the targets are located in a small range bin and the sampling is synchronized with the first target return. In this case, range estimation is not allowed. We will discuss range estimation in the next chapter.

The MIMO radar consists of transmitters and receivers which are nodes of a small scale wireless network and are assumed to be randomly scattered on a disk. The transmit nodes transmit uncorrelated waveforms. Each receive node applies compressive sampling to the received signal to obtain a small number of samples, which the node subsequently forwards to a fusion center. Assuming that the targets are sparsely located in the angle-Doppler space, based on the samples forwarded by the receive nodes the fusion center formulates an ℓ_1-optimization problem, the solution of which yields target angle and Doppler information. The proposed approach achieves the superior resolution of MIMO radar with far fewer samples than required by other approaches. This implies power savings during the communication phase between the receive nodes and the fusion center. Performance in the presence of a jammer is analyzed for the case of slowly moving targets. Issues related to forming the basis matrix that spans the angle-Doppler space, and for selecting a grid for that space are discussed. Extensive simulation results are provided to demonstrate the performance of the proposed approach at different jammer and noise levels.

2.1 Introduction

The application of compressive sampling to a radar system was recently investigated in [34]- [36]. In [34], in the context of radar imaging, compressive sampling was shown to have the potential to reduce the typically required sampling rate and even render matched

filtering unnecessary. In [35], a CS-based data acquisition and imaging algorithm for ground penetrating radar was proposed to exploit the sparsity of targets in the spatial dimension. The approach of [35] was shown to require fewer measurements than standard backprojection methods. In [36], CS was applied in a radar system with a small number of targets, exploiting target sparseness in the time-frequency shift plane. The work of [37] considered DOA estimation of signal sources using CS. Although [37] focussed on communication systems, the proposed approach can be straightforwardly extended to radar systems. In [37], the basis matrix $\mathbf{\Psi}$ was formed by the discretization of the angle space. The source signals were assumed to be unknown, and an approximate version of the basis matrix was obtained based on the signal received by a reference vector. The signal at the reference sensor would have to be sampled at a very high rate in order to construct a good basis matrix.

Throughout this dissertation, we consider a small scale network that acts as a MIMO radar system. Each node is equipped with one antenna, and the nodes are distributed at random on a disk of a certain radius. Without any fixed infrastructure, the distributed antennas in this small network render such MIMO radar more flexible than a fixed antenna array since we can choose the nodes freely. For example, the network nodes could be soldiers that carry antennas on their backpacks. The nodes transmit independent waveforms. We extend the idea of [37] to the problem of angle-Doppler estimation for MIMO radar. Since the number of targets is typically smaller than the number of snapshots that can be obtained, angle-Doppler estimation can be formulated as that of recovery of a sparse vector using CS. Unlike the scenario considered in [37], in MIMO radar the transmitted waveforms are known at each receive node. This information, and also information on the location of transmit nodes, if available, enables each receive node to construct the basis matrix locally, without knowledge of the received signal at a reference sensor or any other antenna. In cases in which the receive nodes do not have location information about the

transmitters, or they do not have the computational power, or they face significant interference, the received samples are transmitted to a fusion center which has access to location information and also to computational power. Based on the received data, the fusion center formulates an augmented ℓ_1-optimization problem the solution of which provides target angle and Doppler information. The performance of ℓ_1-optimization depends on the noise level. A potential jammer would act as noise, and thus affect performance. We provide analytical expressions for the average signal-to-jammer ratio (SJR) and propose a modified measurement matrix that improves the SJR. For the case of stationary targets, the proposed approach is compared to existing methods, such as the Capon, amplitude and phase estimation (APES), generalized likelihood ratio test (GLRT) [14] and multiple signal classification (MUSIC) methods, while for moving targets, comparison to the matched filter method [39] is conducted.

Preliminary results of our work were published in [40]. Independently derived results for MIMO radar using compressive sampling were also published in the same proceedings [41]. The difference between our work and [41] is that in [41] a uniform linear array was considered as a transmit and receive antenna configuration, while in our work we focus on randomly placed transmit and receive antennas, i.e., an infrastructure-less MIMO radar system. Further we investigate the effects of a jammer on estimation performance and propose a modified measurement matrix to suppress the jammer. Note that [41] and other works on CS-based radar, i.e., [34]-[36], did not consider the performance of the CS algorithm in the case of strong interference.

The rest of the Chapter is organized as follows. In Section 2.2 we provide the signal model of a distributed MIMO radar system. In Section 2.3, the proposed approach for angle-Doppler estimation is presented. In Section 2.4 we derive the average SJR for the proposed approach and also discuss a modification of the random measurement matrix that can further improve the SJR. Simulation results are given in Section 2.5 for the cases

of stationary targets and moving targets. Finally, we make some concluding remarks in Section 2.6.

2.2 Signal Model for MIMO Radar

As shown in Fig. 2.1, we consider a MIMO radar system with M_t transmit nodes and N_r receive nodes that are uniformly distributed on a disk of a small radius r. This particular assumption will be used in Section 2.5 for the analytical evaluation of the proposed approach. For simplicity, we assume that targets and nodes lie on the same plane and we consider a clutter-free environment. Perfect synchronization and localization of nodes is also assumed. The extension to the case in which targets and nodes lie in 3-dimension space is straightforward. Let (r_i^t, α_i^t) and (r_i^r, α_i^r) denote the locations in polar coordinates of the i-th transmit and receive antenna, respectively. Then the probability density functions of $r_i^{t/r}$ and $\alpha_i^{t/r}$ are

$$\begin{aligned} f_{r_i^{t/r}}(r_i^{t/r}) &= \frac{2r_i^{t/r}}{r^2},\ 0 < r_i^{t/r} < r \\ \text{and } f_{\alpha_i^{t/r}}(\alpha_i^{t/r}) &= \frac{1}{2\pi},\ -\pi \le \alpha_i^{t/r} < \pi. \end{aligned} \tag{2.1}$$

Let us assume that there are K point targets present. The k-th target is at azimuth angle θ_k and moves with constant radial speed v_k. Its range equals $d_k(t) = d_k(0) - v_k t$, where $d_k(0)$ is the distance between this target and the origin at time equal to zero. Under the far-field assumption, i.e., $d_k(t) \gg r_i^{t/r}$, the distance between the ith transmit/receive antenna and the k-th target d_{ik}^t/d_{ik}^r can be approximated as

$$d_{ik}^{t/r}(t) \approx d_k(t) - \eta_i^{t/r}(\theta_k) = d_k(0) - v_k t - \eta_i^{t/r}(\theta_k) \tag{2.2}$$

where $\eta_i^{t/r}(\theta_k) = r_i^{t/r}\cos(\theta_k - \alpha_i^{t/r})$.

Let $x_i(t)e^{j2\pi ft}$ denote the continuous-time waveform transmitted by the i-th transmit

antenna, where f is the carrier frequency; we assume that all transmit nodes use the same carrier frequency and also that the $x_i(t)$ is periodic with period T_p and narrowband.

The received signal at the k-th target equals

$$y_k(t) = \beta_k \sum_{i=1}^{M_t} x_i(t - d_{ik}^t(t)/c) \exp(j2\pi f(t - \frac{d_{ik}^t(t)}{c})),\ k = 1, \ldots, K \tag{2.3}$$

where $\{\beta_k, k = 1, \ldots, K\}$ are complex amplitudes proportional to the RCS and are assumed to be the same for all the receivers. The latter assumption is consistent with a small network in which the distances between network nodes are much smaller than the distances between the nodes and the targets, i.e., $d_k(t) \gg r_i^{t/r}$. Thus, since they are closely spaced, all receive nodes see the same aspect of the target.

Due to reflection by the target, the l-th antenna element receives

$$\begin{aligned} z_l(t) &= \sum_{k=1}^{K} y_k(t - \frac{d_{lk}^r(t)}{c}) + \epsilon_l(t) \\ &= \sum_{k=1}^{K} \beta_k \sum_{i=1}^{M_t} x_i(t - \frac{d_{ik}^t(t) + d_{lk}^r(t)}{c}) e^{j2\pi f(t - \frac{d_{ik}^t(t) + d_{lk}^r(t)}{c})} + \epsilon_l(t),\ l = 1, \ldots, M_r \end{aligned} \tag{2.4}$$

where $\epsilon_l(t)$ represents noise, which is assumed to be independent and identically distributed (i.i.d.) Gaussian with zero mean and variance σ^2.

For the scenario in which the targets are located in a small range bin and the sampling is synchronized with the first target return, the narrowband assumption on the transmit waveforms allows us to ignore the delay in $x_i(t)$, and consider the delay in the phase term only. Thus, the received baseband signal at the l-th antenna can be approximated as

$$\begin{aligned} z_l(t) &\approx \sum_{k=1}^{K} \beta_k \sum_{i=1}^{M_t} x_i(t) e^{j2\pi f_k t} e^{j\frac{2\pi}{\lambda}(-2d^k(0) + \eta_i^t(\theta_k) + \eta_l^r(\theta_k))} + \epsilon_l(t) \\ &= \sum_{k=1}^{K} \beta_k e^{-j\frac{2\pi}{\lambda}2d_k(0)} e^{j\frac{2\pi}{\lambda}\eta_l^r(\theta_k)} e^{j2\pi f_k t} \mathbf{x}^T(t)\mathbf{v}(\theta_k) + \epsilon_l(t) \end{aligned} \tag{2.5}$$

where λ is the transmitted signal wavelength, $f_k = 2v_k f/c$ is the Doppler shift caused by the k-th target, and

$$\begin{aligned} \mathbf{v}(\theta_k) &= [e^{j\frac{2\pi}{\lambda}\eta_1^t(\theta_k)}, ..., e^{j\frac{2\pi}{\lambda}\eta_{M_t}^t(\theta_k)}]^T \quad (2.6) \\ \text{and } \mathbf{x}(t) &= [x_1(t), ..., x_{M_t}(t)]^T. \quad (2.7) \end{aligned}$$

On letting L be the length of waveforms, $lT_s, l = 0, \ldots, L-1$, denote the time within the pulse (fast time) and T is the pulse repetition interval (PRI), the received samples collected during the m-th pulse are given by

$$\mathbf{z}_{lm} = \begin{bmatrix} z_l((m-1)T + 0T_s) \\ \vdots \\ z_l((m-1)T + (L-1)T_s) \end{bmatrix} = \sum_{k=1}^{K} \gamma_k e^{j\frac{2\pi}{\lambda}\eta_l^r(\theta_k)} e^{j2\pi f_k(m-1)T} \mathbf{D}(f_k)\mathbf{X}\mathbf{v}(\theta_k) + \mathbf{e}_{lm} \quad (2.8)$$

where

$$\begin{aligned} \gamma_k &= \beta_k e^{-j\frac{2\pi}{\lambda}2d_k(0)}, \\ \mathbf{D}(f_k) &= \text{diag}\{[e^{j2\pi f_k 0T_s}, \ldots, e^{j2\pi f_k(L-1)T_s}]\}, \\ \mathbf{e}_{lm} &= [\epsilon_l((m-1)T + 0T_s), \ldots, \epsilon_l((m-1)T + (L-1)T_s)]^T, \\ \text{and } \mathbf{X} &= [\mathbf{x}(0T_s), \ldots, \mathbf{x}((L-1)T_s)]^T \quad (L \times M_t). \quad (2.9) \end{aligned}$$

Throughout this chapter, we make the following assumptions:

- (A1) The targets are slowly moving. Therefore, the Doppler shift within a pulse can be ignored, i.e., $f_k T_p << 1$ for $k = 1, ..., K$, where T_p denotes pulse duration.
- (A2) The radar waveforms are independent across transmit nodes and thus $\int_{t=0}^{T} x_i(t)x_{i'}^*(t+\tau)dt, i \neq i'$ is negligible as compared to $\int_{t=0}^{T} x_i(t)x_{i'}^*(t+\tau)dt$.

2.3 Previous work on DOA and Doppler estimation for MIMO radar

In this section, we describe some well-known DOA and Doppler estimation methods in the literature that will be considered in Chapter 4. These methods will be compared to the approach to be proposed via simulation results.

2.3.1 DOA estimation

We assume stationary targets for DOA estimation and thus only the data during one pulse is considered. Then the received signal at the l-th node in (2.8) is reduced to

$$\mathbf{z}_l = \sum_{k=1}^{K} \gamma_k e^{j\frac{2\pi}{\lambda}\eta_l^r(\theta_k)} \mathbf{X}\mathbf{v}(\theta_k) + \mathbf{e}_l \tag{2.10}$$

Stacking the data of N_r nodes, we have

$$\mathbf{Z} = [\mathbf{z}_1, \ldots, \mathbf{z}_{N_r}]^T = \sum_{k=1}^{K} \gamma_k \mathbf{v}_r(\theta_k)\mathbf{v}^T(\theta_k)\mathbf{X}^T + \mathbf{E}. \tag{2.11}$$

where $\mathbf{v}_r(\theta_k) = [e^{j\frac{2\pi}{\lambda}\eta_1^r(\theta_k)}, ..., e^{j\frac{2\pi}{\lambda}\eta_{N_r}^r(\theta_k)}]^T$ and $\mathbf{E} = [\mathbf{e}_1, \ldots, \mathbf{e}_{N_r}]^T$.

Capon method [14]

The Capon method yields a beamformer $\mathbf{w}$ that can suppress noise, interference and jamming suppression while keeping the desired signal undistorted. In particular, the beamformer $\mathbf{w}$ can be formulated as

$$\min_{\mathbf{w}} \mathbf{w}^H \mathbf{R}\mathbf{w} \; s.t. \; \mathbf{w}^H \mathbf{v}_r(\theta) = 1 \tag{2.12}$$

where $\mathbf{R} = \mathbf{Z}\mathbf{Z}^H$.

The solution to (2.12) is

$$\mathbf{w}^* = \frac{\mathbf{R}^{-1}\mathbf{v}_r(\theta)}{\mathbf{v}_r^H(\theta)\mathbf{R}^{-1}\mathbf{v}_r(\theta)}. \tag{2.13}$$

Applying the LS method to the beamformed output by $\mathbf{w}^*$, we can easily obtain the estimates of target reflectivity as follows

$$\hat{\beta}_k(\theta) = \frac{(\mathbf{w}^*)^H\mathbf{Z}\mathbf{X}^*\mathbf{v}^*(\theta)\mathbf{v}_r^H(\theta)\mathbf{w}}{(\mathbf{w}^*)^H\mathbf{v}_r(\theta)\mathbf{v}^T(\theta)\mathbf{R}_x\mathbf{v}^*(\theta)\mathbf{v}_r^H(\theta)\mathbf{w}} = \frac{\mathbf{v}_r^H(\theta)\mathbf{R}^{-1}\mathbf{Z}\mathbf{X}^*\mathbf{v}^*(\theta)}{\mathbf{v}_r^H(\theta)\mathbf{R}^{-1}\mathbf{v}_r(\theta)\mathbf{v}^T(\theta)\mathbf{R}_x\mathbf{v}^*(\theta)} \tag{2.14}$$

where $\mathbf{R}_x = \mathbf{X}^T\mathbf{X}^*$.

APES method [14]

The APES beamformer aims at minimizing the distance between the output and the desired signal $\mathbf{v}(\theta)\mathbf{X}^T$, i.e.,

$$\min_{\mathbf{w},\beta} \|\mathbf{w}^H\mathbf{Z} - \beta(\theta)\mathbf{v}^T(\theta)\mathbf{X}^T\|^2 \; s.t. \; \mathbf{w}^H\mathbf{v}_r(\theta) = 1. \tag{2.15}$$

The optimal beamformer solving (2.15) is

$$\mathbf{w}^* = \frac{\mathbf{v}_r^H(\theta)\mathbf{Q}^{-1}}{\mathbf{v}_r^H(\theta)\mathbf{Q}^{-1}\mathbf{v}_r(\theta)} \tag{2.16}$$

and the estimate of target reflectivity is given by

$$\hat{\beta}_k(\theta) = \frac{\mathbf{v}_r^H(\theta)\mathbf{Q}^{-1}\mathbf{Z}\mathbf{X}^*\mathbf{v}^*(\theta)}{\mathbf{v}_r^H(\theta)\mathbf{Q}^{-1}\mathbf{v}_r(\theta)\mathbf{v}^T(\theta)\mathbf{R}_x\mathbf{v}^*(\theta)} \tag{2.17}$$

where

$$\mathbf{Q} = \mathbf{R} - \frac{\mathbf{Z}\mathbf{X}^*\mathbf{v}^*(\theta)\mathbf{v}^T(\theta)\mathbf{X}^T\mathbf{Z}^H}{\mathbf{v}^T(\theta)\mathbf{R}_x\mathbf{v}^*(\theta)} \tag{2.18}$$

GLRT method [14]

Let the columns of **E** in (2.11) be independently and identical distributed (i.i.d) circularly symmetric complex Gaussian random vectors with zero-mean and unknown covariance $\mathbf{R}_n$. The GLR is defined as

$$\rho(\theta) = 1 - \left[\frac{\max_{\mathbf{R}_n} f(\mathbf{Z}|\beta = 0, \mathbf{R}_n, \theta)}{\max_{\beta,\mathbf{R}_n} f(\mathbf{Z}|\beta, \mathbf{R_n}), \theta}\right]^{\frac{1}{L}} = 1 - \frac{\mathbf{v}_r^H(\theta)\mathbf{R}^{-1}\mathbf{v}_r(\theta)}{\mathbf{v}_r^H(\theta)\mathbf{Q}^{-1}\mathbf{v}_r(\theta)} \tag{2.19}$$

where

$$f(\mathbf{Z}|\beta, \mathbf{R}_n, \theta) = \pi^{LN_r}|\mathbf{R}_n|^{-L}e^{-\mathrm{Tr}\{\mathbf{R}_n^{-1}(\mathbf{Z}-\beta\mathbf{v}_r(\theta)\mathbf{v}^T(\theta)\mathbf{X})(\mathbf{Z}-\beta\mathbf{v}_r(\theta)\mathbf{v}^T(\theta)\mathbf{X})^H\}} \tag{2.20}$$

One can see from (2.19) that the GLR approaches to 1 if there is a target at θ; otherwise it is close to zero.

MUSIC method [42]

The MUSIC method is one of subspace-based methods. Unlike the three DOA estimation methods described above, the MUSIC does not require to know transmit waveforms. Assuming white noise with covariance matrix $\sigma^2\mathbf{I}$, the covariance matrix of received signal can be represented as

$$\mathbf{R} = \mathbf{V}\mathbf{X}^T\mathbf{X}^*\mathbf{V}^H + \sigma^2\mathbf{I} \tag{2.21}$$

where

$$\mathbf{V} = \sum_{k=1}^{K}\gamma_k\mathbf{v}_r(\theta_k)\mathbf{v}^T(\theta_k) = [\mathbf{v}_r(\theta_1), \ldots, \mathbf{v}_r(\theta_K)]diag\{[\gamma_1, \ldots, \gamma_K]\}[\mathbf{v}(\theta_1), \ldots, \mathbf{v}(\theta_K)]^T \tag{2.22}$$

Subspace-based methods require $N_t > K$ to sperate the noise space from the signal

space. In this case,the term $\mathbf{V}\mathbf{X}^T\mathbf{X}^*\mathbf{V}^H$ has $L - M$ zero eigenvalues. One can see from (2.21) that the eigenvectors denoted by $\mathbf{U}_n$ corresponding to the eigenvalue σ^2 span the noise space and are orthogonal to $\mathbf{V}$, i.e.

$$\mathbf{U}_n^H\mathbf{V} = 0 \rightarrow \mathbf{U}_n^H[\mathbf{v}_r(\theta_1), \ldots, \mathbf{v}_r(\theta_K)] = 0. \tag{2.23}$$

Therefore, the MUSIC "spatial spectrum" is defined as

$$p(\theta) = \frac{\mathbf{v}_r^H(\theta)\mathbf{v}_r(\theta)}{\mathbf{v}_r^H(\theta)(\mathbf{U}_n\mathbf{U}_n^H)^{-1}\mathbf{v}_r(\theta)}. \tag{2.24}$$

If there is a target located at θ, then $p(\theta)$ goes to infinity; otherwise, $p(\theta)$ has small value.

The detection accuracy of the MUSIC method relies on the estimation of noise space. For the sufficiently long signal or adequately high SNR, we can estimate the noise space precisely and thus obtain the desired performance of the MUSIC method.

2.3.2 Doppler estimation [39]

The way to estimate Doppler shift for single-input single-out (SISO) radar has been discussed in Chapter 1. In this section, we consider the Doppler estimation for MIMO radar. The most common method is the matched filtering method (MFM). Based on the signal model (2.8), the angle and Doppler need to be jointly estimated. The matched filter looking for a target at (θ, v) yields

$$c_{MFM}(\theta, v) \triangleq \left| \sum_{m=1} N_p \sum_{l=1}^{N_r} (\mathbf{z}_{lm})^H \left(\gamma_k e^{j\frac{2\pi}{\lambda}\eta_l^r(\theta)} e^{j\frac{4\pi f v}{c}(m-1)T} \mathbf{D}(\frac{2v}{c} f)\mathbf{X}\mathbf{v}(\theta_k) \right) \right|. \tag{2.25}$$

If there is a target located at θ, v, then $(c_{MFM}(\theta, v))$ has large value; otherwise, it is negligible.

2.4 Compressive Sensing for MIMO Radar

Let us discretize the angle and speed space on a fine grid (seen in Fig. 2.2), i.e., respectively, $[\tilde{a}_1, \ldots, \tilde{a}_{N_a}]$ and $[\tilde{b}_1, \ldots, \tilde{b}_{N_b}]$. Let the grid points be arranged first angle-wise and then speed-wise to yield the grid points $(a_n, b_n), n = 1, ..., N_a N_b N_c$. Through this ordering, the grid point $(\tilde{a}_{n_a}, \tilde{b}_{n_b})$ is mapped to point (a_n, b_n) with $n = (n_b - 1)n_a + n_a$.

We can rewrite (2.8) as

$$\mathbf{z}_{lm} = \sum_{n=1}^{N} s_n e^{j\frac{2\pi}{\lambda}\eta_l^r(a_n)} e^{j2\pi b_n(m-1)T} \mathbf{D}(b_n)\mathbf{X}\mathbf{v}(a_n) + \mathbf{e}_{lm} \tag{2.26}$$

where $N = N_a N_b$ and

$$s_n = \begin{cases} \gamma_k, & \text{if the } k\text{-th target is at } (a_n, b_n) \\ 0, & \text{otherwise} \end{cases} . \tag{2.27}$$

In matrix form we have

$$\mathbf{z}_{lm} = \mathbf{\Psi}_{lm}\mathbf{s} + \mathbf{e}_{lm} \tag{2.28}$$

where $\mathbf{s} = [s_1, \ldots, s_N]^T$ and

$$\mathbf{\Psi}_{lm} = [e^{j\frac{2\pi}{\lambda}\eta_l^r(a_1)} e^{j2\pi b_1(m-1)T} \mathbf{D}(b_1)\mathbf{X}\mathbf{v}(a_1), \ldots, e^{j\frac{2\pi}{\lambda}\eta_l^r(a_N)} e^{j2\pi b_N(m-1)T} \mathbf{D}(b_N)\mathbf{X}\mathbf{v}(a_N)]. \tag{2.29}$$

Assuming that there are only a small number of targets, the positions of targets are sparse in the angle-Doppler plane, i.e., $\mathbf{s}$ is a sparse vector. Let us measure linear projections of $\mathbf{z}_{lm}$ as

$$\mathbf{r}_{lm} = \mathbf{\Phi}_{lm}\mathbf{z}_{lm} = \mathbf{\Phi}_{lm}\mathbf{\Psi}_{lm}\mathbf{s} + \tilde{\mathbf{e}}_{lm}, \tag{2.30}$$

where $\mathbf{\Phi}_{lm}$ is an $M \times L$ ($M < L$) zero-mean Gaussian random matrix that has small corre-

lation with $\mathbf{\Psi}_{lm}$, and $\tilde{\mathbf{e}}_{lm} = \mathbf{\Phi}_{lm}\mathbf{e}_{lm}$. M must be larger than the number of targets.

All the receive nodes forward their compressed measurements to a fusion center. We assume that the fusion center has the ability to separate the data of different nodes from each other. This can be done, for instance, if the nodes send their data over different carriers. The fusion center combines the compressively sampled signals due to N_p pulses obtained at N_r receive nodes to form the vector $\mathbf{r}$. It holds that

$$\mathbf{r} = [\mathbf{r}_{11}^T, \ldots, \mathbf{r}_{1N_p}^T, \ldots, \mathbf{r}_{N_r1}^T, \ldots, \mathbf{r}_{N_rN_p}^T]^T = \mathbf{\Theta}\mathbf{s} + \mathbf{E} \tag{2.31}$$

where $\mathbf{\Theta} = [(\mathbf{\Phi}_{11}\mathbf{\Psi}_{11})^T, \ldots, (\mathbf{\Phi}_{1N_p}\mathbf{\Psi}_{1N_p)})^T, \ldots, (\mathbf{\Phi}_{N_r1}\mathbf{\Psi}_{N_r1})^T, \ldots, (\mathbf{\Phi}_{N_rN_p}\mathbf{\Psi}_{N_rN_p)})^T]^T$ and $\mathbf{E} = [\tilde{\mathbf{e}}_{11}^T, \ldots, \tilde{\mathbf{e}}_{1N_p}^T, \ldots, \tilde{\mathbf{e}}_{N_r1}^T, \ldots, \tilde{\mathbf{e}}_{N_rN_p}^T]^T$. Thus, the fusion center can recover $\mathbf{s}$ by applying the Dantzig selector to the convex problem of (3.8) as ([43])

$$\hat{\mathbf{s}} = \min \|\mathbf{s}\|_1 \quad s.t. \ \|\mathbf{\Theta}^H(\mathbf{r} - \mathbf{\Theta}\mathbf{s})\|_\infty < \mu. \tag{2.32}$$

According to [43], the sparse vector $\mathbf{s}$ can be recovered with very high probability if $\mu = (1+t^{-1})\sqrt{2\log N\tilde{\sigma}^2}\sigma_{max}$, where t is a positive scalar, σ_{max} is the maximum norm of columns in the sensing matrix Θ and $\tilde{\sigma^2}$ is the variance of the noise in (3.8). If $\mathbf{\Phi}\mathbf{\Phi}^H = \mathbf{I}$ then $\tilde{\sigma}^2 = \sigma^2$. Determining the best value of μ requires some experimentation. A method that requires an exhaustive search was described in [43]. A lower bound is readily available, i.e., $\mu > \sqrt{2\log N\tilde{\sigma}^2}\sigma_{max}$. Also, μ should not be too large because in that case the trivial solution $\mathbf{s} = \mathbf{0}$ is obtained. Thus, we may set $\mu < \|\Theta^H\mathbf{r}\|_\infty$.

2.4.1 Resolution

The UUP [19][20] indicates that if every set of columns with cardinality less than the sparsity of the signal of interest of the sensing matrix ($\mathbf{\Theta}$ defined in (3.8)) are approximately orthogonal, then the sparse signal can be exactly recovered with high probability. For a

fixed M the correlation of columns of the sensing matrix can be reduced if the number of pulses N_p and/or the number of receive nodes N_r is increased. Intuitively, the increase in N_p and N_r increases the dimension of the sensing matrix columns, thereby rendering the columns less similar to each other. A more formal proof is provided in Appendix I. Moreover, increasing the number of transmit nodes, i.e., M_t, also reduces the correlation of columns; this is also shown in Appendix I.

In general, to achieve high resolution a fine grid is required. However, for fixed N_p, N_r and M_t, decreasing the distance between the grid points would result in more correlated columns in the sensing matrix. Based on the above discussion, the column correlation can be reduced by increasing N_p, N_r or M_t. Also, based on the theory of CS, the effects of a higher column correlation can be mitigated by using a larger number of measurements, i.e., by increasing M. In particular, it was shown in [19] that M should satisfy $M \geq \frac{K\epsilon^2(\log N)^4}{C}$, where ϵ denotes the maximum mutual coherence between the two columns of the sensing matrix and C is a positive constant.

One might tend to think that in order to achieve good resolution one has to involve a lot of measurements, or trasnmit/receive antennas, or pulses, which in turn would involve high complexity. However, extensive simulations suggest that this is not the case. In fact, the proposed approach can match the resolution that can be achieved with conventional methods, while using far fewer received samples, than those used by the conventional methods.

2.4.2 Maximum grid size for the angle-Doppler space

The grid in the angle-Doppler space must be selected so that the targets that do not fall on the chosen grid points can still be captured by the closest grid points. This requires sufficiently high correlation of the signal reflected by each target with the columns of $\boldsymbol{\Theta}$ corresponding to grid points close to the targets in the angle-Doppler plane. However, this requirement goes against the UUP, which requires that every set of columns with cardinality

less than the sparsity of the signal of interest be approximately orthogonal. Thus, there is a tradeoff of the correlation of columns of the sensing matrix and the grid size.

Absent prior information about the targets, we can determine the maximum spacing of adjacent grids in the angle-Doppler space by considering the worst case. Assume that we discretize the angle-Doppler space uniformly with the spacing $(\Delta a, \Delta b)$ as $\mathbf{a} = [(a_1, b_1), \ldots, (a_N, b_N)]$. The worst case scenario is that the targets fall in the middle between two adjacent grid points. Therefore, a practical approach of selecting the grid points is to calculate the correlation of columns corresponding to $(a_i + \frac{\Delta a}{2}, b_i)$ and $(a_i, b_i + \frac{\Delta b}{2})$ with the columns corresponding to (a_i, b_i), $i = 1, \ldots, N$. This can be done by computing the correlation at lag zero of columns corresponding to $(a_i + \frac{\Delta a}{2}, b_i)$ and $(a_i, b_i + \frac{\Delta b}{2})$ with the columns corresponding to (a_i, b_i), for $i = 1, \ldots, N$, and then taking the average. Then, we can vary the step $(\Delta a, \Delta b)$ until the average correlation reaches some threshold. This threshold should be high enough to capture the targets that do not fall on the grid in the angle-Doppler space, and at the same time, it should satisfy the UUP. The adoption of such grid points would ensure that the angle-Doppler estimates of targets would always fall on the grid of the constructed basis matrix.

When the targets are between grid points, the increase in N_p or N_r will not necessarily improve performance. However, simulations show that we can obtain very good performances with very small N_p and N_r. To achieve a similar performance, the conventional matched filter method will require much greater N_p and N_r.

2.4.3 Range of unambiguous speed

Let us assume that the Doppler shift change over the duration (T) of the pulse is negligible as compared to the change between pulses. This is reasonable given the assumption (A1). Given two grid points (a_i, b_i) and (a_i, b_j) in the angle-Doppler space, where $b_i \neq b_j$, the corresponding columns of $\mathbf{\Psi}$ are different if $e^{j2\pi b_i T} \neq e^{j2\pi b_j T}$. Let v_i be the speed corre-

sponding to the Doppler frequency b_i and $\Delta_v^{ij} = v_j - v_i$. It holds that

$$e^{j2\pi b_i T} \neq e^{j2\pi b_j T} \quad \Rightarrow \quad \frac{2\Delta_v^{ij} fT}{c} \neq n, n = \pm 1, \pm 2, \ldots \tag{2.33}$$

Therefore, the range of the unambiguous relative speed between two targets that appear at the same speed satisfies

$$\frac{2\Delta_v^{ij} fT}{c} \leq 1 \Rightarrow \Delta_v^{ij} \leq \frac{c}{2fT}. \tag{2.34}$$

The selection of T affects the range of the unambiguous speed; the smaller the T the larger the range of the unambiguous speed is. We also need a relatively small T to satisfy the assumption that the Doppler shift does not change within the duration of the pulse. On the other hand, a larger T is needed to satisfy the narrowband assumption about the transmitted waveforms. Therefore, T needs to be chosen to balance the above requirements.

2.4.4 Complexity

The proposed approach requires solving the convex programming problem of (2.32). The more targets one would hope to be able to detect the higher the complexity would be. Further, the signals involved are complex. In this case (2.32) can be recast as a SOCP [29], which requires polynomial time in the dimension of the unknown vector.

The requirement of a fine grid further increases the computational complexity. This problem can be mitigated by first performing an initial angle-Doppler estimation using a coarse grid, and then refining the grid points around the initial estimate. Restricting the candidate angle-Doppler space reduces the samples in the angle-Doppler space that are required for constructing the basis matrix, thus reducing the complexity of the ℓ_1-optimization step.

In addition to the computation complexity, the receiver for obtaining the required sam-

ples is also more complex. The schematic diagram of the receiver is shown in Fig. 2.3 (see also [35]).

2.5 Performance Analysis in the presence of a jammer signal

In [43], Candes and Tao showed that if the basis matrix obeys the UUP and the signal of interest **s** is sufficiently sparse, then the square estimation error of the Dantzig selector satisfies with very high probability

$$\| \hat{\mathbf{s}} - \mathbf{s} \|_{\ell_2}^2 \leq C^2 2 log N \times (\sigma^2 + \sum_{i}^{N} \min(s^2(i), \sigma^2)) \tag{2.35}$$

where C is a constant, N denotes the length of **s** and σ^2 is the variance of the noise. It can be easily seen from (4.3) that an increase in the interference power degrades the performance of the Dantzig selector. Thus, in the presence of a jammer that transmits a waveform uncorrelated with the radar transmit waveforms, the performance of the proposed CS method will deteriorate. Next, we provide analytical expressions for the signal-to-jammer ratio at the receive nodes, and propose a modified measurement matrix to suppress the jammer.

2.5.1 Analysis of Signal-to-Jammer Ratio

Suppose that each transmitter transmits N_p pulses. In the presence of a jammer at location (d, θ) the signal received at the l-th receive antenna can be expressed as

$$\mathbf{r}_l = \begin{bmatrix} \mathbf{r}_{l1} \\ \vdots \\ \mathbf{r}_{lN_p} \end{bmatrix} = \underbrace{\sum_{k=1}^{K} \gamma_k e^{j\frac{2\pi}{\lambda}\eta_l^r(\theta_k)} \begin{bmatrix} \mathbf{\Phi}_{l1} e^{j2\pi f_k 0T} \\ \vdots \\ \mathbf{\Phi}_{lN_p} e^{j2\pi f_k (N_p-1)T} \end{bmatrix} \mathbf{D}(f_k)\mathbf{X}\mathbf{v}(\theta_k)}_{\mathbf{r}_{ls}}$$
$$+ \underbrace{e^{-j\frac{2\pi}{\lambda}(d-\eta_l^r(\theta))}\beta \begin{bmatrix} \mathbf{\Phi}_{l1}\tilde{\mathbf{x}}_1 \\ \vdots \\ \mathbf{\Phi}_{lN_p}\tilde{\mathbf{x}}_{N_p} \end{bmatrix}}_{\mathbf{r}_{lj}} + \underbrace{\begin{bmatrix} \mathbf{\Phi}_{l1}\mathbf{e}_{l1} \\ \vdots \\ \mathbf{\Phi}_{lN_p}\mathbf{e}_{lN_p} \end{bmatrix}}_{\mathbf{r}_{ln}} \tag{2.36}$$

where $\tilde{\mathbf{x}}_m = [\tilde{x}_m(0T_s), \ldots, \tilde{x}_m((L-1)T_s)]^T$ contains the samples of the signal transmitted by the jammer during the m-th pulse, and β denotes the square root of the power of the jammer over the duration of one signal pulse.

We assume that for all m, $E\{\tilde{x}_m^*(i)\tilde{x}_m(j)\} = 1/L$ for $i = j$, and 0 otherwise. Thus, $E\{\tilde{\mathbf{x}}_m^H\tilde{\mathbf{x}}_m\} = 1$. Also, we assume that $\tilde{\mathbf{x}}_m$, $m = 1, \ldots, N_p$ are uncorrelated with the main period of the transmitted waveforms. Thus, the effect of the jammer signal is similar to that of additive noise. In the following analysis we assume that the jammer contribution is much stronger than that of additive noise, and therefore we ignore the third term $\mathbf{r}_{ln}$ on the right hand side of (2.36). Later, in our simulations we will consider additive noise in addition to a jammer signal.

We assume that all receive nodes use the same random measurement matrix over N_p pulses, i.e., $\mathbf{\Phi}_l = \mathbf{\Phi}_{l1} = \mathbf{\Phi}_{l2} = \ldots = \mathbf{\Phi}_{lN_p}$. Let $\mathbf{A}_l^{k,k'} = \mathbf{X}^H\mathbf{D}^H(f_k)\mathbf{\Phi}_l^H\mathbf{\Phi}_l\mathbf{D}(f_{k'})\mathbf{X}$ and $q_{i,j}^{k,k'}$ denote the (i, j)-th element of $\mathbf{A}_l^{kk'}$. Thus, the average power of the desirable signal

conditioned on the transmitted waveform can be represented by

$$P_s(l) = E\{\mathbf{r}_{ls}^H \mathbf{r}_{ls} | \mathbf{X}\} = E\{\sum_{k,k'=1}^{K} \underbrace{\gamma_k^* \gamma_{k'} e^{-j\frac{2\pi}{\lambda}(\eta_l^r(\theta_k)-\eta_l^r(\theta_{k'}))}}_{\rho_l(k,k')} \underbrace{(\sum_{m=0}^{N_p-1} e^{-j2\pi(f_k-f_{k'})mT})}_{\mu_{kk'}} \underbrace{\mathbf{v}^H(\theta_k)\mathbf{A}_l^{kk'}\mathbf{v}(\theta_{k'})}_{Q_{kk'}}\}$$

$$= N_p E\{\sum_{k=1}^{K} |\beta_k|^2 Q_{kk}\} + E\{\sum_{k\neq k'} \rho_l(k,k')\mu_{kk'}Q_{kk'}\} \quad (2.37)$$

where $\rho_l(k,k')$ and $Q_{kk'}$ can be further written as

$$\rho_l(k,k') = e^{j\frac{2\pi}{\lambda}[2(d_k(0)-d_{k'}(0))-(\eta_l^r(\theta_k)-\eta_l^r(\theta_{k'}))}\beta_k^*\beta_{k'} \quad (2.38)$$

$$\text{and } Q_{kk'} = \sum_{i,j} q_{i,j}^{k,k'} e^{j\frac{2\pi}{\lambda}(\eta_j^t(\theta_{k'})-\eta_i^t(\theta_k))}\,. \quad (2.39)$$

As defined in Section 3.2, the position of the *i*th TX/RX node is denoted by $(r_i^{t/r}, \alpha_i^{t/r})$ in polar coordinates. Thus it holds that

$$a_{ji}^{k'k} = \eta_j^{t/r}(\theta_{k'}) - \eta_i^{t/r}(\theta_k) = \begin{cases} 2r_i^{t/r}\sin(\frac{\theta_{k'}-\theta_k}{2})\sin(\alpha_i - \frac{\theta_{k'}+\theta_k}{2}) & i = j \\ r_j^{t/r}\cos(\theta_{k'}-\alpha_j) - r_i^{t/r}\cos(\theta_k-\alpha_i) & i \neq j \end{cases} \quad (2.40)$$

Let ψ_0 be deterministic. Based on the assumed statistics of r_i and α_i (see (2.1)), the distribution of $h = \frac{r_i^{t/r}}{r}\sin(\alpha_i^{t/r} - \psi_0)$ is given by ([50])

$$f_h(h) = \frac{2}{\pi}\sqrt{1-h^2}, -1 < h < 1 \quad (2.41)$$

and

$$E\left\{e^{j\alpha h}\right\} = 2\frac{J_1(\alpha)}{\alpha} \quad (2.42)$$

where $J_1(\cdot)$ is the first-order Bessel function of the first kind. Thus, based on (4.15) we can

obtain

$$E\left\{e^{j\frac{2\pi}{\lambda}a_{ji}^{k'k}}\right\} = E\left\{e^{j\frac{2\pi r}{\lambda}\frac{a_{ji}^{k'k}}{r}}\right\} = \begin{cases} 1 & i = j \text{ and } k = k' \\ \varsigma(4\sin(\frac{\theta_{k'}-\theta_k}{2})) & i = j \text{ and } k \neq k' \\ \varsigma^2(2) & i \neq j \end{cases} \tag{2.43}$$

where $\varsigma(x) = 2\frac{J_1(x\frac{\pi r}{\lambda})}{x\frac{\pi r}{\lambda}}$.

Therefore, the average power of the desirable signal $P_s(l)$ taken over the positions of TX/RX nodes can be found to be

$$\begin{aligned} P_s(l) &= N_p E\left\{\sum_{k=1}^{K}|\beta_k|^2 Q_{kk}\right\} + E\left\{\sum_{k\neq k'}\rho_l(k,k')\mu_{kk'}Q_{kk'}\right\} \\ &= N_p\sum_{k=1}^{K}|\beta_k|^2 E\{Q_{kk}\} + \sum_{k\neq k'}E\{\rho_l(k,k')\}\mu_{kk'}E\{Q_{kk'}\} \\ &= N_p\sum_{k=1}^{K}|\beta_k|^2\sum_{i,j}q_{i,j}^{k,k}E\{e^{j\frac{2\pi}{\lambda}a_{ji}^{kk}}\} + \sum_{k\neq k'}\beta_k^*\beta_{k'}e^{j\frac{4\pi}{\lambda}(d_k(0)-d_{k'}(0))}E\{e^{j\frac{2\pi}{\lambda}a_{ll}^{k'k}}\}\mu_{kk'}\sum_{i,j}q_{i,j}^{k,k'}E\{e^{j\frac{2\pi}{\lambda}a_{ji}^{k'k}}\} \\ &= N_p\sum_{k=1}^{K}|\beta_k|^2[\sum_{i}q_{i,i}^{k,k} + \sum_{i\neq j}q_{i,j}^{k,k}\varsigma^2(2)] \\ &\quad + \sum_{k\neq k'}\beta_k^*\beta_{k'}e^{j\frac{4\pi}{\lambda}(d_k(0)-d_{k'}(0))}\varsigma_{kk'}\mu_{kk'}[\varsigma_{kk'}\sum_{i}q_{i,i}^{k,k'} + \sum_{i\neq j}q_{i,j}^{k,k'}\varsigma^2(2)] \end{aligned} \tag{2.44}$$

where $\varsigma_{kk'} = \varsigma(4\sin(\frac{\theta_{k'}-\theta_k}{2}))$.

For many practical radar systems with wavelength λ less than 0.1m, (e.g., most military multimode airborne radars), $2\pi r/\lambda$ is a large number if $r > 5m$. Since the function $\varsigma(x)$ decreases rapidly as x increases, the terms multiplied by $\varsigma^2(2)$ are small enough to be neglected in the above equation. Therefore, (2.44) can be approximated by

$$P_s(l) \approx N_p\sum_{k=1}^{K}|\beta_k|^2\sum_{i}q_{i,i}^{k,k} + \sum_{k\neq k'}\beta_k^*\beta_{k'}e^{j\frac{4\pi}{\lambda}(d_k(0)-d_{k'}(0))}\varsigma_{kk'}{}^2\mu_{kk'}\sum_{i}q_{i,i}^{k,k'}\ . \tag{2.45}$$

Similarly, the average power of the jammer signal over TR/TX locations is given by

$$\begin{aligned} P_j(l) &= E\{\mathbf{r}_{lj}^H \mathbf{r}_{lj}\} = (e^{-j\frac{2\pi}{\lambda}(d-\eta_l^r(\theta))}\beta)(e^{-j\frac{2\pi}{\lambda}(d-\eta_l^r(\theta))}\beta)^* \sum_{m=1}^{N_p} \tilde{\mathbf{x}}_m^H \mathbf{\Phi}_l^H \mathbf{\Phi}_l \tilde{\mathbf{x}}_m \\ &= |\beta|^2 \sum_{m=1}^{N_p} \tilde{\mathbf{x}}_m^H \mathbf{\Phi}_l^H \mathbf{\Phi}_l \tilde{\mathbf{x}}_m. \end{aligned} \tag{2.46}$$

The SJR given the node locations is the ratio of the power of the signal to the power of the jammer. Since the denominator does not depend on node locations, the average SJR equals SJR= $P_s(l)/P_j(l)$.

Some insight into the above obtained expression will be given in the following for some special cases.

2.5.2 SJR based on a modified measurement matrix

Since the jammer signal is uncorrelated with the transmitted signal, the SJR can be improved by correlating the jammer signal with the transmitted signal. Therefore, we propose a measurement matrix of the form

$$\tilde{\mathbf{\Phi}}_l = \mathbf{\Phi}_l' \mathbf{X}^H \ (M \times L) \tag{2.47}$$

where $\mathbf{\Phi}_l'$ is an $M \times M_t$ Gaussian random matrix. Note that $\tilde{\mathbf{\Phi}}_l$ is also Gaussian. As stated in [20], a random measurement matrix with i.i.d. entries, e.g., Gaussian or ±1 random variables, is nearly incoherent with any fixed basis matrix. Therefore, the proposed measurement matrix exhibits low coherence with Ψ_l, thus guaranteeing a stable solution to (2.32). Based on (2.47), the average power of the desirable signal $P_s(l)$ is given by (2.44), except that $Q_{kk'}$ is based on $\mathbf{A}_l^{k,k'} = \mathbf{X}^H \mathbf{D}^H(f_k)\mathbf{X}(\mathbf{\Phi}_l')^H \mathbf{\Phi}_l' \mathbf{X}^H \mathbf{D}(f_{k'})\mathbf{X}$. The average power of the jammer signal is given by (2.46) where $\mathbf{\Phi}_l$ is replaced by $\tilde{\mathbf{\Phi}}_l$.

Let us assume that the M_T transmit nodes emit periodic pulses containing independent

quadrature phase shift keying (QPSK) symbols, and that $\mathbf{X}^H\mathbf{X} = \mathbf{I}_{M_t}$. Also, we assume that $\mathbf{\Phi}_l\mathbf{\Phi}_l^H = \mathbf{\Phi}_l'(\mathbf{\Phi}_l')^H = \mathbf{I}_M$.

Let $\tilde{x}_i(n)$ be expressed as $\vartheta_{in}/\sqrt{L}$, where ϑ_{in} is a random variable with mean zero and variance one. Then the average power of the jammer signal $P_j(l)$ can be rewritten as follows:

$$\begin{aligned} P_j(l) &= |\beta|^2 \sum_{m=1}^{N_p} \tilde{\mathbf{x}}_m^H \mathbf{\Phi}_l^H \mathbf{\Phi}_l \tilde{\mathbf{x}}_m \\ &= |\beta|^2 \sum_{m=1}^{N_p} \sum_{i=j=0}^{L-1} \tilde{x}_m^*(i)\tilde{x}_m(i)c_{ii} + |\beta|^2 \sum_{m=1}^{N_p} \sum_{i\neq j=0}^{L-1} \tilde{x}_m^*(i)\tilde{x}_m(j)c_{ij} \\ &= \frac{1}{L}|\beta|^2 \sum_{m=1}^{N_p} \sum_{i=0}^{L-1} \vartheta_{mi}^*\vartheta_{mi}c_{ii} + \frac{1}{L}|\beta|^2 \sum_{m=1}^{N_p} \sum_{i\neq j=0}^{L-1} \vartheta_{mi}^*\vartheta_{mj}c_{ij} \end{aligned} \tag{2.48}$$

where c_{ij} is the (i, j)-th entry of $\mathbf{\Phi}_l^H\mathbf{\Phi}_l$. Since the entries of $\mathbf{\Phi}_l$ are i.i.d Gaussian variables with zero means and variances $\frac{1}{L}$, $c_{ii}, i = 1, \ldots, L$ are i.i.d chi-square random variables with means $\frac{M}{L}$ and variances $\frac{2M}{L}$; $c_{ij}, i \neq j$ are of mean zero and variance M/L^2. Let us express $c_{ij}, i \neq j$ as $\varrho_{ij}\sqrt{M}/L$, where ϱ_{ij} has zero mean and unit variance. It holds that

$$\begin{aligned} P_j(l) &= |\beta|^2 \sum_{m=1}^{N_p} E\{\vartheta_{mi}^*\vartheta_{mi}c_{ii}\} + \frac{\sqrt{M}}{L^2}|\beta|^2 \sum_{m=1}^{N_p} \sum_{i\neq j=0}^{L-1} \vartheta_{mi}^*\vartheta_{mj}\varrho_{ij} \\ &= |\beta|^2 N_p \frac{M}{L} + \frac{|\beta|^2\sqrt{M}(L-1)}{L} \sum_{m=1}^{N_p} \frac{1}{L(L-1)} \sum_{i\neq j=0}^{L-1} \vartheta_{mi}^*\vartheta_{mj}\varrho_{ij} \\ &= N_p|\beta|^2\frac{M}{L} + \frac{|\beta|^2\sqrt{M}(L-1)}{L} \sum_{m=1}^{N_p} E\{\vartheta_{i,m}^*\vartheta_{j,m}\varrho_{ij}\} \\ &\approx N_p|\beta|^2\frac{M}{L} \end{aligned} \tag{2.49}$$

where we have used the fact that for large L,

$$\frac{1}{L}\sum_{i=0}^{L-1}\vartheta_{mi}^{*}\vartheta_{mi}c_{ii} \quad \rightarrow \quad E\{\vartheta_{mi}^{*}\vartheta_{mi}c_{ii}\} = \frac{M}{L} \tag{2.50}$$

$$\text{and } \frac{1}{L(L-1)}\sum_{i\neq j=0}^{L-1}\vartheta_{mi}^{*}\vartheta_{mj}\varrho_{ij} \quad \rightarrow \quad E\{\vartheta_{mi}^{*}\vartheta_{mj}\varrho_{ij}\} = 0\ . \tag{2.51}$$

Using the measurement matrix $\tilde{\mathbf{\Phi}}_l$ in (2.47) will not affect the average $P_j(l)$ over the jammer signal due to the fact that $\sum_i c_{ii} = \text{Tr}\{\mathbf{X}(\mathbf{\Phi}_l')^H\mathbf{\Phi}_l'\mathbf{X}^H\} = \text{Tr}\{\mathbf{X}^H\mathbf{X}(\mathbf{\Phi}_l')^H\mathbf{\Phi}_l'\} = \text{Tr}\{\mathbf{\Phi}_l'(\mathbf{\Phi}_l')^H\} = \text{Tr}\{\mathbf{I}_M\} = M$.

In the following, we will look into the SJR improvement using $\tilde{\mathbf{\Phi}}_l$ as opposed to $\mathbf{\Phi}_l$, for two different cases, i.e., stationary targets and moving targets.

Stationary Targets

First, let us consider the SJR using the random measurement matrix $\mathbf{\Phi}_l$.

When the targets are stationary, the Doppler shift is zero and so $\mathbf{A}_l^{k,k'} = \mathbf{A}_l = \mathbf{X}^H\mathbf{\Phi}_l^H\mathbf{\Phi}_l\mathbf{X}$. Therefore, the average power of the desired signal can be approximated as

$$P_s(l) \quad \approx \quad N_p\sum_{k=1}^{K}|\beta_k|^2\sum_i q_{i,i} + N_p\sum_{k\neq k'}\beta_k^{*}\beta_{k'}e^{j\frac{4\pi}{\lambda}(d_k(0)-d_{k'}(0))}\varsigma_{kk'}^2\sum_i q_{i,i} \tag{2.52}$$

where $q_{i,j}$ is the (i, j)-th entry of $\mathbf{A}_l$.

Letting $\mathbf{x}_i$ denote the i-th column of $\mathbf{X}$, $\sum_i q_{i,i}$ can be expressed as

$$\begin{aligned}\sum_i q_{i,i} \quad &= \quad \text{Tr}\{\mathbf{A}_l\} = \sum_{i=1}^{M_t}\mathbf{x}_i^H\mathbf{\Phi}_l^H\mathbf{\Phi}_l\mathbf{x}_i = \sum_{i=1}^{M_t}\sum_{m,n=1}^{L}x_i^{*}(m)c_{mn}x_i(n) \\ &= \quad \sum_{i=1}^{M_t}\sum_{m=1}^{L}x_i^{*}(m)x_i(m)c_{mm} + \sum_{i=1}^{M_t}\sum_{m\neq n}^{L}x_i^{*}(m)x_i(n)c_{mn}.\end{aligned} \tag{2.53}$$

where $\Phi_l(m, n)$ is the (m, n)-th entry of $\mathbf{\Phi}_l^H\mathbf{\Phi}_l$.

The entries of $\mathbf{X}$ have zero means and mutually independent; therefore, for sufficiently

long L and M_t it holds that

$$\sum_i q_{i,i} \quad = \quad \frac{M_t}{L} \sum_{m=1}^{L} c_{mm} = \frac{MM_t}{L}. \tag{2.54}$$

Based on (2.54), a concise form of $P_s(l)$ is given by

$$P_s(l) \quad \approx \quad \frac{N_p M M_t \sum_{k=1}^{K} |\beta_k|^2}{L} + \frac{N_p M M_t}{L} \varphi \tag{2.55}$$

where $\varphi = \sum_{k,k',k\neq k'} \beta_k^* \beta_{k'} e^{j\frac{4\pi}{\lambda}(d_k(0)-d_{k'}(0))} \varsigma_{kk'}^2$.

Thus, the SJR corresponding to the random measurement matrix $\mathbf{\Phi}_l$ is

$$SJR_l = \frac{P_s(l)}{P_j(l)} \approx \frac{M_t(\sum_{k=1}^{K} |\beta_k|^2 + \varphi)}{|\beta|^2} \ . \tag{2.56}$$

When using the measurement matrix $\tilde{\mathbf{\Phi}}_l = \mathbf{\Phi}_l' \mathbf{X}^H$, the quantity corresponding to $\mathbf{A}_l^{k,k'}$ is

$$\tilde{\mathbf{A}}_l^{k,k'} = \tilde{\mathbf{A}}_l = \mathbf{X}^H \mathbf{X} (\mathbf{\Phi}_l')^H \mathbf{\Phi}_l' \mathbf{X}^H \mathbf{X} = (\mathbf{\Phi}_l')^H \mathbf{\Phi}_l' \ . \tag{2.57}$$

It holds that $\sum_i q_{i,i} = \mathrm{Tr}\{(\mathbf{\Phi}_l')^H \mathbf{\Phi}_l'\} = \mathrm{Tr}\{\mathbf{\Phi}_l' (\mathbf{\Phi}_l')^H\} = M$. Similarly, the average power of the desired signal can be approximated as

$$P_s(l) \quad \approx \quad N_p M (\sum_{k=1}^{K} |\beta_k|^2 + \varphi). \tag{2.58}$$

Therefore, the SJR corresponding to the random measurement matrix $\tilde{\mathbf{\Phi}}_l$ is

$$SJR_l = \frac{P_s(l)}{P_j(l)} \approx \frac{L(\sum_{k=1}^{K} |\beta_k|^2 + \varphi)}{|\beta|^2} \ . \tag{2.59}$$

From (2.56) and (2.59), it can be seen that the use of $\tilde{\mathbf{\Phi}}_l$ instead of $\mathbf{\Phi}_l$ can improve SJR by a factor of L/M_t when $L > M_t$. The SJR can be improved by an increase in L. However,

increasing L will require a higher T_s when the pulse duration is fixed. This will increase the bandwidth of the signal. It is interesting to note that the SJR of (2.56) and (2.59) does not depend on the the number of measurements, M.

Slowly Moving Targets

Based on the measurement matrix $\mathbf{\Phi}_l$, and considering the Doppler shift, we have $\mathbf{A}_l^{k,k'} = \mathbf{X}^H\mathbf{D}^H(f_k)\mathbf{\Phi}_l^H\mathbf{\Phi}_l\mathbf{D}(f_{k'})\mathbf{X}$. Due to the assumption (A1), we have

$$\sum_i q_{i,i}^{k,k'} = \mathrm{Tr}\{\mathbf{A}_l^{k,k'}\} = \mathrm{Tr}\{\mathbf{X}^H\mathbf{D}^H(f_k)\mathbf{\Phi}_l^H\mathbf{\Phi}_l\mathbf{D}(f_{k'})\mathbf{X}\} \approx \frac{MM_t}{L}. \tag{2.60}$$

Thus, $P_s(l)$ for the slowly moving targets with $f_pT << 1$ is approximately the same as that of stationary targets.

Let us now consider the measurement matrix $\tilde{\mathbf{\Phi}}_l$. Let c_{ij}^k denote the (i, j)-th entry of $\mathbf{X}^H\mathbf{D}^H(f_k)\mathbf{X}$ and note that c_{ij}^k is given by $c_{ij}^k = \sum_{n=0}^{L-1} x_i^*(n)x_j(n) * e^{j2\pi f_k nT_s}$. In scenarios in which L is relatively large, the following approximations are readily derived:

$$c_{ij}^k \begin{cases} = & \frac{1}{L}\frac{1-e^{j2\pi f_k LT_s}}{1-e^{j2\pi f_k T_s}} & i = j \\ \approx & 0 & i \neq j \end{cases}. \tag{2.61}$$

Since the off-diagonal elements are small compared with the diagonal elements, they can be ignored.

Then, we obtain the following approximation

$$\mathbf{A}_l^{k,k} = \mathbf{X}^H\mathbf{D}^H(f_k)\mathbf{X}(\mathbf{\Phi}_l')^H\mathbf{\Phi}_l'\mathbf{X}^H\mathbf{D}(f_k)\mathbf{X} \approx (\mathbf{\Phi}_l')^H\mathbf{\Phi}_l'. \tag{2.62}$$

Therefore, the SJR of slowly moving targets with $f_pT << 1$ is approximately equal to that of stationary targets for both random measurement matrices.

2.6 Simulation Results

The goal of this section is to demonstrate the ability of the proposed MIMO radar approach, denoted in the figures as CS, to pick up targets in the presence of noise and/or a jammer, and also show the effect on the various parameters involved. In each case the performance is compared against other methods that have been proposed in the context of MIMO radar (here referred to as "conventional") in order to quantify weaknesses and advantages. For the case of stationary targets, the conventional methods tested here are the methods of Capon, APES, GLRT [14] and MUSIC [52], while for moving targets, comparison to the matched filter method [39] is conducted.

In our simulations we consider a MIMO radar system with the transmit/receive antennas uniformly distributed on a disk of radius 10m. The carrier frequency is $f = 5GHz$ and the pulse repetition interval is $T = 1/4000s$. Each transmit node uses uncorrelated QPSK waveforms. The received signal is corrupted by zero mean Gaussian noise. We also consider a jammer that transmits waveforms uncorrelated to the signal waveforms. For simulation purposes we take the jamming waveforms to be white Gaussian [51]. The SNR is defined as the ratio of power of transmit waveform to that of thermal noise at a receive node. Throughout this dissertation, we use `CVX` to solve the Dantzig selector in (2.32). `CVX` is a package for specifying and solving convex programs [48][49].

2.6.1 Stationary Targets

The presence of a target can be seen in the plot of the magnitude of $\hat{\mathbf{s}}$ obtained by (2.32). We will refer to this vector as the *target information vector*. The location and magnitude of a peak in that plot provides target location and RCS magnitude, respectively. The proposed approach results in a clean plot away from the target locations, and well distinguished peaks corresponding to the targets. This is a desirable behavior for target detection, as it would result in small probability of false alarm. To demonstrate the appearance of the graph we

define the peak-to-ripple ratio (PRR) metric as follows. For the k-th target, PRR_k is the ratio of the square amplitude of the DOA estimate at the target azimuth angle to the sum of the square amplitude of DOA estimates at other angles except at the jammer location, i.e., $PRR_k = \frac{|s_k|^2}{\mathbf{s}^H\mathbf{s} - \sum_{i=1}^{K} |s_k|^2 - |s_j|^2}$, where $\mathbf{s}$ is defined in (2.27); s_k and s_j denote the elements of $\mathbf{s}$ corresponding to the location of the k-th target and the jammer, respectively. A clean plot would yield a high PPR, while a plot with a lot of ripples would yield a low PRR.

A metric that shows the degree to which a jammer is suppressed, namely the peak-to-jammer ratio (PJR), is also used here. PJR is defined as the ratio of the average square amplitude of the DOA estimates at the target angles to the square amplitude of DOA estimates at the jammer, i.e., $PJR = \frac{\frac{1}{K}\sum_{i=1}^{K} |s_k|^2}{|s_j|^2}$. Unlike PRR, PJR is averaged over all targets. In this way, the jammer is considered to be suppressed only if the peak amplitude at the jammer location is much smaller than the peak amplitude at any target location.

The results that we show represent $1,000$ Monte Carlo simulations over independent waveforms and noise realizations. To better show the statistical behavior of the methods we plot the cumulative density function (CDF) of PPR and PJR, i.e., $Probability(PPR < x)$ and $Probability(PJR < x)$, where PPR is the sum of $PRR_k, k = 1, \ldots, K$.

Targets falling on the grid

We consider the following scenario. Two targets are located at angles $\theta_1 = 0.2^{\text{o}}$and $\theta_2 = -0.2^{\text{o}}$. The corresponding reflection coefficients are $\beta_1 = \beta_2 = 1$. A jammer is located at angle 7^{o} and transmits an unknown zero-mean Gaussian random waveform with variance $\beta^2 = 400$. Additive white Gaussian noise is added at the receive nodes. The ratio of the power of transmitted waveforms at each transmit node to the variance of the additive Gaussian noise The number of transmit antennas is fixed at $M_t = 30$. For the purpose of reducing computation time, the angle space is taken to be $[-8^{\text{o}}, 8^{\text{o}}]$, and is sampled with increments of 0.2^{o} from -8^{o} to 8^{o}, i.e., $\mathbf{a} = [-8^{\text{o}}, -7.8^{\text{o}}, \ldots, 7.8^{\text{o}}, 8^{\text{o}}]$. $M = 30$ random

measurements of one pulse are used to feed the Dantzig selector. Since the MUSIC method requires the number of receive antennas to be greater than the number of targets, when only one receive antenna is used we compare the proposed CS method with only the Capon, APES and GLRT methods. The comparison methods are using $L = 512$ samples to obtain their estimates, while the proposed approach uses $M = 30$ samples. The result of one realization for the case of one receive node is shown in Fig. 2.4. One can observe the cleaner appearance of the graph corresponding to the proposed approach, where the two targets appear correctly except with a small error in the magnitude of the target RCS. The CDF of the corresponding PRR and PJR are also shown in the same figure. One can clearly see that with one receive antenna the comparison methods yield PRR close to 1, which is indicative of severe ripples.

In general, an increase in the length of waveforms L leads to improved PRR and PJR for all methods. In the following results we fix L to 512. For the comparison methods, L represents the number of samples needed to obtain target information. For CS, the number of samples used to extract target information is M.

For the scenario of Fig. 2.4, the effect of the threshold μ is evaluated in terms of the empirical CDF of the PRR and the amplitude estimate of RCS, and the results are shown in Fig. 2.5. One can can see that the increase in μ can lead to fewer ripples but at the same time it degrades the amplitude estimate of RCS. In the following, the value of μ used in each case will be shown on the corresponding figures.

For the same target and jammer configuration as above, we now examine the effect of different levels of jammer strength. We consider the scenario where $N_r = 10$ receive nodes participate in the estimation. For the case of CS, each node sends to the fusion center $M = 30$ received samples, while for the comparison methods, each node sends to the fusion center $L = 512$ received samples. In Fig. 2.6 we show the CDF of PPR and PJR corresponding to jammer variance $\beta^2 = 400, 1600$ and 3600 and SNR equal to 0 dB. One can

see that for CS, the probability of low PRR and PJR increases when the jammer becomes stronger. In particular, there is some non-zero probability that the PRR will be close to 10^{-7}. Such cases are rare and occur when one of the two targets is missed. The decrease in the threshold μ can improve the DOA estimates at the target locations and reduce the probability of missing one of the targets. The cost, however, would be an increase in ripples. The performance of the proposed approach can be improved, i.e., the rare low PRR values can be completely avoided by increasing N_r, or M. This is demonstrated in Fig. 2.7, where the strong jammer case of Fig. 2.6 is considered, i.e., $\beta^2 = 3600$, and N_r is increased to 30. We should note here that it does not help to increase M beyond M_t as the maximal rank of Φ_l' is M_t.

Next, we consider the same scenario as above but let the two targets be at variable distance d in the angle domain. Figure 2.8 demonstrates performances for the cases $d = 0.2^o, 0.3^o, 0.4^o$in the presence of a strong jammer with variance $\beta^2 = 3600$. The SNR is 0 dB, $N_r = 10$ and $M = 30$. One can see that the comparison methods produce good level PRR. Regarding the PJR, as expected, MUSIC fails, Capon and APES result in is PRR≈ 1 most of the time, while GLRT performs well all the time. The proposed CS approach performs well with a few exceptions in which a PRR or PJR less than 1 is obtained with very small probability. Again, the CS method performance can be improved by increasing N_r and/or M.

Based on the above results, the performance of the proposed approach for the jammer dominated scenario can be made at least comparable to that of the conventional methods while using about 5.8% ($= 30/512$) of the number of samples required by the conventional methods.

Next, we study a thermal noise dominated case, i.e., SNR=-40dB. Figure 2.9 shows PRR and PJR performance for different values of jammer variance, i.e., $\beta^2 = 400, 1600$ and 3600. In all cases the parameters are $N_r = 10$, $M_t = M = 30$ and the targets were separated

by $d = 0.4^{o}$. CS yields good performance even in the presence of both a strong jammer and thermal noise. The PRR performance of other methods appears to deteriorate at this noise level. The performances for targets with spacing $d = 0.2^{o}$,$0.3^{o}$and $0.4^{o}$are given in Fig. 2.10 for $N_r = 20$, $M_t = M = 30$ and $\beta^2 = 400$. As in the case of a strong jammer, the decrease in the spacing d does not affect the performance significantly. In this thermal noise dominated case, CS appears to perform very well in terms of PRR and PJR, while the comparison methods appear to be very noisy. To further examine this case, we consider two additional performance measures, i.e., mean squared error (MSE) and probability of false alarm (PFA), which are computed based on the obtained estimate $\hat{\mathbf{s}}$ as follows. A new vector, $\hat{\mathbf{s}}^t$ is formed; if $\hat{s}_i$ is greater than some threshold then $\hat{s}_i^t = 1$, otherwise, $\hat{s}_i^t = 0$. The MSE is calculated as $MSE = \|\hat{\mathbf{s}}_t - \mathbf{s}_t\|_2^2/N$, where $\mathbf{s}_t$ is an $N \times 1$ vector that contains zeros everywhere except at angles corresponding to target locations, where it is 1. The PFA measures the probability of 1 occurring in $\hat{\mathbf{s}}$ at non-target locations. Figure 2.11 shows the MSE based on $8,000$ Monte Carlo simulations. Note that the performance of MUSIC is not shown here since MUSIC always yields a peak at the jammer location. One can see that the simple thresholding described above helps the comparison methods, and if the threshold is picked appropriately all methods can produce a low angle MSE and PFA. However, the MSE corresponding to the CS method is less sensitive to the particular threshold than other methods. For the milder jammer case ($\beta = 20$), the CS approach exhibits slightly better "best MSE performance" than the comparison methods, while in the stronger jammer case ($\beta = 60$) the GLRT outperforms CS for most thresholds. For the strong jammer case, the MSE and PFA of CS are compared to those of the GLRT for different numbers of samples, L in Fig. 2.12. One can see that for the strong jammer case ($\beta = 60$) CS performs comparably to the GLRT with $L = 256$. Thus, in the strong jammer case, CS still achieves good performance with fewer samples than the GLRT, except that the savings in terms of number of samples is smaller. For CS, the trend of an increasing MSE as the threshold

increases can be explained by the fact that one of the two targets can be missed as the threshold increases. The GLRT relies on the Gaussian assumption for the noise and jammer signals, which is totally valid in our simulations. Thus, unlike the other methods, the GLRT can suppress the jammer completely. We should note that the specific values of MSE and PFA depend on the kind of thresholding performed. For example, applying thresholding on a nonlinear transformation of the estimated vector can give different values of MSE and PFA, and the best results for each method are not necessarily obtained based on the same non-linear transformation. Determining the best thresholding method is outside the scope of this disseration.

Targets falling off the grid points

In this section, we consider scenarios in which targets do not fall on the grid points. This is a case of practical interest, as the target locations are unknown, and thus the best grid in not known in advance. We first select the proper step to discretize the angle space following the procedures described in Section 2.4.2. The angle space is sampled by increments of $0.2^{o}$from $-8^{o}$to 8^{o}, i.e., $\mathbf{a} = [-8^{o}, -7.8^{o}, \ldots, 7.8^{o}, 8^{o}]$. We assume that four targets of interest are located at $\theta_k = \{-1.1^{o}, -0.3^{o}, 0.3^{o}, 1.1^{o}\}$. Their reflection coefficients are $\{\beta_k = 1, k = 1, 2, 3, 4\}$. A jammer is still located at 7^{o}. Since the targets are located between the grid points, we cannot plot PRR and PJR as in the case of targets on the grid points. Therefore, we show the mean plus and minus one standard deviation (std) for the amplitude of the DOA estimate at each grid point. The results are shown in Fig. 2.13. The power of the jammer was 400 (left column of Fig. 2.13) and 3600 (right column). Based on Fig. 2.13, it can be seen that with the proper grid points, the proposed method can capture well the targets that do not fall on grid points. The next best method is the GLRT which captures the targets but exhibits high variance as indicated by the shaded region around the mean.

2.6.2 Moving Targets

We continue to consider orthogonal QPSK waveforms and a jammer located at $7^o$with power 400. The SNR is still set to be 0 dB and each receive node collects $M = 30$ measurements. Figures 2.14 and 2.15 show the target scene of the proposed CS method and the matched filter approach [39] for targets on the grid points and off the grid points, respectively. The matched filter correlates the receive signal with the transmit signal distorted by different Doppler shifts and steering vectors.

Targets falling onto the grid points

We assume the presence of three targets located at $\{\theta_k = -1^o, 0^o, 1^o\}$ that are moving at the speed of $\{v_k = 60m/s,\ 70m/s,\ 80m/s\}$, respectively. We sample the angle-Doppler space by the increment (0.5^o,$5m$) as

$$\mathbf{a} = [(-8^o, 50m/s), (-7.5^o, 50m/s), \ldots, (8^o, 50m/s), (-8^o, 55m/s), \ldots, (8^o, 110m/s)] \quad (2.63)$$

Figure 2.14 shows the target scene for one realization corresponding to $N_1 = 1$ receive nodes (left column of the figure), and also $N_r = 10$ (right column of the figure). We can see that the performance of the matched filtering method is inferior to that of the CS approach even when using the data of 30 pulses. The proposed CS approach can yield the desired performances even with a single receive node and as low as 5 pulses. Comparing the left column and right column of Fig. 2.14, one can see the effect of the number of receive antennas N_r. The increase in N_r can reduce the number of pulses required to produce good performance.

Targets falling off the grid points

In this section, we consider the scenarios in which targets that do not fall on grid points. From simulations (the corresponding figure is not given here because of space limitations), we found that the column correlation is more sensitive to the angle step than the speed step, since $fT_s << 1$. This indicates that in the initial estimation, the grid points should be closely spaced in the angle axis and relatively sparser in the speed axis. Then the resolution of target detection can be improved by taking denser samples of the angle-Doppler space around the initial angle-Doppler estimate.

Like the scenarios with the stationary targets, the angle dimension is sampled by increments of $0.2^{o}$and the step of the speed dimension is set to $5m/s$. Three targets are moving at speeds of $\{v_k = 62.5m/s,\ 72.5m/s,\ 82.5m/s\}$ in the directions of $\{\theta_k = -1.1^{o},\ 0.1^{o},\ 1.1^{o}\}$. Fig.2.15 demonstrates that the proposed method can capture the targets that fall out of the grid points in both angle and speed dimensions and it can outperform the conventional matched filter method. Moreover, we can see that an increase in N_p or N_r will not necessarily improve performance for the targets between grid points. This is because an increase in the dimension of the basis vectors will decrease the correlation of columns in the basis matrix, which contradicts the requirement for capturing the targets out of the grid points 2.4.2. The performance in the case of more closely spaced targets, i.e., $d = 0.4^{o}$is shown in Fig. 2.16.

2.7 Conclusions

We have proposed a MIMO radar system that can be implemented by a small-sized wireless network. Network nodes serve as transmitters or receivers. Transmit nodes transmit uncorrelated waveforms. Each receive node applies compressive sampling to the received signal to obtain a small number of samples, which the node subsequently forwards to a fusion center. Assuming that the targets are sparsely located in the angle-Doppler space,

the fusion center formulates an ℓ_1-optimization problem, the solution of which yields target angle and Doppler information. For the stationary case, the performance of the proposed approach has been compared to that of conventional approaches that have been proposed in the context of MIMO radar. The comparison scenario assumes that each receive node forwards the received signal to a fusion center, where Capon, APES, GLRT or MUSIC is implemented to obtain target information. The proposed approach can extract target information based on a small number of measurements from one of more receive nodes. In particular, for a mild jammer, the proposed method has been shown to be at least as good as the Capon, APES, GLRT and MUSIC techniques while using a significantly smaller number of samples. In the case of strong thermal noise and strong jammer, the proposed method performs slightly worse than the GLRT method. In that case, its performance is still acceptable, especially if one takes into account the fact that it uses significantly fewer samples than GLRT. For the case of moving targets, the proposed approach has been compared to conventional matched filtering, and has been shown to perform better in both single and multiple receive nodes cases.

An important feature of the proposed approach is energy savings. If the fusion center implemented the proposed CS approach, it would require nodes to forward M samples each, as opposed to L samples that would be needed if the fusion center were to implement the conventional methods. In order to meet a certain performance level, M is typically significantly smaller than L, i.e., fewer samples would be needed for the CS implementation as compared to the implementation of conventional methods. This translates into energy savings during the transmission of the samples from the receive nodes to the fusion center. The obtained savings would be significant in prolonging the life of the wireless network.

2.8 Appendices: The effects of N_r, N_p, M_t on the correlation of columns in the sensing matrix

2.8.1 The effect of the number of pulses on the column correlation in the sensing matrix

The sensing matrix for the l-th receive antenna $\mathbf{\Theta}_l$ is given by

$$\mathbf{\Theta}_l = \begin{bmatrix} \mathbf{\Phi}_l \mathbf{\Psi}_{l1} \\ \vdots \\ \mathbf{\Phi}_l \mathbf{\Psi}_{lN_p} \end{bmatrix} \tag{2.64}$$

where $\mathbf{\Psi}_{lm}, m = 1, \ldots, N_p$, is defined in (2.29).

On letting $\mathbf{g}_k$ denote the i-th column of $\mathbf{\Theta}_l$, the correlation of columns $\mathbf{g}_k$ and $\mathbf{g}_{k'}$ equals

$$p_{kk'} = |<\mathbf{g}_k, \mathbf{g}_{k'}>| = \begin{cases} N_p |\mathbf{v}^H(a_k)\mathbf{B}_l^{kk}\mathbf{v}(a_k)| & k = k' \\ |\frac{sin(\pi(b_k - b_{k'})N_pT)}{\sin(\pi(b_k - b_{k'})T)}| |\mathbf{v}^H(a_k)\mathbf{B}_l^{kk'}\mathbf{v}(a_{k'})| & k \neq k' \end{cases} . \tag{2.65}$$

where $\mathbf{B}_l^{kk'} = \mathbf{X}^H\mathbf{D}^H(b_k)\mathbf{\Phi}_l^H\mathbf{\Phi}_l\mathbf{D}(b_{k'})\mathbf{X}$.

For a given pair $(k, k'), k \neq k'$, the ratio of $|<\mathbf{g}_k, \mathbf{g}_k>|$ to $|<\mathbf{g}_k, \mathbf{g}_{k'}>|$, i.e., $h_{kk'}$, reveals the effect of N_p on the correlation of the two columns. It holds that

$$h_{kk'} \propto \frac{N_p}{|\sin(\pi(b_k - b_{k'})N_pT)|} . \tag{2.66}$$

Let assume that T has been fixed. As long as $(b_k - b_{k'})N_pT \leq 1$, $h_{kk'}$ increases with N_p, and attains the maximum value when $(b_k - b_{k'})N_pT = 1$, because the cross correlation of $\mathbf{g}_k$ and $\mathbf{g}_{k'}$ becomes zero. Therefore, the increase in N_p can improve the performance of CS estimation of (2.32) as long as $(b_k - b_{k'})N_pT \leq 1$. This indicates that if $(b_k - b_{k'})N_pT \leq 1$ for each pair of $(k, k'), k \neq k'$, the increase in N_p can always improve the performances of CS

estimation. For a conventional radar, the number of pulses can also improve the resolution of Doppler estimates since the Doppler shift creates greater change between pulses.

2.8.2 The effect of the number of receive antennas on the column correlation in the sensing matrix

Next, we investigate the effect of the number of receive antennas N_r on the correlation of columns in the sensing matrix. For simplicity, we assume that only the received data collected during the n-th pulse is considered and the random measurement matrix $\mathbf{\Phi}$ is constant over receive antennas. Then the sensing matrix $\mathbf{\Theta}$ can be represented as

$$\Theta = \begin{bmatrix} \mathbf{\Phi\Psi}_{1n} \\ \vdots \\ \mathbf{\Phi\Psi}_{N_r n} \end{bmatrix}. \tag{2.67}$$

Thus, the correlation of columns $\mathbf{g}_i$ and $\mathbf{g}_j$ equals

$$\begin{aligned} p_{ij} &= |<\mathbf{g}_i, \mathbf{g}_j>| = \left|\sum_{l=1}^{N_r} e^{j\frac{2\pi}{\lambda}(\eta_l^r(a_j)-\eta_l^r(a_i))}\right| \left|e^{j2\pi(n-1)T(b_j-b_i)}\mathbf{v}^H(a_i)\mathbf{X}^H\mathbf{D}^H(b_i)\mathbf{\Phi}^H\mathbf{\Phi}\mathbf{D}(b_j)\mathbf{X}\mathbf{v}(a_j)\right| \\ &= \begin{cases} N_r|\mathbf{v}^H(a_i)\mathbf{B}^{i,j}\mathbf{v}(a_j)| & i = j \\ |\sum_{l=1}^{N_r} e^{j\frac{2\pi}{\lambda}(\eta_l^r(a_j)-\eta_l^r(a_i))}||\mathbf{v}^H(a_i)\mathbf{B}^{i,j}\mathbf{v}(a_j)| & i \neq j \end{cases} \end{aligned} \tag{2.68}$$

where $\mathbf{B}^{i,j} = \mathbf{X}^H\mathbf{D}^H(b_i)\mathbf{\Phi}^H\mathbf{\Phi}\mathbf{D}(b_j)\mathbf{X}$.

Thus the ratio of $|<\mathbf{g}_i, \mathbf{g}_j>|$ to $|<\mathbf{g}_i, \mathbf{g}_i>|$ is

$$h_{ij} \propto \frac{1}{N_r}\left|\sum_{l=1}^{N_r} e^{j\frac{2\pi}{\lambda}(\eta_l^r(a_j)-\eta_l^r(a_i))}\right|. \tag{2.69}$$

Since the receive nodes are randomly and independently distributed, $\frac{1}{N_r}|\sum_{l=1}^{N_r} e^{j\frac{2\pi}{\lambda}(\eta_l^r(a_j)-\eta_l^r(a_i))}|$ approaches 0 as N_r becomes large. Therefore, the correlation of two columns in the sensing

matrix can be reduced when the number of receive antennas is increased.

2.8.3 The effect of the number of transmit antennas on the column correlation in the sensing matrix

Finally, let us see the effect of the number of transmit nodes on the correlation of columns. For simplicity, we assume $N_r = N_p = 1$. Then $\mathbf{v}^H(a_i)\mathbf{B}^{i,j}\mathbf{v}(a_j)$ can be rewritten as

$$\begin{aligned}\mathbf{v}^H(a_i)\mathbf{B}^{i,j}\mathbf{v}(a_j) &= \sum_{k,p} v_k(a_j)v_k^*(a_i)B_{p,p}^{i,j}/L + \underbrace{\sum_{k}\sum_{p\neq q} v_k(a_j)v_k^*(a_i)x_k(q)x_k^*(p)B_{p,q}^{i,j}}_{\sigma_1^{ij}} \\ &\quad + \underbrace{\sum_{k\neq k'}\sum_{p,q} v_k(a_j)v_{k'}^*(a_i)x_k(q)x_{k'}^*(p)B_{p,q}^{i,j}}_{\sigma_2^{ij}} \qquad (2.70)\end{aligned}$$

$$\approx \begin{cases} \frac{MM_t}{L} + \sigma_1^{ii} + \sigma_2^{ii} & i = j \\ \frac{M\sum_k v_k(a_j)v_k^*(a_i)}{L} + \sigma_1^{ij} + \sigma_2^{ij} & i \neq j \end{cases} \qquad (2.71)$$

where v_k and $B_{p,q}^{i,j}$ denote the k-th entry of $\mathbf{v}$ and the (p,q)-th entry of $\mathbf{D}^H(b_i)\mathbf{\Phi}^H\mathbf{\Phi}\mathbf{D}(b_j)$, respectively.

Thus, the ratio of $|<\mathbf{g}_i,\mathbf{g}_j>|$ to $|<\mathbf{g}_i,\mathbf{g}_i>|$ is

$$h_{ij} = \left|\frac{\frac{M\sum_k v_k(a_j)v_k^*(a_i)}{L} + \sigma_1^{ij} + \sigma_2^{ij}}{\frac{MM_t}{L} + \sigma_1^{ii} + \sigma_2^{ii}}\right| = \left|\frac{\frac{M\sum_k v_k(a_j)v_k^*(a_i)}{M_tL} + \frac{\sigma_1^{ij}}{M_t} + \frac{\sigma_2^{ij}}{M_t}}{\frac{M}{L} + \frac{\sigma_1^{ii}}{M_t} + \frac{\sigma_2^{ii}}{M_t}}\right|. \qquad (2.72)$$

It can easily be seen that the numerator approaches 0 as M_t approaches infinity. Therefore, the correlation of two columns of the sensing matrix can be reduced by employing a large number of transmit nodes M_t.

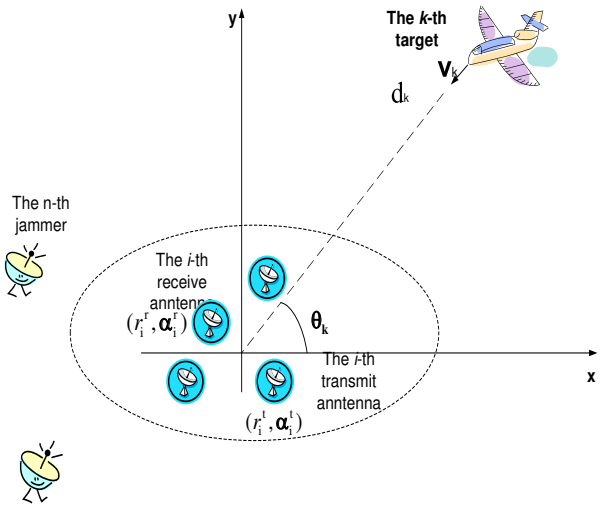

Figure 2.1: Illustration of a MIMO radar system.

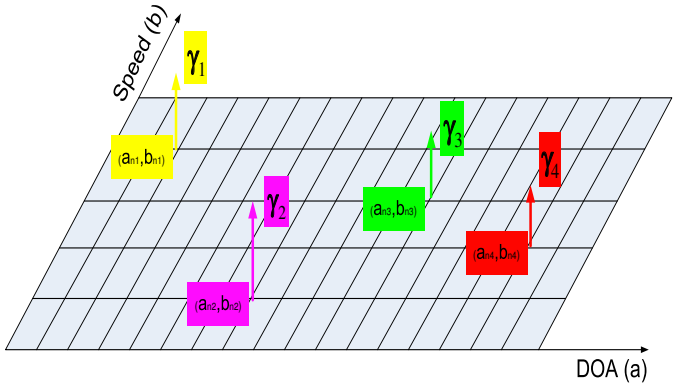

Figure 2.2: The discretized angle-speed plain.

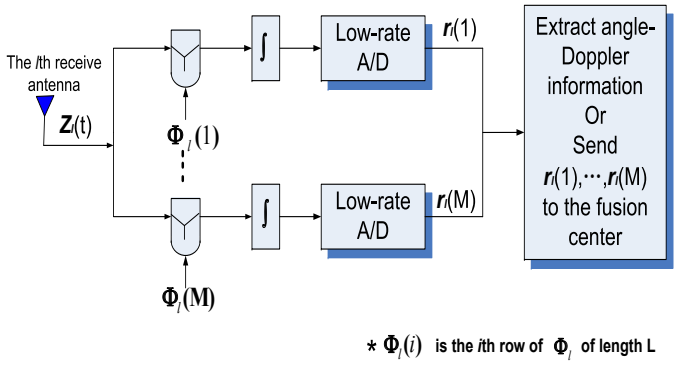

Figure 2.3: Schematic diagram of the receiver. Φ_l denotes the measurement matrix for the lth receive node.

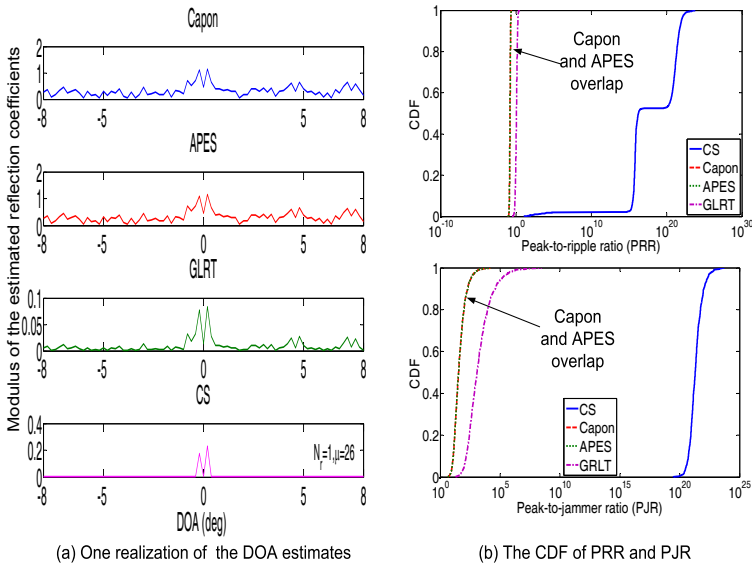

Figure 2.4: One realization of the DOA estimates (left column) and CDF of PRR and PJR (right column), for $N_r = 1$, $M_t = M = 30$, $\beta^2 = 400$, SNR= 0 dB and $\mu = 26$.

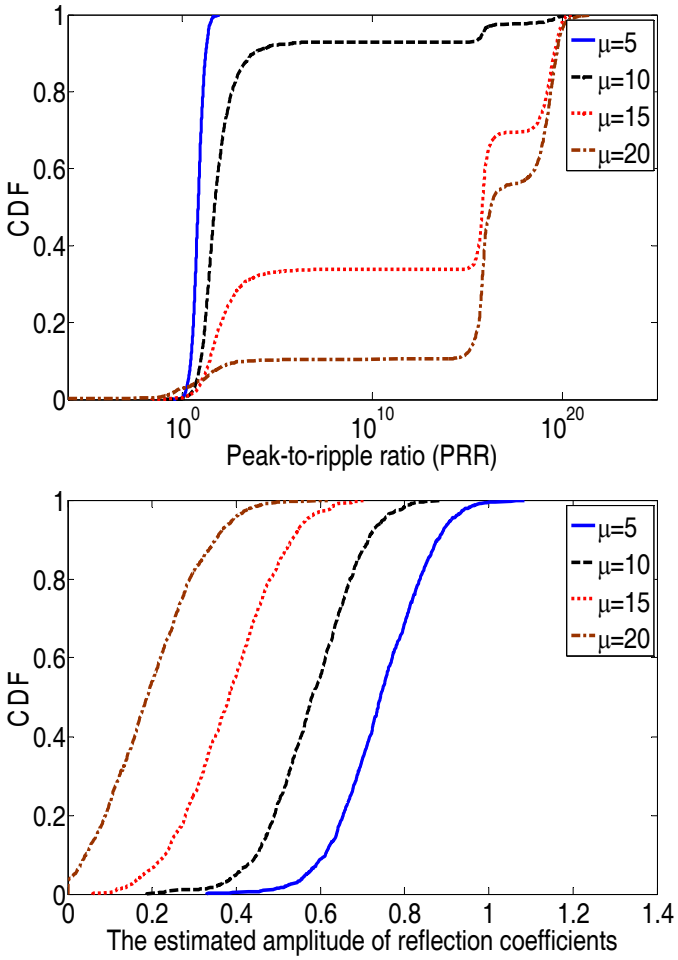

Figure 2.5: CDF of PRR (top) and amplitude estimate of RCS (bottom).

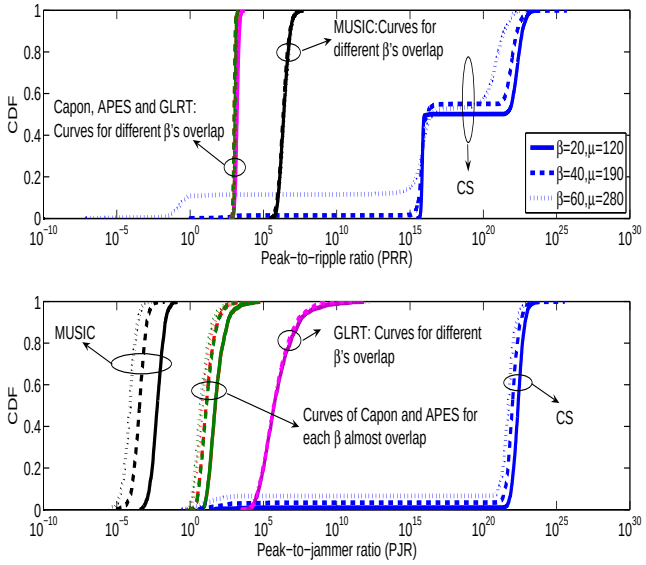

Figure 2.6: CDF of PRR and SJR for $\beta = 20, 40, 60$ with $N_r = 10, M_t = M = 30$ and SNR= 0 dB. The corresponding thresholds are $\mu = 120, 190$ and 280.

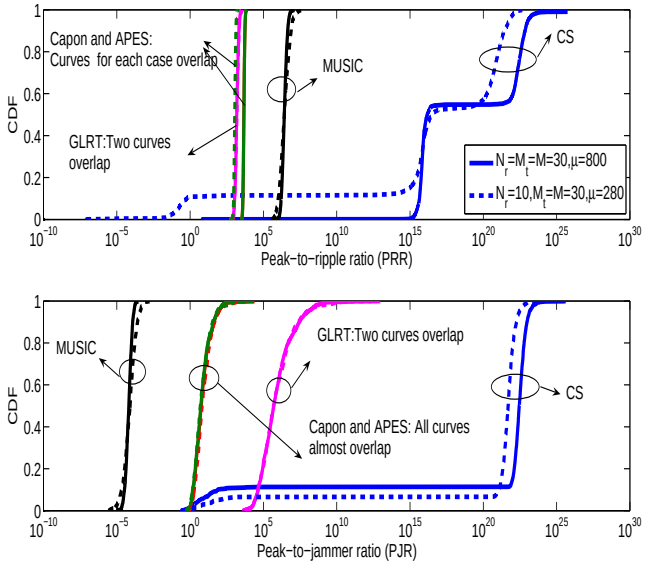

Figure 2.7: CDF of PRR and SJR for $\beta^2 = 3600$ and SNR=0 dB. Two cases are shown, ($N_r = 10, M_t = 30, M = 30$) and ($N_r = 30, M_t = 30, M = 30$). The corresponding thresholds are $\mu = 280$ and 800.

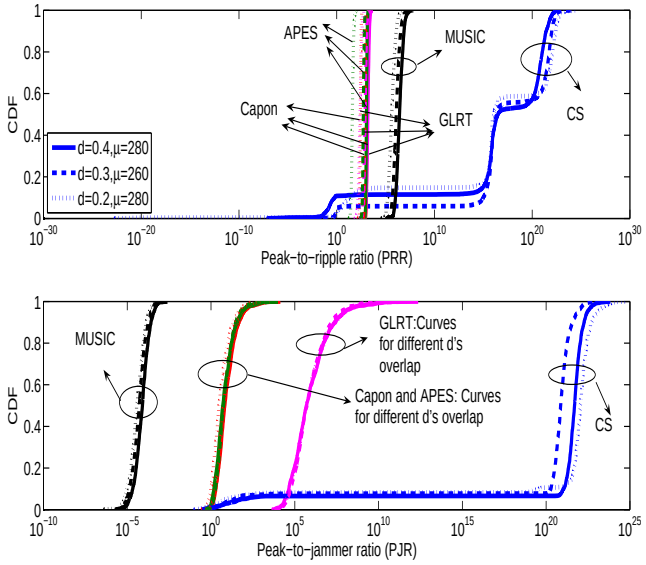

Figure 2.8: DOA estimates of two targets with spacing $d = 0.4^{o}$,$0.3^{o}$and 0.2^{o}, for $N_r = 10, M_t = M = 30$, SNR=0 dB and $\beta^2 = 3600$. The corresponding thresholds are $\mu = 280, 260$ and 280.

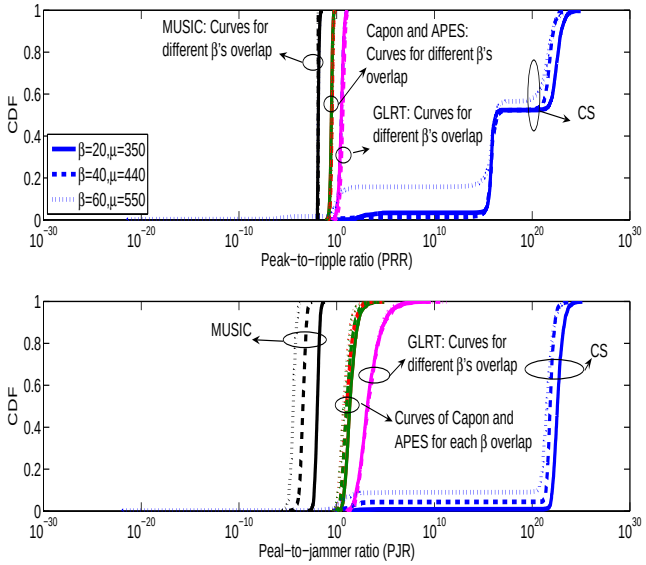

Figure 2.9: CDF of PRR and PJR for $\beta = 20, 40$ and 60 with $N_r = 20, M_t = M = 30$ and SNR=-40 dB. The corresponding thresholds are $\mu = 350, 440$ and 550.

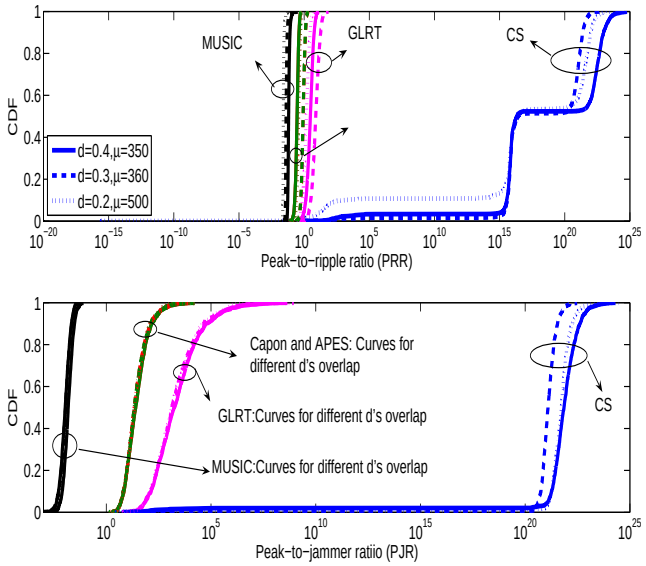

Figure 2.10: CDF of PRR and PJR for two targets with spacing $d = 0.4^{o}$,$0.3^{o}$and 0.2^{o}, for $N_r = 20$, $M_t = M = 30$, SNR=−40 dB and $\beta = 20$.

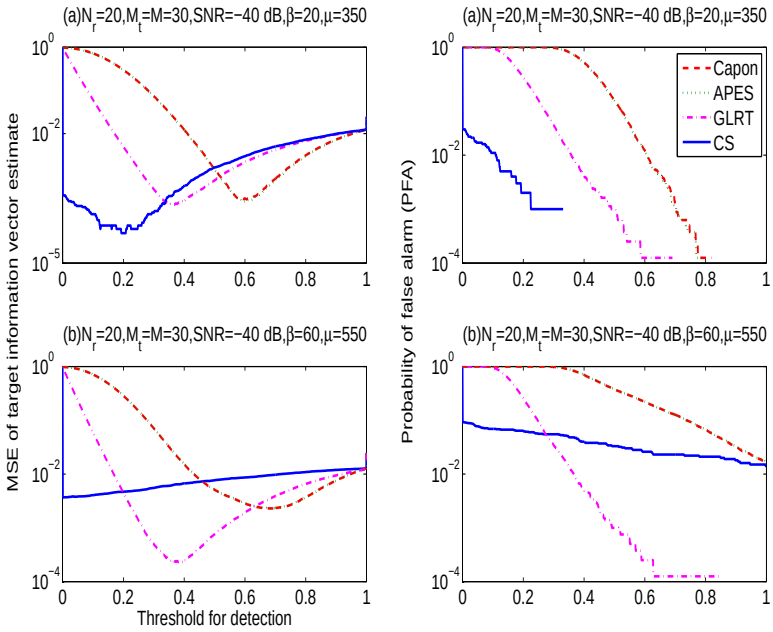

Figure 2.11: MSE of target information vector and probability of false alarm (PFA) for two targets with spacing $d = 0.4^{o}$for $N_r = 20$, $M_t = M = 30$ and SNR= −40 dB.

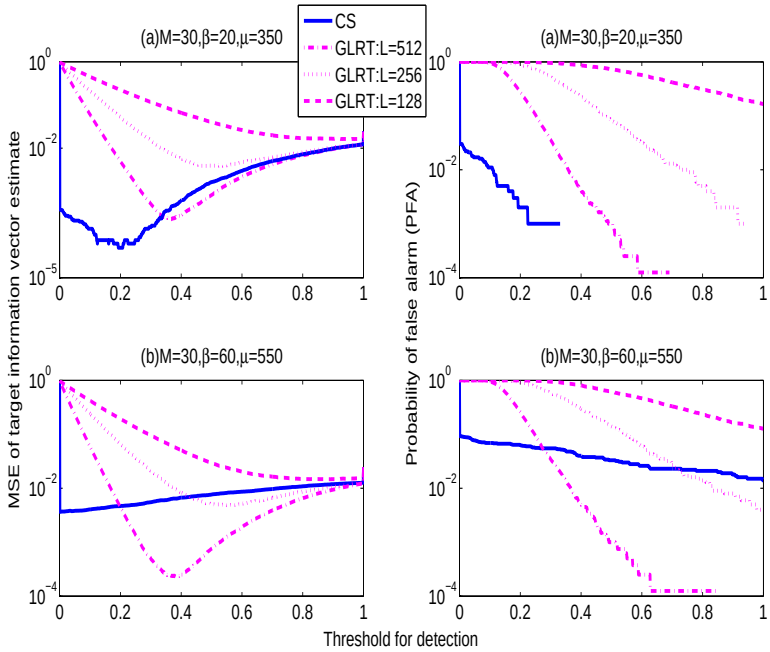

Figure 2.12: MSE of target information vector and probability of false alarm (PFA) for two targets with spacing $d = 0.4^{o}$for $N_r = 20, M_t = M = 30$ and SNR= -40 dB. The length of transmit sequence within a pulse and receive samples per pulse for CS is 512 and 30, respectively.

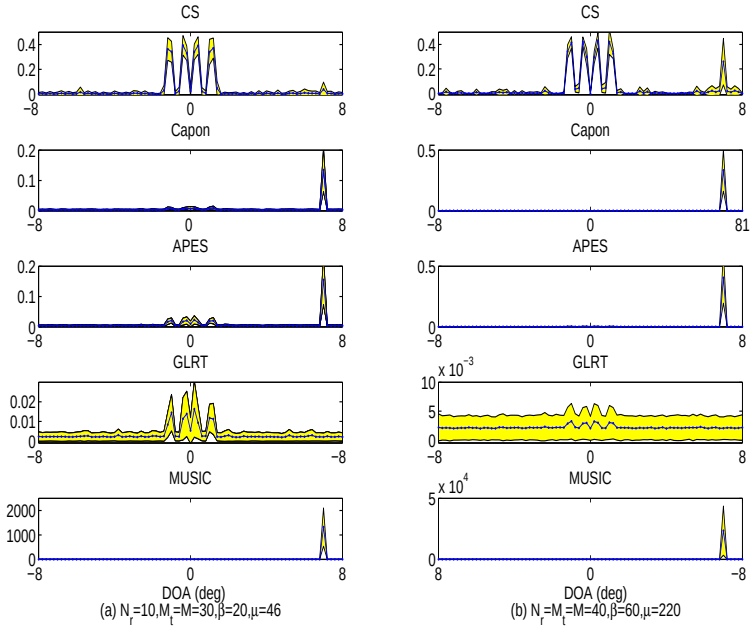

Figure 2.13: Modulus of DOA estimates for four targets that do not fall on grid points. The dotted line is the mean of DOA estimates. The yellow region is the area bounded by the curves mean ± std.

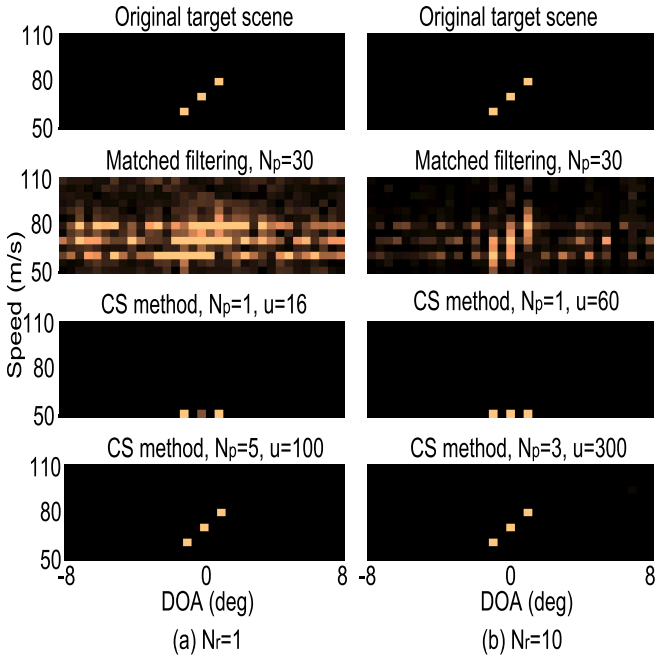

Figure 2.14: Angle-Doppler estimates for three targets on the grid points. The targets are located at {-1º, 0º, 1º}. $M_t = M = 30$, SNR= 0 dB and $\beta^2 = 400$.

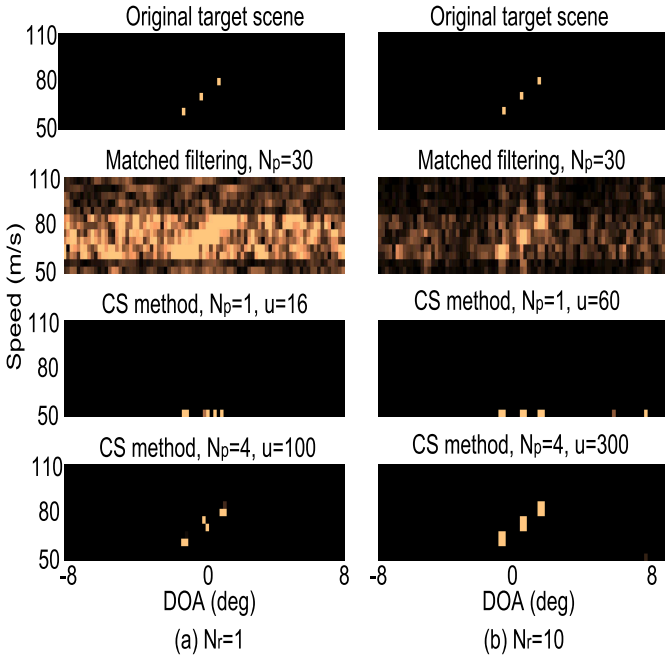

Figure 2.15: Angle-Doppler estimates for three targets that do not fall on the grid points. The targets are located at {-1.1°, 0.1°, 1.1°}. $M_t = M = 30$, $\beta^2 = 400$ and SNR= 0 dB.

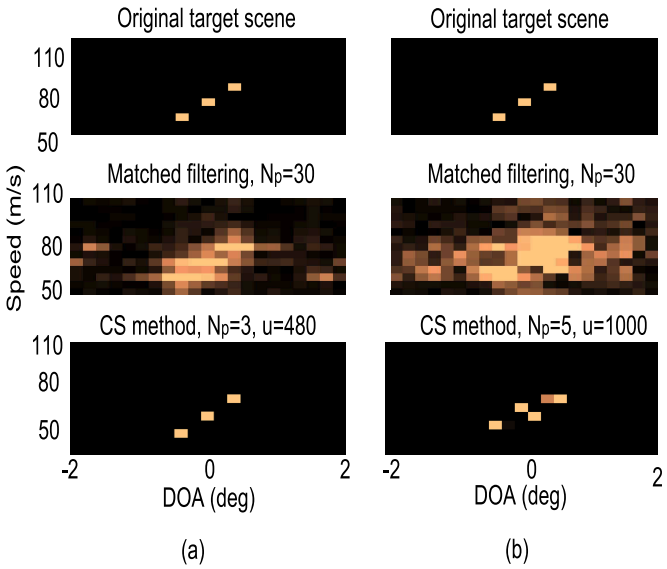

Figure 2.16: Angle-Doppler estimates for three targets on and off grid points. $N_r = 10$, $M_t = M = 30$, SNR= 0 dB, $\beta^2 = 400$ and $d = 0.4°$.

3. CSSF MIMO Radar: Low-Complexity Compressive Sensing Based MIMO Radar That Uses Step Frequency

In Chapter 2, we focus on DOA and Doppler estimation only for the case in which the targets are located in a small range bin and the sampling is synchronized with the first target return. Such assumptions do not allow for range estimation. In this chapter, we consider a more general case without those assumptions and propose a new approach, namely CSSF MIMO radar, which applies the technique of step frequency (SF) to CS-based MIMO radar. The proposed approach enables high resolution range, angle and Doppler estimation, while transmitting narrowband pulses. The problem of joint angle-Doppler-range estimation is first formulated to fit the CS framework, i.e., as an ℓ_1 optimization problem. Direct solution of this problem entails high complexity as it employs a basis matrix whose construction requires discretization of the angle-Doppler-range space. Since high resolution requires fine space discretization, the complexity of joint range, angle and Doppler estimation can be prohibitively high. For the case of slowly moving targets, a technique is proposed that achieves significant complexity reduction by successively estimating angle-range and Doppler in a decoupled fashion and by employing initial estimates obtained via matched filtering to further reduce the space that needs to be digitized. Numerical results show that the combination of CS and SF results in a MIMO radar system that has superior resolution and requires far less data as compared to a system that uses a matched filter with SF.

3.1 Introduction

The application of CS to step-frequency radar (SFR) [55]-[57] was investigated in [58]-[60]. SFR transmits pulse trains of varying frequency. Thus, although the individual pulses

are relatively long in duration and are narrowband, the transmit signal is effectively wideband. Since range resolution increases with the signal bandwidth, SFR achieves high range resolution. At the same time, SFR does not suffer from low SNR at the receiver typically associated with wideband systems that rely on short duration pulses. In [60], it was found that the CS approach can significantly reduce the number of pulses required by SFR to achieve a certain resolution. A CS-based data acquisition and imaging method was proposed in [58] for stepped-frequency continuous-wave ground penetrating radars, and in [59] CS was applied to stepped-frequency through-the-wall radar imaging. In both cases it was shown that the CS approach can provide a high-quality radar image using many fewer data samples than conventional methods.

In this chapter, we consider a more general scenario than that of Chapter 2 in which range estimation is excluded. The methods of Chapter 2 assume that the targets are located in a small range bin and the sampling is synchronized with the first target return. Such assumptions do not allow for range estimation. In this chapter, the targets can be located across several range bins. We propose CSSF MIMO radar, an approach that applies step frequency to CS-based MIMO radar. Two types of CSSF MIMO radar systems are considered, i.e., linear step-frequency radar (LSFR), and random step-frequency radar (RSFR), and their effects on the CS approach are studied. The proposed approach enables high resolution range as well as angle and Doppler estimation. The problem of joint angle-Doppler-range estimation is first formulated to fit the CS framework, i.e., as an ℓ_1 optimization problem. Solving this problem entails high complexity as it employs a basis matrix whose construction requires discretization of the angle-Doppler-range space. The complexity increases with the size of the basis matrix, or equivalently, as the discretization step decreases; the latter step needs to be as small as possible as it sets the lower limit of resolution. For slowly moving targets, a technique is proposed that successively estimates angle-range and Doppler in a decoupled fashion, and employs initial estimates obtained via

a MF to further reduce the space that needs to be digitized. In [61] and [62], information on the support of a sparse signal was used in the minimization process resulting in complexity reduction. In our case, we do not explore the role of initial estimates on the minimization process, as they are not expected to be very reliable. Instead, we use them only as a guide for the construction of the basis matrix. The preliminary results of CSSF MIMO radar and the decoupled scheme were published in [63] and [64] which consider the same signal models as in [40] and [53]. This chapter extends the work of [63] and [64] to the general scenario aforementioned and offers an mathematic insight into CSSF MIMO.

The rest of the chapter is organized as follows. In Section 3.2, we provide the signal model of a CS-based MIMO radar system. In Section 3.3, we introduce the proposed CSSF MIMO radar system. A decoupled scheme for CSSF MIMO is described in Section 3.4. Simulation results are given in Section 3.5 for the case of slowly moving targets. Finally, we make some concluding remarks in Section 3.6.

3.2 Signal Model for CS-based MIMO Radar

Let us consider the same setting as in Chapter 2. The target return from the k-th target arriving at the l-th antenna during the m-th pulse is

$$y_{lm}^{k}(t) = \sum_{i=1}^{M_t} \beta_k x_i(t - (d_{ik}^{t}(t) + d_{lk}^{r}(t))/c) \exp(j2\pi f(t - (d_{ik}^{t}(t) + d_{lk}^{r}(t))/c)). \tag{3.1}$$

The demodulated baseband signal corresponding to a single target can be approximated by

$$y_{lm}^{k}(t) \approx \sum_{i=1}^{M_t} \beta_k x_i(t - 2d_k(0)/c) \exp(-j2\pi f(d_{ik}^{t}(t) + d_{lk}^{r}(t))/c). \tag{3.2}$$

In the above equation, the time delays in the received waveforms due to the k-th target are all the same and equal to $2d_k(0)/c$. This approximation is enabled by the assumption of narrowband transmit waveforms, slowly moving targets and colocated nodes. The fact that

the targets can be in different range bins implies that the delays corresponding to different targets will be different. Therefore, sampling the received signal and ensuring that all target returns fall in the sampling window would require time delay estimation. However, in a CS scenario, there are not enough data to obtain such estimates using traditional methods, e.g., the matched filtering method. In the following, we will extract the range and angle information simultaneously using the CS approach without assuming availability of time delay estimates.

The compressed samples collected by the *l*-th antenna during the *m*-th pulse can be expressed as

$$\mathbf{r}_{lm} = \sum_{k=1}^{K} \beta_k e^{j2\pi p_{lmk}} \mathbf{\Phi}_l \mathbf{D}(f_k) \mathbf{C}_{\tau_k} \mathbf{X} \mathbf{v}(\theta_k) + \mathbf{\Phi}_l \mathbf{n}_{lm} \tag{3.3}$$

where

(i) $p_{lmk} = \frac{-2d_k(0)f}{c} + \frac{\eta_l^r(\theta_k)f}{c} + f_k(m-1)T$, where $f_k = \frac{2v_k f}{c}$ is the Doppler shift induced by the *k*-th target; $\text{diag}\{\mathbf{X}^H\mathbf{X}\} = [1, \ldots, 1]^T$; $lT_s, l = 0, \ldots, L-1$, represent the time within the pulse (fast time) and thus the pulse duration is $T_p = LT_s$;

(ii) $\mathbf{\Phi}_l$ is the $M \times (L + \tilde{L})$ measurement matrix for the *l*-th receive node where $\tilde{L}T_s$ is the maximum time delay and known in advance. The measurement matrix has elements that are independent and identically distributed (i.i.d) Gaussian random variables;

(iii) $\mathbf{v}(\theta_k) = [e^{j\frac{2\pi f}{c}\eta_1^t(\theta_k)}, ..., e^{j\frac{2\pi f}{c}\eta_{M_t}^t(\theta_k)}]^T$ and $\mathbf{D}(f_k) = \text{diag}\{[e^{j2\pi f_k 0T_s}, \ldots, e^{j2\pi f_k(L-1)T_s}]\}$;

(iv) $\tau_k = \lfloor \frac{2d_k(0)}{cT_s} \rfloor$ and $\mathbf{C}_{\tau_k} = [\mathbf{0}_{L\times\tau_k}, \mathbf{I}_L, \mathbf{0}_{L\times(\tilde{L}-\tau_k)}]^T$. Here, we assume that the target returns completely fall within the sampling window of length $(L + \tilde{L})T_s$, and that T_s is small enough so that the rounding error in the delay is small, i.e., $x_i(t - \tau_k) \approx x_i(t - \lfloor \frac{2d_k(0)}{cT_s} \rfloor)$.

(v) $\mathbf{n}_{lm}$ is the interference at the *l*-th receiver during the *m*-th pulse, which includes a jammer's signal and thermal noise.

Let us discretize the angle, speed and range space on a fine grid, i.e., respectively, $[\tilde{a}_1, \ldots, \tilde{a}_{N_a}]$, $[\tilde{b}_1, \ldots, \tilde{b}_{N_b}]$ and $[\tilde{c}_1, \ldots, \tilde{c}_{N_c}]$. Let the grid points be arranged first angle-wise, then range-wise, and finally speed-wise to yield the grid points (a_n, b_n, c_n), $n = 1, ..., N_a N_b N_c$. Through this ordering, the grid point $(\tilde{a}_{n_a}, \tilde{b}_{n_b}, \tilde{c}_{n_c})$ is mapped to point (a_n, b_n, c_n) with $n = (n_b - 1)n_a n_c + (n_c - 1)n_a + n_a$. We assume that the discretization step is small enough so that each target falls on some angle-speed-range grid point. Then (3.3) can be rewritten as

$$\mathbf{r}_{lm} = \mathbf{\Phi}_l \left(\sum_{n=1}^{N} s_n e^{j2\pi q_{lmn}} \mathbf{D}\left(\frac{2b_n f}{c}\right) \mathbf{C}_{\lfloor \frac{2c_n}{cT_s} \rfloor} \mathbf{X}\mathbf{v}(a_n) + \mathbf{n}_{lm} \right) \tag{3.4}$$

where $s_n = \begin{cases} \text{reflection coefficient of the target,} & \text{if there is a target at } (a_n, b_n, c_n) \\ 0, & \text{if there is no target at } (a_n, b_n, c_n) \end{cases}$, $N = N_a N_b N_c$, and

$$q_{lmn} = \frac{-2c_n f}{c} + \frac{\eta_l^r(a_n) f}{c} + \frac{2b_n f(m-1)T}{c}. \tag{3.5}$$

In matrix form we have

$$\mathbf{r}_{lm} = \mathbf{\Theta}_{lm}\mathbf{s} + \mathbf{\Phi}_l \mathbf{n}_{lm} \tag{3.6}$$

where $\mathbf{s} = [s_1, ..., s_N]^T$ and

$$\mathbf{\Theta}_{lm} = \mathbf{\Phi}_l \underbrace{\left[e^{j2\pi q_{lm1}} \mathbf{D}(2b_1 f/c) \mathbf{C}_{\lfloor \frac{2c_1}{cT_s} \rfloor} \mathbf{X}\mathbf{v}(a_1), \ldots, e^{j2\pi q_{lmN}} \mathbf{D}(2b_N f/c) \mathbf{C}_{\lfloor \frac{2c_N}{cT_s} \rfloor} \mathbf{X}\mathbf{v}(a_N) \right]}_{\mathbf{\Psi}_{lm}}. \tag{3.7}$$

According to the CS formulation, $\mathbf{\Theta}_{lm}$ is the sensing matrix and $\mathbf{\Psi}_{lm}$ is the basis matrix.

Combining the output of N_p pulses at N_r receive antennas the fusion center can formulate the equation

$$\mathbf{r} \triangleq [\mathbf{r}_{11}^T, \ldots, \mathbf{r}_{1N_p}^T, \ldots, \mathbf{r}_{N_r N_p}^T]^T = \mathbf{\Theta}\mathbf{s} + \mathbf{n} \tag{3.8}$$

where

$$\mathbf{\Theta} = [(\mathbf{\Theta}_{11})^T, \ldots, (\mathbf{\Theta}_{1N_p})^T, \ldots, (\mathbf{\Theta}_{N_rN_p})^T]^T \tag{3.9}$$

and

$$\mathbf{n} = [(\mathbf{\Phi}_1\mathbf{n}_{11})^T, \ldots, (\mathbf{\Phi}_1\mathbf{n}_{1N_p})^T, \ldots, (\mathbf{\Phi}_{N_r}\mathbf{n}_{N_rN_p})^T]^T. \tag{3.10}$$

Subsequently, using the predefined measurement matrices, $\mathbf{\Phi}_l,\ l = 1, ..., N_r$, based on the discretization of the angle-speed-range space, and also based on knowledge of the waveform matrix **X**, the fusion center recovers **s** by applying the Dantzig selector.

3.3 Introducing Step Frequency to CS-MIMO radar

Let us consider a MIMO radar system in which the carrier frequency of the *m*-th pulse equals

$$f_m = f + \Delta f_m \tag{3.11}$$

where f is the center carrier frequency and Δf_m denotes the frequency step, $m = 1, \ldots, N_p$.

The baseband samples collected by the *l*-th antenna during the *m*-th pulse can be expressed as

$$\tilde{\mathbf{r}}_{lm} = \mathbf{\Phi}_l \sum_{k=1}^{K} \beta_k e^{j2\pi\tilde{p}_{lmk}} \mathbf{D}(f_{mk})\mathbf{C}_{\tau_k}\mathbf{X}\mathbf{v}_m(\theta_k) + \mathbf{\Phi}_l\mathbf{n}_{lm} \tag{3.12}$$

where

$$f_{mk} = \frac{2v_k f_m}{c}, \mathbf{v}_m(\theta_k) = [e^{j\frac{2\pi f_m}{c}\eta_1^t(\theta_k)}, ..., e^{j\frac{2\pi f_m}{c}\eta_{M_t}^t(\theta_k)}]^T$$
$$\text{and } \tilde{p}_{lmk} = \frac{-2d_k(0)f_m}{c} + \frac{\eta_l^r(\theta_k)f_m}{c} + f_{mk}(m-1)T. \tag{3.13}$$

Then, based on discrete grid points of the angle-speed-range space, (3.12) can be rewritten as

$$\begin{aligned} \tilde{\mathbf{r}}_{lm} &= \mathbf{\Phi}_l \tilde{\mathbf{\Psi}}_{lm}\mathbf{s} + \mathbf{\Phi}_l \mathbf{n}_{lm} \\ &= \tilde{\mathbf{\Theta}}_{lm}\mathbf{s} + \mathbf{\Phi}_l \mathbf{n}_{lm} \end{aligned} \tag{3.14}$$

where

$$\tilde{\mathbf{\Psi}}_{lm} = [e^{j2\pi\tilde{q}_{lm1}}\mathbf{D}(2b_1 f_m/c)\mathbf{C}_{\lfloor\frac{2c_1}{cT_s}\rfloor}\mathbf{X}\mathbf{v}_m(a_1), \ldots, e^{j2\pi\tilde{q}_{lmN}}\mathbf{D}(2b_N f_m/c)\mathbf{C}_{\lfloor\frac{2c_N}{cT_s}\rfloor}\mathbf{X}\mathbf{v}_m(a_N)],$$
$$\tilde{q}_{lmn} = \frac{-2c_n f_m}{c} + \frac{\eta_l^r(a_n)f_m}{c} + \frac{2b_n f_m(m-1)T}{c},$$
$$\text{and } \tilde{\mathbf{\Theta}}_{lm} = \mathbf{\Phi}_l \tilde{\mathbf{\Psi}}_{lm}. \tag{3.15}$$

At the fusion center, the compressively sampled signals due to N_p pulses obtained at N_r receive nodes are stacked as

$$\tilde{\mathbf{r}} \triangleq \tilde{\mathbf{\Theta}}\mathbf{s} + \mathbf{n} \tag{3.16}$$

where

$$\tilde{\mathbf{\Theta}} = [(\tilde{\mathbf{\Theta}}_{11})^T, \ldots, (\tilde{\mathbf{\Theta}}_{1N_p})^T, \ldots, (\tilde{\mathbf{\Theta}}_{N_r N_p})^T]^T. \tag{3.17}$$

Recovery of $\mathbf{s}$ is performed as in (2.32) where $\mathbf{\Theta}$ is replaced with $\tilde{\mathbf{\Theta}}$.

3.3.1 Range resolution

In this subsection we study the relationship between range resolution and the ambiguity function. For the conventional radar systems that uses a matched filter to extract target information, the ambiguity function (AF) characterizes the response to a point target and determines resolution. Let us assume that there is a target at (θ, d, v). The matched filter looking for a target at (θ', d', v') yields

$$\chi(\Delta d, \Delta v, \theta, \theta') = \sum_{l=1}^{N_r} \sum_{i,i'=1}^{M_t} \sum_{m=1}^{N_p} \chi_{i,i',m}(\Delta d, \Delta v) e^{j2\pi f_m \frac{\eta_i^t(\theta)+\eta_l^r(\theta)-\eta_{i'}^t(\theta')-\eta_l^r(\theta')-2\Delta d}{c}} \tag{3.18}$$

where $\Delta d = d - d'$, $\Delta v = v - v'$ and

$$\chi_{i,i',m}(\Delta d, \Delta v) \triangleq \int_t x_i(t) x_{i'}^*(t + 2\Delta d/c) e^{j2\pi f_m \frac{2\Delta v}{c} t} dt. \tag{3.19}$$

Equation (3.18) is the AF for SF MIMO radar, where SF MIMO radar refers to MIMO radar that uses the SF technique. Unlike the AF for MIMO radar [65], the carrier frequency is varying between pulses in (3.18).

To investigate the range resolution let us set $\Delta v = 0$ and $\theta = \theta'$. Then, the AF becomes

$$\begin{aligned}
\chi(\Delta d, 0, \theta, \theta) &= N_r \sum_{i,i'=1}^{M_t} \sum_{m=1}^{N_p} \chi_{i,i',m}(\Delta d, 0) e^{j2\pi f_m \frac{\eta_i^t(\theta)-\eta_{i'}^t(\theta)-2\Delta d}{c}} \\
&= N_r \underbrace{\sum_{m=1}^{N_p} e^{j2\pi f_m(-2\Delta d/c)}}_{\chi_1(\Delta d)} \underbrace{\sum_{i=i'} \int_t x_i(t) x_{i'}^*(t + 2\Delta d/c)\, dt}_{\chi_2(\Delta d)} \\
&\quad + \underbrace{N_r \sum_{m=1}^{N_p} \sum_{i \neq i'} e^{j2\pi f_m \frac{\eta_i^t(\theta)-\eta_{i'}^t(\theta)-2\Delta d}{c}} \int_t x_i(t) x_{i'}^*(t + 2\Delta d/c)\, dt}_{\Delta\chi(\Delta d)}
\end{aligned} \tag{3.20}$$

Due to (A2), the term $\Delta\chi(\Delta d)$ is negligible as compared to the product $\chi_1(\Delta d)\chi_2(\Delta d)$ in (3.20). One can see that $\chi_1(\Delta d)$ and $\chi_2(\Delta d)$ are respectively the AF of SF single-input single-output (SISO) radar and MIMO radar, both for $\Delta v = 0$ and $\theta = \theta'$. It can seen from (3.20) that a colocated MIMO radar has no gain on range resolution as compared to a SISO radar, i.e., the range resolution of MFSF MIMO radar is at least equal to the best between the range resolution of SF SISO radar and SISO radar, where MFSF MIMO radar refers to matched filter based MIMO radar that uses the SF technique.

In [66], in a study of CS-based SISO radar, it was observed that the maximum value of the correlation of two different columns of the basis matrix is equal to the second largest value of the discrete AF surface. The recovery performance of CS approaches, however, is directly related to the column correlation of the sensing matrix rather than the basis matrix. Unlike [66], we next study the relation of the AF and the column correlation of the sensing matrix for the proposed CSSF MIMO radar. This analysis will provide a clue for comparing the resolution of CS and matched filter in the context of SF MIMO radar, i.e., CSSF MIMO radar and MFSF MIMO radar.

On letting $\mathbf{p}_k$ denote the column of the sensing matrix $\tilde{\mathbf{\Theta}}$ corresponding to the k-th grid point in the angle-speed-range space, we have

$$
\begin{aligned}
< \mathbf{p}_k, \mathbf{p}_{k'} > &= \sum_{l=1}^{N_r}\sum_{m=1}^{N_p} e^{j2\pi(\tilde{q}_{lmk}-\tilde{q}_{lmk'})}\mathbf{v}_m^H(a_{k'})\mathbf{X}^H\mathbf{C}^H_{\lfloor\frac{2c_{k'}}{cT_s}\rfloor}\mathbf{D}^H\left(\frac{2b_{k'}f_m}{c}\right)\underbrace{\mathbf{\Phi}_l^H\mathbf{\Phi}_l}_{\mathbf{A}}\underbrace{\mathbf{D}\left(\frac{2b_k f_m}{c}\right)\mathbf{C}_{\lfloor\frac{2c_k}{cT_s}\rfloor}\mathbf{X}\mathbf{v}_m(a_k)}_{\mathbf{g}_k} \\
&= \sum_{l=1}^{N_r}\sum_{m=1}^{N_p}\sum_{p,q=1}^{L+\tilde{L}} e^{j2\pi(\tilde{q}_{lmk}-\tilde{q}_{lmk'})}g^*_{k'}(p)g_k(q)A(p,q) \\
&= \sum_{l=1}^{N_r}\sum_{m=1}^{N_p}\sum_{p,q=1}^{L+\tilde{L}}\sum_{i,i'=1}^{M_t} A(p,q)e^{j2\pi f_m(\eta_i^t(a_k)+\eta_l^r(a_k)-\eta_{i'}^t(a_{k'})-\eta_l^r(a_{k'})-2\Delta d_{kk'}+2\Delta v_{kk'}(m-1)T+2T_s(b_k(q-1)-b_{k'}(p-1)))/c} \\
&\cdot x_i\left((q-1)T_s-\frac{2c_k}{c}\right)x^*_{i'}\left((p-1)T_s-\frac{2c_{k'}}{c}\right) \qquad (3.21)
\end{aligned}
$$

where $\Delta d_{kk'} = c_k - c_{k'}$ and $\Delta v_{kk'} = b_k - b_{k'}$. For simplicity, in the above we assumed that

the receive nodes use the same measurement matrix; thus the index l was dropped in $\mathbf{A}$.

Taking the elements of the measurement matrix $\mathbf{\Phi}$ to be independent and Gaussian $\mathcal{N}(0, \frac{1}{L+\tilde{L}})$, the expectation of $< \mathbf{p}_k, \mathbf{p}_{k'} >$ with respect to the elements of $\mathbf{\Phi}$ equals

$$\begin{aligned} E\{< \mathbf{p}_k, \mathbf{p}_{k'} >\} = \frac{M}{L+\tilde{L}} \sum_{l=1}^{N_r} \sum_{m=1}^{N_p} \sum_{i,i'=1}^{M_t} & e^{j2\pi f_m(\eta_i^t(a_k)+\eta_l^r(a_k)-\eta_{i'}^t(a_{k'})-\eta_l^r(a_{k'})-2\Delta d_{kk'}+2\Delta v_{kk'}(m-1)T)/c} \\ & \cdot \sum_{p=1}^{L+\tilde{L}} x_i\left((p-1)T_s - \frac{2c_k}{c}\right) x_{i'}^*\left((p-1)T_s - \frac{2c_{k'}}{c}\right) e^{j2\pi f_m(2T_s(p-1)\Delta v_{kk'})/c} \\ & \propto \chi(\Delta d_{kk'}, \Delta v_{kk'}, a_k, a_{k'}). \end{aligned} \tag{3.22}$$

One can see from the above equation that the expectation of the column correlation of the sensing matrix is proportional to the discrete AF. To focus on the range resolution we set $a_k = a_{k'}$ and $\Delta v_{kk'} = 0$. Essentially, the range resolution of MFSF MIMO radar corresponds to the smallest range difference between two targets, $\Delta d_{kk'}$, that sets the AF to zero. Based on the UUP in [32], however, the coherence of the sensing matrix does not have to be zero for exact recovery; a small level of coherence is good enough. Therefore, CS-based radar systems have the potential to improve range resolution. This possibility will be confirmed via simulations in Section 4.3 (see Fig. 3.2).

3.3.2 The effect of signal bandwidth on CSSF-MIMO radar

In an LSFR system, the carrier frequency increases by a constant step between pulses, i.e., $\Delta f_m = (m-1)\Delta f$. This type of SF radar can be efficiently implemented using the Inverse Discrete Fourier Transform (IDFT) [55]; however, it suffers from range ambiguity if the distance between a target and receive nodes exceeds the value $R_u = \frac{cT}{2}$. The range ambiguity can be removed by randomly choosing the step frequency within a fixed bandwidth at the expense of increased sidelobe as compared to the LSFR [67]. In this section, we investigate the effect of the number of pulses N_p (or equivalently, the bandwidth) on

range resolution for two types of CSSF MIMO radar, i.e., LSFR and RSFR, in terms of the coherence of the sensing matrix (see (4.44)). Consistent with [67], which discussed convectional radar systems using the MFM, we find that the RSFR requires more pulses than LSFR to achieve the same range resolution for CS-based MIMO radar.

Since an increase in the number of receive nodes does not improve the range resolution, for simplicity we consider one receive node only. The correlation of columns $\mathbf{p}_k$ and $\mathbf{p}_{k'}$ for $a_k = a_{k'}$ and $b_k = b_{k'}$ equals

$$p_{kk'} = |<\mathbf{p}_k, \mathbf{p}_{k'}>| = \left|\sum_{m=1}^{N_p}\sum_{p,q=1}^{L+\tilde{L}} e^{j2\pi f_m(-2\Delta d_{kk'})/c} g_{k'}^*(p) g_k(q) A(p,q)\right|$$
$$= \left|\sum_{m=1}^{N_p} e^{j2\pi f_m(-2\Delta d_{kk'})/c} \sum_{p,q=1}^{L+\tilde{L}} A(p,q) e^{j2\pi f_m(2T_s b_k(q-p))/c} \left(\sum_{i=1}^{M_t} Q_{kk'}(m,p,q,i,i) + \sum_{i\neq i'}^{M_t} Q_{kk'}(m,p,q,i,i')\right)\right| \tag{3.23}$$

where

$$Q_{kk'}(m,p,q,i,i') = e^{j2\pi f_m(\eta_i^t(a_k)-\eta_{i'}^t(a_k))/c} x_i\left((q-1)T_s - \frac{2c_k}{c}\right) x_{i'}^*\left((p-1)T_s - \frac{2c_{k'}}{c}\right). \tag{3.24}$$

Due to (A1) and the discretized version of (A2), we can ignore the Doppler shift within a pulse and the second term $\sum_{i\neq i'}^{M_t} Q_{kk'}(m,p,q,i,i')$ in (3.23). Therefore, (3.23) becomes

$$p_{kk'} \approx \left|\sum_{m=1}^{N_p} e^{j2\pi f_m(-2\Delta d_{kk'})/c} \sum_{p,q=1}^{L+\tilde{L}} A(p,q) \sum_{i=1}^{M_t} x_i\left((q-1)T_s - \frac{2c_k}{c}\right) x_i^*\left((p-1)T_s - \frac{2c_{k'}}{c}\right)\right|. \tag{3.25}$$

Eq. (3.25) can be rewritten as

$$p_{kk'} \approx \begin{cases} N_p \rho_{kk} & k = k' \\ \underbrace{\left| \sum_{m=1}^{N_p} e^{j\alpha_{kk'}(f+\Delta f_m)} \right|}_{h(\mathbf{\Delta f})} \rho_{kk'} & k \neq k' \end{cases} \tag{3.26}$$

where $\mathbf{\Delta} f = [\Delta f_1, \ldots, \Delta f_{N_p}]$,

$$\rho_{kk'} = \left| \sum_{p,q=1}^{L+\tilde{L}} \sum_{i=1}^{M_t} A(p,q) x_i((q-1)T_s - \frac{2c_k}{c}) x_i^*((p-1)T_s - \frac{2c_{k'}}{c}) \right|$$

$$\text{and } \alpha_{kk'} = -\frac{4\pi \Delta d_{kk'}}{c}. \tag{3.27}$$

Then, the coherence of the sensing matrix $\tilde{\mathbf{\Theta}}$ corresponding to columns $\mathbf{p}_k$ and $\mathbf{p}_{k'}$ can be written as

$$\mu_{kk'}(\tilde{\mathbf{\Theta}}) = \frac{p_{kk'}}{\sqrt{p_{kk} p_{k'k'}}} \approx \frac{h(\mathbf{\Delta f}) \rho_{kk'}}{N_p \sqrt{\rho_{kk} \rho_{k'k'}}}. \tag{3.28}$$

Linear step frequency

If the carrier frequency increases by a constant step Δf between adjacent pulses, i.e., $\Delta f_m = (m-1)\Delta f$, then

$$\mu_{kk'}(\tilde{\mathbf{\Theta}}) \approx \frac{|1 - e^{j\alpha_{kk'} \Delta f N_p}| \rho_{kk'}}{|1 - e^{j\alpha_{kk'} \Delta f}| N_p \sqrt{\rho_{kk} \rho_{k'k'}}} \propto \frac{|\sin(\frac{1}{2}\alpha_{kk'} \Delta f N_p)|}{N_p}. \tag{3.29}$$

It can be easily seen that an increase in N_p tends to reduce the coherence and thus improves the range resolution.

Let $\alpha_{kk'ii'}^{pq}$ denote the travel-time difference between the signals sent from the transmit node i to the target located at the kth grid point at time instant pT_s, and from the transmit

node i' to the target located at the k'th grid point at time instant qT_s. It holds that

$$\alpha_{kk'ii'}^{pq} = (-2\Delta d_{kk'} + 2T_s b_k(q-p) + \eta_i^t(a_k) - \eta_{i'}^t(a_k))/c. \tag{3.30}$$

Regarding the approximation error, the term discarded in (3.25) is

$$\begin{aligned}\tilde{p}_{kk'} &= \sum_{m=1}^{N_p} e^{j2\pi f_m(-2\Delta d_{kk'})/c} \sum_{p,q=1}^{L+\tilde{L}} A(p,q) e^{j2\pi f_m(2T_s b_k(q-p))/c} \sum_{i\neq i'}^{M_t} Q_{kk'}(m,p,q,i,i') \\ &= \sum_{p,q=1}^{L+\tilde{L}} \frac{1-e^{j2\pi N_p \Delta f \alpha_{kk'ii'}^{pq}}}{1-e^{j2\pi \Delta f \alpha_{kk'ii'}^{pq}}} e^{j2\pi f \alpha_{kk'ii'}^{pq}} A(p,q) \sum_{i\neq i'}^{M_t} x_i\left((q-1)T_s - \frac{2c_k}{c}\right) x_{i'}^*\left((p-1)T_s - \frac{2c_{k'}}{c}\right).\end{aligned} \tag{3.31}$$

The amplitude of $\frac{1-e^{j2\pi N_p \Delta f \alpha_{kk'ii'}^{pq}}}{1-e^{j2\pi \Delta f \alpha_{kk'ii'}^{pq}}} e^{j2\pi f \alpha_{kk'ii'}^{pq}}$ is bounded by N_p. For independent waveforms, the approximation error $\tilde{p}_{kk'}$ in (3.23) is always negligible as compared to $p_{kk'}$.

Let μ_t denote the maximum coherence of $\tilde{\mathbf{\Theta}}$ that guarantees exact recovery of the sparse vector with high probability via the Dantzig selector. The minimum number of pulses required to achieve a certain resolution can be obtained by solving

$$\begin{aligned} N_p^* = \min\ & N_p \\ s.t.\ & \frac{|1-e^{j\alpha_{kk'}\Delta f N_p}|\rho_{kk'}}{|1-e^{j\alpha_{kk'}\Delta f}|N_p\sqrt{\rho_{kk}\rho_{k'k'}}} \leq \mu_t, \\ & k,k' = 1,\ldots,N \text{ and } k \neq k'. \end{aligned} \tag{3.32}$$

The above problem is easy to solve, for example by trying different values for N_p; however, it requires a value for μ_t. In [54], a rough estimate of μ_t in the presence of mild interference was offered. In general, μ_t must be determined experimentally.

Random step frequency

Assuming that the frequency steps over pulses are i.i.d uniform random variables, i.e., $\Delta f_m \sim U(0, 2b)$, the expectation of square coherence over Δf_m is given by

$$E\{\mu_{kk'}^2(\tilde{\boldsymbol{\Theta}})\} = E\left\{\frac{\left|\sum_{m=1}^{N_p} e^{j\alpha_{kk'}(f+\Delta f_m)}\rho_{kk'}\right|^2}{N_p^2\rho_{kk}\rho_{k'k'}}\right\}$$
$$= \frac{\rho_{kk'}^2}{\rho_{kk}\rho_{k'k'}}\left(\frac{1}{N_p} + \frac{N_p^2 - N_p}{N_p^2}\frac{\sin^2(\alpha_{kk'}b)}{\alpha_{kk'}^2 b^2}\right). \tag{3.33}$$

For a fair comparison, we set LSFR and RSFR to cover the same frequency band, i.e., set b equal to $\Delta f(N_p - 1)/2$. Then (3.33) can be rewritten as

$$E\{\mu_{kk'}^2(\tilde{\boldsymbol{\Theta}})\} = \frac{\rho_{kk'}^2}{\rho_{kk}\rho_{k'k'}N_p}\left(1 + \frac{4\sin^2(\frac{1}{2}(N_p-1)\alpha_{kk'}\Delta f)}{(N_p-1)\alpha_{kk'}^2\Delta f^2}\right)$$
$$= \frac{\rho_{kk'}^2}{\rho_{kk}\rho_{k'k'}N_p}\left(1 + \frac{\sin^2(\frac{1}{2}(N_p-1)\alpha_{kk'}\Delta f)}{(N_p-1)(2\pi\Delta f\Delta d_{kk'}/c)^2}\right). \tag{3.34}$$

As the term $(2\pi\Delta f\Delta d_{kk'}/c)^2$ increases, the expected value of the squared coherence becomes approximately equal to $1/N_p$. This holds when the product of radian frequency step $2\pi\Delta f$ and the range spacing of grid points $\Delta d_{kk'}$ is comparable to the speed of light c.

Since the coherence of the sensing matrix for RSFR cannot be obtained directly, we instead compare the squared coherence of the sensing matrix for LSFR and RSFR. For large N_p, we find from (3.29) and (3.34) that the squared coherence for LSFR and RSFR decreases inverse proportionally to N_p^2 and N_p, respectively. This implies that more pulses are required by RSFR to achieve the desired performance with all other parameters, i.e., M_t, N_r and M, being equal.

Before ending this section, we note that the expectation of the approximation error in

(3.23) can be represented by

$$\tilde{p}_{kk'} = \sum_{p,q=1}^{L+\tilde{L}} e^{j2\pi\alpha^{pq}_{kk'ii'}(N_p-1)\Delta f/2+f} \frac{N_p}{N_p-1} \frac{2\sin(\pi\alpha^{pq}_{kk'ii'}(N_p-1)\Delta f)}{\alpha^{pq}_{kk'ii'}2\pi\Delta f} A(p,q) \cdot \sum_{i\neq i'}^{M_t} x_i\left((q-1)T_s - \frac{2c_k}{c}\right) x^*_{i'}\left((p-1)T_s - \frac{2c_{k'}}{c}\right) \quad (3.35)$$

where one can see that a decrease in the product of $\alpha^{pq}_{kk'ii'}$ (seen in (3.30)) and the radian frequency step, $2\pi\Delta f$, increases both the approximation error and the squared coherence. Given $\alpha^{pq}_{kk'ii'}$, an increase in Δf would reduce the approximation error $\tilde{p}_{kk'}$. However, this would increase the bandwidth required by RSFR.

3.4 Decoupled estimation of angle, velocity and range with reduced complexity

Solving the ℓ_1 minimization problem of (2.32) requires polynomial time in the dimension of **s**. For the discretization discussed in Section II, the joint estimation of angle, velocity and range requires complexity of $O((N_aN_bN_c)^3)$ [29][43]. For large values of N_a, N_b and N_c, the computational cost of the CS approach would be prohibitive. In the following, we propose a decoupled angle-velocity-range estimation approach which reduces the search space and thus the computational complexity.

The scheme needs some initial rough estimates of angle and range. One way to obtain those estimates is to use the MFM, which requires forwarding to the fusion center Nyquist sampled data from one pulse. In the following, all N_r nodes in the system sample all received pulses in a compressive fashion, except $\tilde{N}_r$ nodes, which sample the first received pulse at the Nyquist rate and all remaining pulses in a compressive fashion. Those Nyquist rate samples will be used to obtain coarse estimates of angle and range via the MFM.

The fusion center performs the following operations (also see Fig. 3.1).

(i) *STEP1: Angle and range estimation*

This step uses the first pulse forwarded by each receive node. A fine grid, (a_{n_1}, c_{n_1}), $\ldots, (a_{n_{K_1}}, c_{n_{K_1}})$, is constructed around the MFM initial estimates. Then the sensing matrix is constructed as

$$\tilde{\mathbf{\Theta}}_1 = \mathbf{\Phi}_{l1}[e^{j2\pi f_1(-2c_{n_1}+\eta_l^r(a_{n_1}))/c}\mathbf{C}_{\lfloor\frac{2c_{n_1}}{cT_s}\rfloor}\mathbf{X}\mathbf{v}_m(a_{n_1}), \ldots, e^{j2\pi f_1(-2c_{n_{K_1}}+\eta_l^r(a_{n_{K_1}}))/c}\mathbf{C}_{\lfloor\frac{2c_{n_{K_1}}}{cT_s}\rfloor}\mathbf{X}\mathbf{v}_m(a_{n_{K_1}})] \tag{3.36}$$

where

$$\mathbf{\Phi}_{lm} = \begin{cases} \mathbf{I}_{L+\tilde{L}}, & l = 1, \ldots, \tilde{N}_r,\ m = 1 \\ \text{the measurement matrix of size } M \times (L+\tilde{L}), & \text{otherwise} \end{cases}. \tag{3.37}$$

The received signals, $\tilde{\mathbf{r}}_{11}, \ldots, \tilde{\mathbf{r}}_{N_r 1}$, are stacked in a vector, i.e.,

$$\tilde{\mathbf{r}}_1 = \tilde{\mathbf{\Theta}}_1\mathbf{s} + \mathbf{n}_1 \tag{3.38}$$

where $\tilde{\mathbf{r}}_1 = [\tilde{\mathbf{r}}_{11}^T, \ldots, \tilde{\mathbf{r}}_{N_r 1}^T]^T$. By applying the Dantzig selector to (3.38), new and refined angle-range information is obtained.

Thanks to the initial estimates, the search area in the angle-range plane is significantly reduced and thus the computational load of CS is lightened. Due to the fact that only one pulse from each receive node is used, the range resolution at this step is limited by $\frac{c}{2B}$, where B is the signal bandwidth. The obtained range estimates will be refined in the next step in which the fusion center will jointly process the entire pulse train. Also, due to assumption (A1), Doppler information cannot be extracted at this step.

(ii) *STEP 2: Range resolution improvement and Doppler estimation*

In this step the fusion center processes the entire pulse train forwarded by each re-

ceive node. The range space around the range estimates obtained in Step 1 is discretized into finer grid points. Based on a discretization of the Doppler space, the refined range grid points and the angle estimates obtained in Step 1, i.e., $(a_{m_1}, b_{m_1}, c_{m_1})$, $\ldots$, $(a_{m_{K_2}}, b_{m_{K_2}}, c_{m_{K_2}})$, the fusion center formulates a sensing matrix and extracts angle-Doppler-range information in a CS fashion.

To further reduce the complexity of CS reconstruction, the MFM can be applied before CS to provide angle-Doppler-range estimates around which a finer grid can be constructed and used by CS. In that case MFM would be applied based on the grid points $(a_{m_1}, b_{m_1}, c_{m_1}), \ldots, (a_{m_{K_2}}, b_{m_{K_2}}, c_{m_{K_2}})$.

For the case in which there are stationary targets and moving targets, the angle estimation can be further improved by taking into account Doppler information.

Assuming that the MFM is used for initial estimation, the complexity of two steps is respectively $O(N_a N_c(\tilde{N}_r L + (N_r - \tilde{N}_r)M) + K_1^3)$ and $O(K_2(\tilde{N}_r(L-M) + N_r N_p M) + K_3^3)$, where K_3 is the number grid points used by CS at Step 2. Generally, it holds that $K_1^3 + K_3^3 \ll N_a N_c(\tilde{N}_r L + (N_r - \tilde{N}_r)M) + K_2(\tilde{N}_r(L-M) + N_r N_p M)$ for a small number of targets. Therefore, the computational load is mostly due to the initial estimation. As compared to the complexity of the joint angle-Doppler-range CS approach, i.e., $O((N_a N_b N_c)^3$, considerable computations can be saved by using the proposed decoupled scheme for large values of N_a, N_b and N_c.

The computation savings, however, may be obtained at the expense of detection accuracy, unless the initial estimates provided by the initial estimation method are reliable. *Reliable estimates* here refer to the initial estimates whose distances to the true target locations are within the resolution cell that is determined by the initial estimation. Then all the targets can be captured based on the finer angle-range grid points constructed around the reliable initial estimates. For the instance of the MFM, the performance in providing good initial estimates depends on several factors; (i) the signal-to-interference ratio (SIR), which

can be improved by employing more data; (ii) angular, range or Doppler resolution, which is improved by increasing N_r or N_p; (iii) the distance between the adjacent grid points. (In the worst case in which the targets fall midway between grid points, the targets may fail to be captured by the closest grid points if the spacing of adjacent grid points is too large. An empirical approach to select grid spacing was discussed in [53]. That approach is also applicable to the MFM); and (iv) the threshold for hard detection. A small threshold should be used in order to reduce the miss probability. However, this implies that more grid points need to be considered for the CS approach following the MFM as compared to a larger threshold. In summary, the performance of the MFM can be improved at the expense of more transmit power and increased complexity.

3.5 Simulation Results

We consider a MIMO radar system with transmit and receive nodes uniformly distributed on a disk of radius 10m. The carrier frequency is $f = 5GHz$. Each transmit node uses orthogonal Hadamard waveforms of length $L = 512$ and unit power. The received signal is corrupted by zero-mean Gaussian noise. The signal-to-noise ratio (SNR) is defined as the inverse of the power of thermal noise at a receive node. A jammer is located at angle 7^o and transmits an unknown Gaussian random waveform. The targets are assumed to fall on the grid points. Throughout this section, the CS approach uses a measurement matrix with Gaussian entries.

3.5.1 Range resolution of the CS-based SFR and conventional SFR

In this subsection we provide some simulation results to show the superiority of CSSF MIMO radar as compared to MFSF MIMO radar in terms of range resolution. Figure 3.2 shows the normalized amplitude estimates of target reflection coefficients for CSSF MIMO radar and MFSF MIMO radar in one realization. Since the multiple colocated an-

tennas fail to improve range resolution, we consider a single transmit and receive antenna here for simplicity. Let $M = 10$, $N_p = 30$ and the carrier frequencies be randomly selected within the frequency band $[5, 5.029]GHz$. The CSSF radar uses 10 measurements per pulse while MFSF radar obtains 665 measurements per pulse. Various values of SNR are considered. The spacing between two adjacent grid points is $2m$. There are six targets at ranges [1024, 1028, 1032, 1036, 1040, 1044]m. Figure 3.2 shows that the peaks corresponding to all targets can be distinguished from each other for the CSSF radar while for the MFSF radar some peaks are lost. This verifies the observations of Section 3.3.1 that CSSF radar has the potential to achieve higher range resolution than does MFSF radar.

3.5.2 Range estimation for CSSF MIMO radar

The goal of this subsection is to test the performance of CSSF MIMO radar based on LSF and RSF. Figure 3.3 compares the numerical and theoretical squared coherence of the sensing matrix corresponding to two adjacent grid points in the range plane for different numbers of pulses and various values of the linear frequency step $\Delta f = 1MHz$, $4MHz$ and $8MHz$. All the results shown in Fig. 3.3 are the numerical squared coherence averaged over 100 independent and random runs and the theoretical squared coherence for LSFR and RSFR calculated based on (3.29) and (3.33). We consider the case in which $M_t = M = 10$, $N_r = 1$ and the grid step is $\Delta c = 7.5m$. For a fair comparison, we choose random step frequencies within the same frequency band as in LSFR, i.e., $f + [0, (N_p - 1)\Delta f]$. It can be easily seen that the numerical squared coherence of the sensing matrix for LSFR perfectly matches with the theoretical results in (3.29). The numerical squared coherence of the sensing matrix for RSFR approaches the theoretical results in (3.33) as Δf increases and approaches $1/N_p$ as the number of pulses increases. It is also verified by Fig. 3.3 that LSFR exhibits lower coherence of the sensing matrix than does RSFR.

Figure 3.4 shows the receiver operating characteristic (ROC) curves of the range esti-

mates produced by the random and linear step-frequency technique based on 200 random and independent runs. Here, the probability of detection (PD) is the percentage of cases in which all the targets are detected. The probability of false alarm (PFA) is the percentage of cases in which false targets are detected. We consider a case in which the angle and speed of three targets are the same and assumed to be known. In each independent run, the target angle and speed are randomly generated. The ranges of three targets are fixed to $1005m$, $1010m$ and $1045m$, respectively. The power of the jammer signal is 4 and SNR= 0dB. We can see that the use of LSF yields better performance than randomly choosing the carrier frequency within the same frequency band. In this particular case, CS-based RSFR requires 12 pulses to generate the ROC performance that can be achieved by CS-based LSFR using only 9 pulses. The performance of LSFR and RSFR based on the MFM is also shown in Fig. 3.4. It can be seen that the former using 12 pulses is far better than the latter with the same number of pulses. It can also be seen that CSSF MIMO radar outperforms MFSF MIMO radar.

3.5.3 The joint angle-Doppler-range estimation of CSSF MIMO radar

Figure 3.5 shows the ROC curves of the angle-speed-range estimates yielded by CSSF MIMO radar using the decoupled scheme. The angle-speed-range estimates have been obtained based on 200 random and independent runs. The cases in which $M_t = 10$, $N_r = \tilde{N}_r = 7$ and $N_p = 12$ are shown in Fig. 3.5. The azimuth angle and range of three targets are randomly generated in each run but the spacing of angle and range between targets are fixed to 0.3^o and $7.5m$, respectively. The speeds of three targets are $10m/s, 30m/s$, and $60m/s$. The power of the jammer signal is 4 and SNR= 0dB. The performance of MFSF MIMO radar, shown in Fig. 3.5, is obtained in the same decoupled fashion, i.e., 1) estimate target angle and range based on a single pulse; then refine the angle estimates based on the finer angle grid points around the initial angle estimates by using the MFM; and then

2) process the entire pulse train to extract angle-speed-range information by discretizing the speed space, constructing finer range grid points around the initial range estimates and utilizing the initial angle estimates obtained in 1). One can see that MFSF MIMO radar is inferior to CSSF MIMO radar even when using far more measurements than the latter.

3.6 Conclusions

We have presented a CSSF MIMO radar system that applies SF to CS-based MIMO radar. The technique of SF can significantly improve range resolution. We have shown that CSSF MIMO radar has the potential to achieve better resolution than MFSF MIMO radar, and that more pulses are required by RSFR than by LSFR to achieve the desired performance with all other parameters being the same. The angle-Doppler-range estimation requires discretization of the angle-Doppler-range space into a large number of grid points, which would increase the complexity of the CS approach. We have presented a CSSF MIMO radar scheme that by decoupling angle-range estimation and Doppler estimation achieves significant complexity reduction. The proposed technique applies to slowly moving targets and relies on initial rough angle-range estimates. Assuming that the initial estimates do not miss any targets, the proposed low complexity scheme maintains the high resolution of the CS approach.

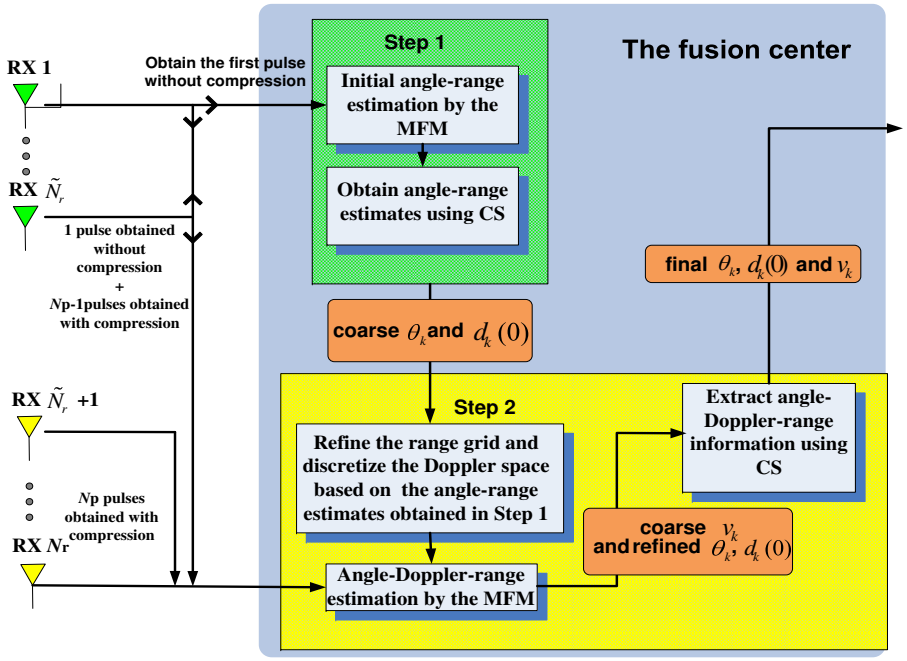

Figure 3.1: Schematic diagram of the proposed decoupled scheme.

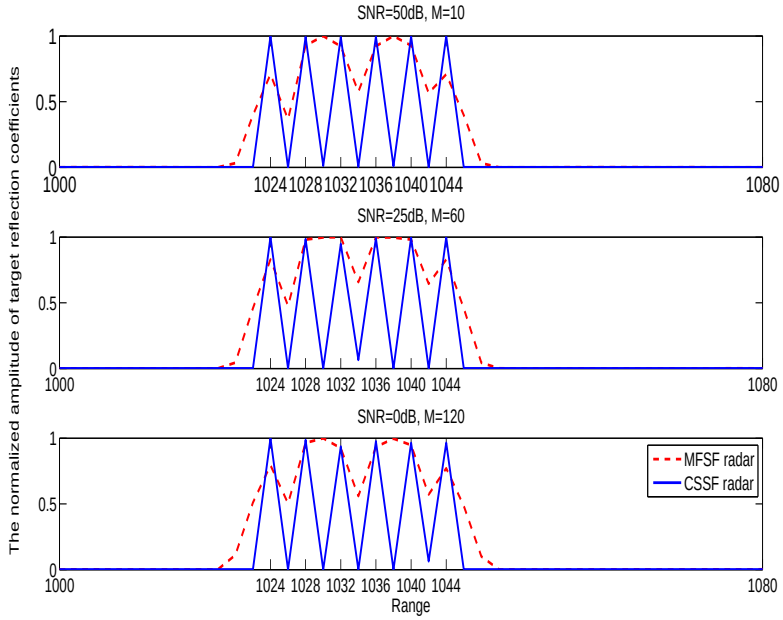

Figure 3.2: Normalized amplitude estimates of target reflection coefficients for the CSSF radar and MFSF radar (one realization for $M_t = N_r = 1$ and $N_p = 30$).

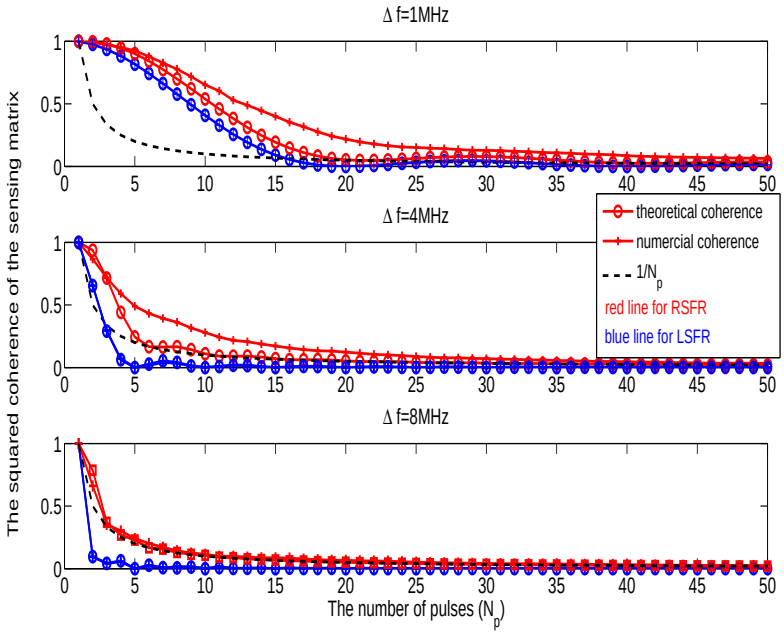

Figure 3.3: Average squared coherence of the sensing matrix for different numbers of pulses N_p over 100 independent and random runs ($\Delta f = 4 \times 10^6$, $M = M_t = 10$ and $N_r = 1$). The distance of two grid points in the range plane is $\Delta c = 7.5m$.

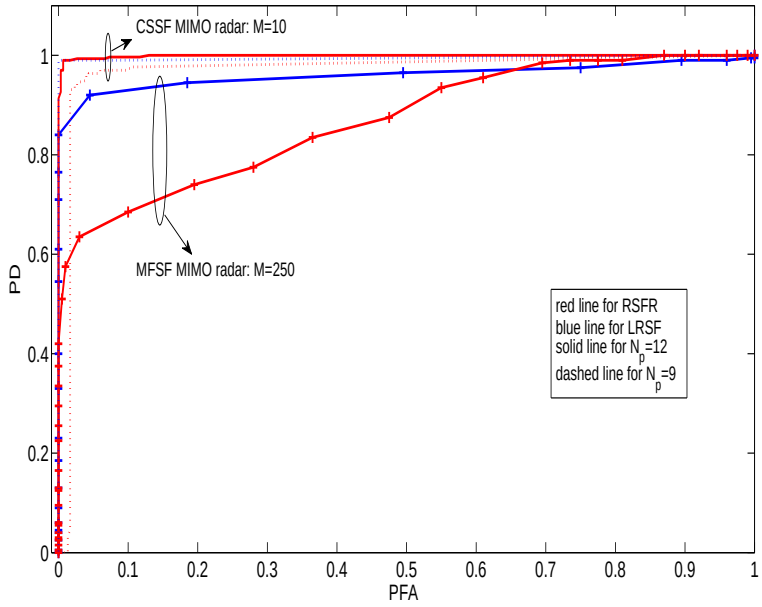

Figure 3.4: ROC of range estimates obtained with linearly and randomly stepped frequency CSSF MIMO radar and MFSF MIMO radar ($M = M_t = 10$, $N_r = 1$ and $\Delta f = 1MHz$).

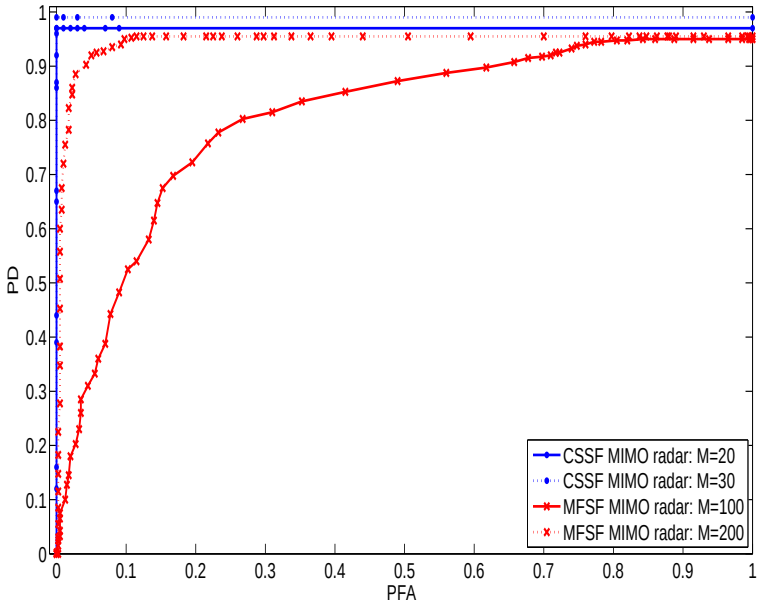

Figure 3.5: ROC of target detection based on angle-speed-range estimates yielded by the proposed decoupled scheme in Section 3.4 for CSSF MIMO radar and MFSF MIMO radar ($M_t = 10, N_r = \tilde{N}_r = 7$ and $N_p = 12$).

4. Measurement matrix design

In Chapter 2, we have proposed a measurement matrix that enables high SIR as compared to the Gaussian random measurement matrix. However, this measurement matrix is only applicable to the case in which the targets are located in a small range bin and the sampling is synchronized with the first target return. In this chapter, we propose new measurement matrices for the general scenario considered in Chapter 3 without confining targets in the same range bin and without requiring sampling synchronization.We design measurement matrices that achieve some optimality measure that is function of the coherence of the sensing matrix (CSM) and/or signal-to-interference ratio (SIR). The first approach determines the measurement matrix by minimizing a criterion that is a linear combination of CSM and the inverse of SIR. The second one, in order to reduce complexity, imposes a structure on the measurement matrix, and the components of the structure are designed to enhance SIR while keeping the CSM comparable to that of the conventional measurement matrix, e.g., the Gaussian random measurement matrix. A reduced complexity suboptimal construction for the first measurement matrix is also proposed. It is shown via simulations that the proposed measurement matrices can improve detection accuracy as compared to a Gaussian random measurement matrix.

4.1 Introduction

UUP [20][32] indicates that if every set of sensing matrix columns with cardinality less than the sparsity of the signal of interest is approximately orthogonal, then the sparse signal can be exactly recovered with high probability. This implies that $\mathbf{\Phi}$ is incoherent with $\mathbf{\Psi}$. For an orthonormal basis matrix, use of a random measurement matrix leads to a sensing matrix that obeys the UUP with overwhelming probability [31]. The entries of

such measurement matrix can be taken from a Gaussian distribution, symmetric Bernoulli distribution, and could be randomly sampled from a Fourier matrix or any orthonormal matrix. In this chapter, we term as *conventional approach* the CS recovery via a Gaussian measurement matrix.

In this chapter, we consider the general scenario considered in Chapter 3, in which the targets might be located across several range bin and the sampling is asynchronized with the first target return. The performance of the CS approach degrades in the presence of strong interference and with increased coherence among the columns of the sensing matrix. We propose two designs for the measurement matrix. The first design aims at decreasing CSM and at the same time enhancing SIR. The measurement matrix is obtained by solving a convex optimization problem and depends on the basis matrix, which in turn depends on space discretization. This optimization problem might involve high complexity due to a large number of variables and constraints involved. A reduced complexity suboptimal construction for the first measurement matrix is also proposed. The second approach targets only SIR improvement. It is constructed based on the transmit signal waveforms and accounts for all possible discretized delays of target returns within a given time window. It is shown that depending on the waveforms used, the latter measurement matrix can significantly improve SIR while it results in CSM comparable that of a random Gaussian measurement matrix.

The rest of the chapter is organized as follows. In Section 4.2 we introduce the two proposed measurement matrices and provide the analysis related to the second measurement matrix. Simulation results are given in Section 4.3 for the cases of slowly moving targets. Finally, we make some concluding remarks in Section 4.4.

4.2 Measurement matrix design

In this section, we discuss the design of the measurement matrix in order to improve the detection performance of CS-MIMO radar. We assume that all the nodes utilize the same measurement matrix, defined as $\mathbf{\Phi}$, which does not vary with time for simplicity. Under the assumption (A1), the Doppler shift within a pulse can be ignored. Recall that the received signal at the l-th node during the m-th pulse can be formulated as (eq. (3.3))

$$\mathbf{r}_{lm} = \sum_{k=1}^{K} \beta_k e^{j2\pi p_{lmk}} \mathbf{\Phi} \mathbf{C}_{\tau_k} \mathbf{X} \mathbf{v}(\theta_k) + \mathbf{\Phi} \mathbf{n}_{lm} \tag{4.1}$$

and the sensing matrix for the l-th node is given by (eq. (3.7))

$$\mathbf{\Theta}_l = \mathbf{\Phi}[e^{j2\pi q_{lm1}} \mathbf{C}_{\lfloor \frac{2c_1}{cT_s} \rfloor} \mathbf{X} \mathbf{v}(a_1), \ldots, e^{j2\pi q_{lmN}} \mathbf{C}_{\lfloor \frac{2c_N}{cT_s} \rfloor} \mathbf{X} \mathbf{v}(a_N)]. \tag{4.2}$$

Generally, there are two factors that affect the performance of CS. The first one is the coherence of the sensing matrix. UUP requires low coherence to guarantee exact recovery of the sparse signal. Although the CSM always serves as a tool that examines the necessary conditions for the CS approach, it does reflect the behavior of the sensing matrix in many cases. Furthermore, the simplicity of the CSM render itself a practical performance criterion for the CS application in real systems. The second factor is SIR. If the basis matrix obeys the UUP and the signal of interest $\mathbf{s}$ is sufficiently sparse, then the square estimation error of the Dantzig selector satisfies with very high probability [43]

$$\| \hat{\mathbf{s}} - \mathbf{s} \|_{\ell_2}^2 \leq C^2 2 log N \times (\sigma^2 + \sum_{i}^{N} \min(s^2(i), \sigma^2)) \tag{4.3}$$

where C is a constant. It can be easily seen from (4.3) that an increase in the interference power degrades the performance of the Dantzig selector.

4.2.1 The measurement matrix #1: The goal is to reduce the coherence of the sensing matrix and at the same time increase SIR

The coherence of two columns of the sensing matrix, $\mathbf{\Theta}$, corresponding to the k-th and k'-th grid point is given by

$$\mu_{kk'}(\mathbf{\Theta}) = \frac{\left|\sum_{m=1}^{N_p}\sum_{l=1}^{N_r} e^{j2\pi(q_{lmk}-q_{lmk'})}\left(\mathbf{\Phi}\mathbf{C}_{\lfloor\frac{2c_{k'}}{cT_s}\rfloor}\mathbf{X}\mathbf{v}(a_{k'})\right)^H \mathbf{\Phi}\mathbf{C}_{\lfloor\frac{2c_k}{cT_s}\rfloor}\mathbf{X}\mathbf{v}(a_k)\right|}{N_r\sqrt{\sum_{m=1}^{N_p}\left\|\mathbf{\Phi}\mathbf{C}_{\lfloor\frac{2c_k}{cT_s}\rfloor}\mathbf{X}\mathbf{v}(a_k)\right\|_2^2\sum_{m=1}^{N_p}\left\|\mathbf{\Phi}\mathbf{C}_{\lfloor\frac{2c_{k'}}{cT_s}\rfloor}\mathbf{X}\mathbf{v}(a_{k'})\right\|_2^2}}$$
$$= \frac{\left|\sum_{m=1}^{N_p}\sum_{l=1}^{N_r} e^{j2\pi(q_{lmk}-q_{lmk'})}\mathbf{u}_{k'}^H\mathbf{\Phi}^H\mathbf{\Phi}\mathbf{u}_k\right|}{N_rN_p\sqrt{\mathbf{u}_k^H\mathbf{\Phi}^H\mathbf{\Phi}\mathbf{u}_k\mathbf{u}_{k'}^H\mathbf{\Phi}^H\mathbf{\Phi}\mathbf{u}_{k'}}} \tag{4.4}$$

where $\mathbf{u}_k = \mathbf{C}_{\lfloor\frac{2c_k}{cT_s}\rfloor}\mathbf{X}\mathbf{v}(a_k)$.

Let the interference waveform at the lth receive node during the mth pulse be Gaussian distributed, i.e., $n_{lm}(t) \sim \mathcal{CN}(0,\sigma^2)$. Let us also assume that the noise waveforms are independent across receive nodes and between pulses. Then the average power of the interference can be represented by

$$P_n = E\{\sum_{m=1}^{N_p}\sum_{l=1}^{N_r}(\mathbf{\Phi}\mathbf{n}_{lm})^H\mathbf{\Phi}\mathbf{n}_{lm}\} = N_pN_r\sigma^2\mathrm{Tr}\{\mathbf{\Phi}^H\mathbf{\Phi}\}. \tag{4.5}$$

The average power of the echo reflected by the ith target located on the k_ith grid point of the angle-range space is approximately equal to

$$P_s^i \approx |\beta_i|^2N_r\sum_{m=1}^{N_p}\mathbf{u}_{k_i}^H\mathbf{\Phi}^H\mathbf{\Phi}\mathbf{u}_{k_i}. \tag{4.6}$$

Therefore, the SIR equals

$$\mathrm{SIR} = \frac{\sum_{i=1}^{K}|\beta_i|^2\sum_{m=1}^{N_p}\mathbf{u}_{k_i}^H\mathbf{\Phi}^H\mathbf{\Phi}\mathbf{u}_{k_i}}{\sigma^2N_p\mathrm{Tr}\{\mathbf{\Phi}^H\mathbf{\Phi}\}}. \tag{4.7}$$

The precise manner in which CSM and SIR affect the performance of the CS approach is unknown. Although theoretical bounds for the ℓ_2-norm of the estimation error have been proposed [26]-[43], the bounds are hard to obtain. Furthermore, those bounds might not be relevant in applications in which the quantity of interest is the location of the non-zero elements of the sparse signal rather than the non-zero values themselves. This is the case for the problem at hand. In [44] the upper bound on the probability of error under the *optimal* decision rule was derived. Although that upper bound is related to the detection of non-zero elements, it cannot be used for the measurement matrix design as it is rather loose in some practical cases and it has a complicated form. In this paper, we determine the measurement matrix by optimizing a linear combination of the CSM and the reciprocal of SIR.

The overall CSM is here taken as the maximum coherence produced by a pair of cross columns in the sensing matrix. This criterion works well for a uniform sensing matrix but might not capture the behavior of the sensing matrix in which the coherence of most column pairs is small [45]. However, that coherence metric is widely used for the CS scenario due to its simplicity [45][46]. The optimization problem becomes

$$\min_{\mathbf{\Phi}}(\max_{k\neq k'}\mu_{kk'}^2(\mathbf{\Theta})+\lambda\frac{1}{\mathrm{SIR}})\ \ (C1) \tag{4.8}$$

where λ is a positive weight, which reflects the tradeoff between the coherence and SIR.

Since (4.8) is not a convex problem, two steps are taken to address this issue. First, we solve (4.8) with respect to $\mathbf{B}=\mathbf{\Phi}^H\mathbf{\Phi}$ instead of $\mathbf{\Phi}$. Furthermore, the norm of columns in the sensing matrix is set to 1, i.e., $N_rN_p\mathbf{u}_k^H\mathbf{\Phi}^H\mathbf{\Phi}\mathbf{u}_k=1,\ k=1,...,N$, so that we can avoid

the fractional expression of $\mu_{kk'}(\boldsymbol{\Theta})$ and $\frac{1}{\mathrm{SIR}}$. Thus (4.8) can be reformulated as

$$\begin{aligned}
\min_{t,\mathbf{B}} \quad & t + \lambda \mathrm{Tr}\{\mathbf{B}\} \\
s.t. \quad & \left| \sum_{m=1}^{N_p} \sum_{l=1}^{N_r} e^{j2\pi(q_{lmk'} - q_{lmk})} \mathbf{u}_{k'}^H \mathbf{B} \mathbf{u}_k \right|^2 \leq t, \\
& k = 1, \ldots, N, k' = k+1, \ldots, N \\
& N_r \sum_{m=1}^{N_p} \mathbf{u}_k^H \mathbf{B} \mathbf{u}_k = 1, \ k = 1, \ldots, N, \\
& \mathbf{B} \geq 0, \ t \geq 0.
\end{aligned} \tag{4.9}$$

which is a convex problem with respect to **B**. The first term in the objective refers to the maximum coherence of cross columns in the sensing matrix; the second term is proportional to the noise power which is a linear function of **B**. Once **B** is available, **Φ** can be easily obtained. On letting **B** be factorized by the eigendecomposition $\mathbf{B} = \mathbf{V}\boldsymbol{\Sigma}\mathbf{V}^{\mathbf{H}}$, we can obtain the measurement matrix #1 as

$$\boldsymbol{\Phi}_{\#1} = \sqrt{\tilde{\boldsymbol{\Sigma}}}\tilde{\mathbf{V}}^H \tag{4.10}$$

where $\tilde{\boldsymbol{\Sigma}}$ is a diagonal matrix that contains the nonzero eigenvalues of **Σ** on its diagonal and $\tilde{\mathbf{V}}$ includes the eigenvectors corresponding to the nonzero eigenvalues.

$\boldsymbol{\Phi}_{\#1}$ solved from ($C1$) might increase very low coherence of some pair of columns in order to minimize the maximum CSM, i.e., the coherence of different pairs of columns will spread more evenly than the conventional measurement matrix. This might not be desirable in some cases. Another criteria for evaluating the CSM is the sum of coherence of all pairs of columns in the sensing matrix (SCSM). The measurement matrix **Φ** obtained by minimizing the SCSM can increase the number of pairs of columns which yield low

coherence. It can be solved from

$$\min_{\mathbf{\Phi}}\left(\sum_{k\neq k'}\mu_{kk'}^{2}(\mathbf{\Theta})+\lambda\frac{1}{\mathrm{SIR}}\right)\ (C2) \tag{4.11}$$

The proposed methods of optimizing the measurement matrix, i.e., ($C1$) and ($C2$), can reduce the coherence of cross columns in the sensing matrix without amplifying the interference. This will improve the detection performance of the CS-based MIMO radar system, however, this will incur a computation load as compared to using the conventional measurement matrix. The number of complex variables to be solved in the convex problem of (4.9) is $\frac{(\tilde{L}+L+1)(\tilde{L}+L)}{2}$. The computation complexity would be prohibitively high for large values of $\tilde{L}+L$. For a large number of grid points N, we have to deal with a large number of constraints. The optimal measurement matrix might be obtained and stored offline based on knowledge of grid points in the angle-range space. However, it would need to be updated once the basis matrix varies with the search area of interest. This would bring heavy burden to radar systems and thus might render the real-time application impossible. Therefore, ways to alleviate the computational load are worthy of being exploited. A suboptimal scheme for the measurement matrix #1 that involves lower complexity is discussed next.

Let us impose a structure on the measurement matrix to be determined by the optimization problem of ($C2$) as follows:

$$\mathbf{\Phi}_{\#1}=\mathbf{W}\mathbf{\Phi} \tag{4.12}$$

where $\mathbf{W}$ is an $((L+\tilde{L})\times\tilde{M})$ unknown matrix to be determined and $\mathbf{\Phi}$ is a $\tilde{M}\times M_t(\tilde{L}+1)$ Gaussian random matrix. Then the number of variables in $\mathbf{W}$ can be controlled by changing the value of $\tilde{M}$. Furthermore, the structure in (4.12) enables a two-step processing for CS-based MIMO radar that simplifies the hardware of receive nodes. In particular, a receive node linearly compresses the incident signal by using $\mathbf{\Phi}$. At the fusion center, all the signal

forwarded by receive nodes are first multiplied by $\mathbf{W}$ and then jointly processed to extract target information. We can think of $\mathbf{W}$ as a post processing. In this way, the received nodes require no information of $\mathbf{W}$, which reduces the communication overhead for the fusion center and nodes.

In order to render the convex problem tractable, the norm of columns in the sensing matrix is forced to be a constant. This increases the number of constraints. If the number of variables is not sufficiently high, there might not be enough degrees of freedoms to decrease the coherence of the sensing matrix as compared to the original one. Since the number of constraints equals the number of grid points, it can be decreased by reducing the search area. This can be done by considering the grid points around the initial angle-range estimates if they are available.

4.2.2 The measurement matrix #2: The goal is to improve SIR only

Although the suboptimal construction in (4.12) significantly reduces the number of variables, solving (4.9) still requires high computation loads. Besides, $\mathbf{\Phi}_{\#1}$ must be adapted to a particular basis matrix. To avoid these two defects of $\mathbf{\Phi}_{\#1}$, another measurement matrix that targets SIR improvement only is proposed in this section. As in [53], we impose a special structure on the measurement matrix, i.e., $\mathbf{\Phi}_{\#2} = \mathbf{\Phi}\mathbf{W}^H$, where $\mathbf{\Phi}$ is an $M \times \tilde{M}$ ($M \leq \tilde{M}$) zero-mean Gaussian random matrix and $\mathbf{W}$ is an $(L + \tilde{L}) \times \tilde{M}$ deterministic matrix satisfying $\text{diag}\{\mathbf{W}^H\mathbf{W}\} = [1, \ldots, 1]^T$. The above structure serves two purposes. First, the matrix $\mathbf{W}$ can be selected to improve the detection performance of the CS approach at the receiver. Second, $\mathbf{\Phi}_{\#2}$ is always a Gaussian random matrix regardless of $\mathbf{W}$. With the appropriate $\mathbf{W}$, the measurement matrix in the form of $\mathbf{\Phi}\mathbf{W}^H$ might not increase the CSM as compared to the conventional one. Otherwise, a $\mathbf{W}$ that is highly correlated with the basis matrix would invalidate the UUP. Unlike the design of $\mathbf{\Phi}_{\#1}$, the measurement matrix proposed in this section targets SIR improvement only.

The average power of the echo reflected by the kth target with respect to node locations, conditioned on the transmit waveforms is approximately equal to

$$\begin{aligned} P_s^k &\approx |\beta_k|^2 N_r N_p E\{\mathrm{Tr}\{\mathbf{\Phi}\mathbf{C}_{\tau_k}\mathbf{X}\mathbf{v}(\theta_k)(\mathbf{\Phi}\mathbf{C}_{\tau_k}\mathbf{X}\mathbf{v}(\theta_k))^H\}\} \\ &\approx |\beta_k|^2 N_r N_p \mathrm{Tr}\{\mathbf{\Phi}\mathbf{C}_{\tau_k}\mathbf{X}E\{\mathbf{V}_k\}\mathbf{X}^H\mathbf{C}_{\tau_k}^H\mathbf{\Phi}^H\} \end{aligned} \tag{4.13}$$

where $\mathbf{V}_k = \mathbf{v}(\theta_k)\mathbf{v}^H(\theta_k)$ and its (i, j)th entry can be expressed as $V_k(i, j) = e^{j\frac{2\pi f}{c}(r_i^t\cos(\theta_k-\alpha_i)-r_j^t\cos(\theta_k-\alpha_j))}$. The Doppler shift within a pulse is ignored in (4.13) due to assumption (A1). Since the nodes are uniformly dispersed on a disk of radius r, the distribution of $h = \frac{r_i^{t/r}}{r}\sin(\alpha_i^{t/r} - \psi_0)$ is given by ([50])

$$f_h(h) = \frac{2}{\pi}\sqrt{1-h^2}, -1 < h < 1 \tag{4.14}$$

so that

$$E\left\{e^{j\alpha h}\right\} = 2\frac{J_1(\alpha)}{\alpha} \tag{4.15}$$

where $J_1(\cdot)$ is the first-order Bessel function of the first kind. Thus, based on (4.15) we can obtain ([53])

$$\begin{aligned} &E\left\{e^{j\frac{2\pi f}{c}(r_i^t\cos(\theta_k-\alpha_i)-r_j^t\cos(\theta_{k'}-\alpha_j))}\right\} \\ &= \begin{cases} 1 & i = j \text{ and } k = k' \\ \varsigma(4\sin(\frac{\theta_{k'}-\theta_k}{2})) & i = j \text{ and } k \neq k' \\ \varsigma^2(2) & i \neq j \end{cases} \end{aligned} \tag{4.16}$$

where $\varsigma(x) = 2\frac{J_1(x\frac{\pi r f}{c})}{x\frac{\pi r f}{c}}$. As observed in [53], the terms multiplied by $\varsigma^2(2)$ are small enough

and can be neglected. Then the average power P_s^k in (4.13) can be further approximated by

$$\begin{aligned} P_s^k &\approx |\beta_k|^2 N_p N_r \mathrm{Tr}\{\mathbf{\Phi}\mathbf{W}^H \mathbf{C}_{\tau_k} \mathbf{X}\mathbf{X}^H \mathbf{C}_{\tau_k}^H \mathbf{W}\mathbf{\Phi}^H\} \\ &\approx \frac{|\beta_k|^2 M N_p N_r}{\tilde{M}} \mathrm{Tr}\{\mathbf{W}^H \mathbf{C}_{\tau_k} \mathbf{X}\mathbf{X}^H \mathbf{C}_{\tau_k}^H \mathbf{W}\}. \end{aligned} \tag{4.17}$$

Inserting $\mathbf{\Phi}_{\#2}$ into (4.5), the average power of the interference can be represented by

$$P_n = \sigma^2 N_p N_r \mathrm{Tr}\{\mathbf{\Phi}\mathbf{W}^H\mathbf{W}\mathbf{\Phi}^H\} = \sigma^2 N_p N_r \sum_{q=1}^{M} \sum_{i,j} \Phi_{qi} w_{ij} \Phi_{qj}^* \approx \sigma^2 N_p N_r M \tag{4.18}$$

where Φ_{ij} and w_{ij} are the (i, j)-th entries of $\mathbf{\Phi}$ and $\mathbf{W}^H\mathbf{W}$, respectively. The approximation in (4.18) uses the constraint $\mathrm{diag}\{\mathbf{W}^H\mathbf{W}\} = [1, \ldots, 1]^T$ and the fact that $\sum_{q=1}^{M} \sum_{i \neq j} \Phi_{qi} w_{ij} \Phi_{qj}^* \approx 0$ for sufficiently large $\tilde{M}$ due to $\Phi_{qi} \sim \mathcal{N}(0, 1/\tilde{M})$.

Based on (4.17) and (4.18), the SIR is given by

$$SIR_k = P_s^k / P_n \approx \frac{|\beta_k|^2}{\sigma^2 \tilde{M}} \mathrm{Tr}\{\mathbf{W}^H \mathbf{Q}_{\tau_k} \mathbf{W}\} \tag{4.19}$$

where $\mathbf{Q}_{\tau_k} = \mathbf{C}_{\tau_k} \mathbf{X}\mathbf{X}^H \mathbf{C}_{\tau_k}^H$ is an $(L + \tilde{L}) \times (L + \tilde{L})$ matrix of rank M_t. The matrix $\mathbf{W}$ that maximizes SIR_k can be obtained by solving

$$\begin{aligned} \mathbf{W}^* = \max_{\mathbf{W}, \tilde{M}} & \frac{|\beta_k|^2}{\sigma^2 \tilde{M}} \mathrm{Tr}\{\mathbf{W}^H \mathbf{Q}_{\tau_k} \mathbf{W}\} \\ s.t.\ & \mathrm{diag}\{\mathbf{W}^H\mathbf{W}\} = [1, \ldots, 1]^T_{\tilde{M} \times 1}. \end{aligned} \tag{4.20}$$

It can be easily seen that $\mathbf{W}^*$ is the eigenvector corresponding to the largest eigenvalue of $\mathbf{Q}_{\tau_k}$. Since the largest eigenvalue of $\mathbf{Q}_{\tau_k}$ is not greater than $\mathrm{Tr}\{\mathbf{Q}_{\tau_k}\} = M_t$, the maximum SIR_k is bounded by

$$Bound\ 1: \ \frac{|\beta_k|^2}{\sigma^2} \leq SIR_k \leq \frac{|\beta_k|^2 M_t}{\sigma^2}. \tag{4.21}$$

The upper bound is achieved when the rank of $\mathbf{X}$ equals 1, i.e., all the transmit nodes send out the same waveforms. When orthogonal waveforms are utilized, i.e., $\mathbf{X}^H\mathbf{X} = \mathbf{I}_{M_t}$, the SIR_k reaches the lower bound.

However, the solution $\mathbf{W}^*$ would invalidate the conditions for the application of CS since a pulse is equivalently compressed to a single measurement. Fortunately, there are multiple equally large eigenvalues when $\mathbf{X}^H\mathbf{X} = \mathbf{I}_{Mt}$. In this case $\mathbf{Q}_{\tau_k}$ has M_t nonzero eigenvalues which are all equal to 1. Therefore, for a fixed $\tilde{M}$, $\tilde{M} \leq M_t$, the optimal $\mathbf{W}$ contains the $\tilde{M}$ eigenvectors of $\mathbf{Q_k}$ corresponding to eigenvalue 1 and achieves the maximum $SIR_k = \frac{|\beta_k|^2}{\sigma^2}$. Since the maximum SIR_k is independent of $\tilde{M}$, any matrix containing $\tilde{M}$, $\tilde{M} \leq M_t$, eigenvectors of $\mathbf{Q}$ corresponding to eigenvalue 1 would give rise to the maximum SIR_k. However, $\tilde{M} = M_t$ results in smaller coherence of the sensing matrix than any $\tilde{M}$ less than M_t due to the fact that the rank of $\mathbf{W}$ is $\tilde{M}$. Therefore, the optimal $\mathbf{W}$ is

$$\mathbf{W}^{**} = \mathbf{C}_{\tau_k}\mathbf{X}. \tag{4.22}$$

For the case of completely coherent transmit waveforms in which the upper bound in (4.21) is achieved, the resulting $\mathbf{W}^{**}$ is rank deficient.

Unfortunately, $\mathbf{W}^{**}$ is not achievable since the time delay induced by a target is unknown at the receiver. To address this issue, we replace SIR_k in the objective function in (4.20) with the average value of SIR_k with respect to the time delay, denoted by $\overline{SIR_k}$. Let the time delay induced by the kth target follow discrete uniform distribution, i.e., $p(\tau_k = k) = \frac{1}{\tilde{L}+1}, k = 0, \ldots, \tilde{L}$. Then the average value of SIR_k can be expressed as

$$\overline{SIR_k} = \frac{|\beta_k|^2}{\sigma^2\tilde{M}} \sum_{\tau=0}^{\tilde{L}} \frac{1}{\tilde{L}+1} \mathrm{Tr}\{\mathbf{W}^H\mathbf{Q}_\tau\mathbf{W}\} = \frac{|\beta_k|^2}{\sigma^2\tilde{M}} \frac{1}{\tilde{L}+1} \mathrm{Tr}\{\mathbf{W}^H\mathbf{C}\mathbf{W}\} \tag{4.23}$$

where

$$\mathbf{C} = \sum_{\tau=0}^{\tilde{L}} \mathbf{Q}_\tau = [\mathbf{C}_0\mathbf{X}, \ldots, \mathbf{C}_{\tilde{L}}\mathbf{X}][\mathbf{C}_0\mathbf{X}, \ldots, \mathbf{C}_{\tilde{L}}\mathbf{X}]^H. \tag{4.24}$$

Therefore, the optimization problem that maximizes $\overline{SIR}_k$ can be rewritten as

$$\begin{aligned} \mathbf{W}^* = & \max_{\mathbf{W},\tilde{M}} \overline{SIR}_k \\ & s.t.\ \mathrm{diag}\{\mathbf{W}^H\mathbf{W}\} = [1, \ldots, 1]^T_{\tilde{M}\times 1}. \end{aligned} \tag{4.25}$$

One can see again that the solution to (4.25) is the eigenvector corresponding to the largest eigenvalue of $\mathbf{C}$. Unlike (4.20), we fail to find the close-form solution to (4.25) that has sufficiently high rank. Besides, the problem (4.25) is non-convex. This further prevents us from obtaining a desired solution that validates the conditions for the application of CS.

Inspired by the form of (4.22), we propose a feasible and simple $\mathbf{W}$ by taking all the possible delays into account:

$$\mathbf{W} = [\mathbf{C}_0\mathbf{X}, \ldots, \mathbf{C}_{\tilde{L}}\mathbf{X}]. \tag{4.26}$$

Since $\mathbf{C}_i\mathbf{X}$ contains eigenvectors corresponding to the largest eigenvalues of $\mathbf{Q}_i$, utilizing (4.26) results in the average SIR_k bounded by

$$\textit{Bound } 2: \ \frac{|\beta_k|^2}{\sigma^2}\frac{1}{\tilde{L}+1} + \Delta \le \overline{SIR}_k \le \frac{|\beta_k|^2}{\sigma^2}\frac{M_t}{\tilde{L}+1} + \Delta \tag{4.27}$$

where Δ denotes $\frac{|\beta_k|^2}{\sigma^2 M_t(\tilde{L}+1)^2}\mathrm{Tr}\{\sum_{\tau'\neq\tau}\mathbf{X}^H\mathbf{C}_\tau^H\mathbf{Q}_{\tau'}\mathbf{C}_\tau\mathbf{X}\}$. One can see that *Bound* 2 would be reduced to *Bound* 1 when $\tilde{L} = 0$.

Next, we will examine the SIR yielded by the proposed measurement matrix $\mathbf{\Phi}_{\#2} = \mathbf{\Phi}\mathbf{W}^H$ based on three types of waveforms, rectangular pulse, independently generated

quadrature phase shift keying (QPSK) waveforms and Hadamard codes. As shown below, using $\mathbf{\Phi}_{\#2}$ can suppress interference uncorrelated with the transmit waveforms, and maintains coherence as low as the Gaussian random measurement matrix with the proper waveforms.

SIR under the conventional measurement matrix

Let us consider a conventional measurement matrix $\mathbf{\Phi}_c$, which is an $M\times(L+\tilde{L})$ Gaussian random matrix and $\mathrm{Tr}\{\mathbf{\Phi}_c\mathbf{\Phi}_c^H\} = M$. The average power of the interference is $P_n = \sigma^2 M$ (see (4.5)).

Let $\mathbf{S}_i$ be a square matrix, formed by shifting the main diagonal of $\mathbf{I}_L$ up by i. It can be easily seen that $\mathbf{S}_i^H = \mathbf{S}_{-i}$. The average power of the target returns from K targets at a receive node, conditioned on the transmit waveforms, is given by

$$P_s = E\{\mathbf{r}^H\mathbf{r}|\mathbf{X}\} = \sum_k P_s^k + \sum_{k\neq k'} P_s^{k,k'} \tag{4.28}$$

where

$$\begin{aligned} P_s^k &= |\beta_k|^2 E\{\mathrm{Tr}\{\mathbf{\Phi}_c\mathbf{C}_{\tau_k}\mathbf{X}\mathbf{v}(\theta_k)(\mathbf{\Phi}\mathbf{C}_{\tau_k}\mathbf{X}\mathbf{v}(\theta_k))^H\}\} \\ &\approx |\beta_k|^2 \mathrm{Tr}\{\mathbf{\Phi}_c\mathbf{C}_{\tau_k}\mathbf{X}\mathbf{X}^H\mathbf{C}_{\tau_k}^H\mathbf{\Phi}_c^H\} \\ &\approx \frac{M_t M|\beta_k|^2}{L+\tilde{L}} \end{aligned} \tag{4.29}$$

and

$$P_s^{k,k'} \approx \underbrace{\beta_k^*\beta_{k'}\varsigma^2\left(4\sin\left(\frac{\theta_k-\theta_{k'}}{2}\right)\right)e^{\frac{4\pi f(d_k(0)-d_{k'}(0))}{c}}}_{\gamma_{kk'}}\frac{M}{L+\tilde{L}}\mathrm{Tr}\{\mathbf{X}^H\mathbf{S}_{\tau_k-\tau_{k'}}\mathbf{X}\}. \tag{4.30}$$

SIR for the measurement matrix $\mathbf{\Phi}_{\#2}$

The proposed measurement matrix $\mathbf{\Phi}_{\#2} = \mathbf{\Phi}\mathbf{W}^H$ results in the same average interference power as the matrix $\mathbf{\Phi}_c$. The average power of the desired signal conditioned on the transmit waveforms, $\tilde{P}_s$, however, will improve. Like (4.28), $\tilde{P}_s$ can be partitioned into the sum of the autocorrelation, $\tilde{P}_s^k$, and cross correlation, $\tilde{P}_s^{k,k'}$, of the returns from K targets. It holds that

$$\begin{aligned}
\tilde{P}_s^k &= |\beta_k|^2 E\{\mathrm{Tr}\{\tilde{\mathbf{\Phi}}_{\#2}\mathbf{C}_{\tau_k}\mathbf{X}\mathbf{v}(\theta_k)(\tilde{\mathbf{\Phi}}_{\#2}\mathbf{C}_{\tau_k}\mathbf{X}\mathbf{v}(\theta_k))^H\}\} \\
&\approx |\beta_k|^2 \mathrm{Tr}\{\mathbf{\Phi}\mathbf{W}^H\mathbf{C}_{\tau_k}\mathbf{X}\mathbf{X}^H\mathbf{C}_{\tau_k}^H\mathbf{W}\mathbf{\Phi}^H\} \\
&\approx \frac{|\beta_k|^2 M}{(\tilde{L}+1)M_t}\mathrm{Tr}\{\mathbf{W}^H\mathbf{C}_{\tau_k}\mathbf{X}\mathbf{X}^H\mathbf{C}_{\tau_k}^H\mathbf{W}\} \\
&= \frac{|\beta_k|^2 M}{(\tilde{L}+1)M_t}\sum_{q=0}^{\tilde{L}}\mathrm{Tr}\{\mathbf{X}^H\mathbf{S}_{q-\tau_k}\mathbf{X}\mathbf{X}^H\mathbf{S}_{q-\tau_k}^H\mathbf{X}\} \qquad (4.31)
\end{aligned}$$

and

$$P_s^{k,k'} \approx \frac{\gamma_{kk'}M}{(\tilde{L}+1)M_t}\sum_{q=0}^{\tilde{L}}\mathrm{Tr}\{\mathbf{X}^H\mathbf{S}_{\tau_k-q}\mathbf{X}\mathbf{X}^H\mathbf{S}_{q-\tau_{k'}}\mathbf{X}\}. \qquad (4.32)$$

For orthogonal, or randomly generated waveforms across transmit nodes, $\tilde{P}_s^k$ always dominates the average power of the desired signal. In order to increase $\tilde{P}_s^k$, the quantity $\mathrm{Tr}\{\mathbf{X}^H\mathbf{S}_{q-\tau_k}\mathbf{X}\mathbf{X}^H\mathbf{S}_{q-\tau_k}^H\mathbf{X}\}$ in (4.31) needs to be as large as possible. $\mathbf{X}^H\mathbf{S}_m\mathbf{X}$ can be expressed as

$$\mathbf{X}^H\mathbf{S}_m\mathbf{X} = \begin{cases} \mathbf{X}_{1:L-m}^H\mathbf{X}_{m+1:L}, & m \geq 0 \\ \mathbf{X}_{1-m:L}^H\mathbf{X}_{1:L+m}, & \text{otherwise} \end{cases} \qquad (4.33)$$

where $\mathbf{X}_{i:j}$ denotes the matrix that contains the rows of $\mathbf{X}$ indexed from i to j.

Eq. (4.33) implies that the non-circular autocorrelation of the waveform sequence of a transmit node, i.e., $R_i(\tau) = \int_{t=0}^{T_p} x_i(t)x_i^*(t-\tau), i = 1, \ldots, M_t$, should be insensitive to the shift.

This essentially requires a narrowband signal. Based on this principle, the best candidate is a rectangular pulse and the maximum $\tilde{P}_s$ becomes

$$\tilde{P}_s = \frac{MM_t}{(\tilde{L}+1)} \sum_{k=1}^{K} \sum_{q=0}^{\tilde{L}} |\beta_k|^2 \left(\frac{L-|q-\tau_k|}{L} \right)^2 + \frac{MM_t}{(\tilde{L}+1)} \sum_{k \neq k'} \sum_{q=0}^{\tilde{L}} \gamma_{kk'} \frac{(L-|\tau_k - q|)(L-|q-\tau_{k'}|)}{L^2}$$
$$\leq MM_t \left(\sum_{k=1}^{K} |\beta_k|^2 + \sum_{k \neq k'} \gamma_{kk'} \right). \tag{4.34}$$

The equality holds only if targets induce identical delays and the sampling window of length exactly covers the duration of target returns. Obviously, transmit nodes cannot share the same waveforms. This is because the transmit waveforms are required to be orthogonal, or randomly generated in order to maintain low coherence of the basis matrix.

Similarly, the minimum average power of the desired signal is achieved when the randomly generated QPSK waveforms are utilized. This is because the random generated QPSK waveforms cover the widest bandwidth for the fixed pulsed duration T_p and the length of waveforms L. $\tilde{P}_s$ for the randomly generated QPSK waveforms is given by

$$\tilde{P}_s \approx \frac{M}{(\tilde{L}+1)} \sum_{k=1}^{K} |\beta_k|^2 (\sum_{q=0, q \neq \tau_k}^{\tilde{L}} M_t \frac{L-|q-\tau_k|}{L^2} + 1). \tag{4.35}$$

For orthogonal Hadamard waveforms that are of less bandwidth than the random generated QPSK waveforms, the average power of the desired signal is given by

$$\tilde{P}_s \approx \frac{M}{(\tilde{L}+1)} \sum_{k=1}^{K} \sum_{q=0}^{\tilde{L}} |\beta_k|^2 \left(\frac{L-|q-\tau_k|}{L} \right)^2. \tag{4.36}$$

Recall that $\mathbf{W}^*$ corresponding to the true delay gives rise to the maximum received signal power. Adding the terms $\mathbf{C}_{\tilde{\tau}_\mathbf{k}}\mathbf{X}, \tilde{\tau}_k \neq \tau_k$ to $\mathbf{W}$ (see (4.19)) would lower $\tilde{P}_s^k$. When a coarse delay estimate is available, we need to consider the delays around the coarse delay only and thus the length of sampling window can be shortened. This enables to reduce the number

of possible delays considered for the construction of $\mathbf{W}$. Therefore, $\tilde{P}_s^k$ can be improved for the waveforms considered above if the coarse delay is available.

The SIR gain

Let SIR_p and SIR_c denote the SIR obtained by using $\mathbf{\Phi}_{\#2}$ and conventional measurement matrices, respectively. When transmitting Hadamard codes, the SIR gain induced by using the proposed measurement matrix can be expressed as

$$\begin{aligned} r_{Ha} = \frac{P_s}{\tilde{P}_s} &\approx \frac{\frac{M}{(\tilde{L}+1)} \sum_{k=1}^{K} \sum_{q=0}^{\tilde{L}} |\beta_k|^2 \left(\frac{L-|q-\tau_k|}{L}\right)^2}{\sum_{k=1}^{K} \frac{M_t M |\beta_k|^2}{L+\tilde{L}}} \\ &= \frac{L+\tilde{L}}{M_t(\tilde{L}+1)L^2} \frac{\sum_{k=1}^{K} |\beta_k|^2 C_k}{\sum_{k=1}^{K} |\beta_k|^2} \end{aligned} \tag{4.37}$$

where

$$C_k = \sum_{q=0}^{\tilde{L}} (L - |q-\tau_k|)^2 = (\tilde{L}+1-2L)(\tau_k - \tilde{L}/2)^2 + \sum_{q=L-\tilde{L}}^{L} q^2 + \frac{(2L-\tilde{L}-1)\tilde{L}^2}{4}. \tag{4.38}$$

For a fixed $\tilde{L}$ and L, with $0 \le \tilde{L} \le 2L-1$, C_k can be bounded as

$$\sum_{q=L-\tilde{L}}^{L} q^2 \le C_k \le \sum_{q=L-\tilde{L}}^{L} q^2 + \frac{(2L-\tilde{L}-1)\tilde{L}^2}{4}. \tag{4.39}$$

Therefore, lower and upper bounds on the SIR gain using Hadamard codes are given

$$\frac{(L+\tilde{L})\sum_{q=L-\tilde{L}}^{L} q^2}{M_t(\tilde{L}+1)L^2} \le r_{Ha} \le \frac{(L+\tilde{L})(\sum_{q=L-\tilde{L}}^{L} q^2 + \frac{(2L-\tilde{L}-1)\tilde{L}^2}{4})}{M_t(\tilde{L}+1)L^2}. \tag{4.40}$$

Similarly, the SIR gain using randomly generated QPSK waveforms are bounded by

$$\frac{(L+\tilde{L})(\sum_{q=L-\tilde{L}}^{L} q + \frac{L^2}{M_t} - L)}{(\tilde{L}+1)L^2} \le r_{QPSK} \le \frac{(L+\tilde{L})(\sum_{q=L-\tilde{L}}^{L} q + \frac{\tilde{L}^2}{4} + \frac{L^2}{M_t} - L)}{(\tilde{L}+1)L^2}. \tag{4.41}$$

As long as $\tilde{L} < L$ and $M_t < L$, r_{QPSK} is always greater than 1. When $\frac{\sum_{q=L-\tilde{L}}^{L} q^2}{M_t \sum_{q=L-\tilde{L}}^{L} q} > 1$, the lower bound on r_{Ha} is higher than that on r_{QPSK}. For a sufficiently long L and moderate M_t, r_{Ha} would be superior to r_{QPSK}. Based on (4.34) and (4.36), one can infer that the SIR gain using the rectangular pulse is approximately M_t times greater than using Hadamard codes.

The CSM based on the suboptimal measurement matrix #2

In this section, we will examine the effect of the proposed $\mathbf{W}$ in (4.26) on the coherence of sensing matrix. For simplicity, we consider stationary targets and the possible delays for constructing $\mathbf{W}$ are based on the range grid points used to form the basis matrix. Then the sensing matrix with the measurement matrix $\mathbf{\Phi}_{\#2}$, or the Gaussian random matrix can be respectively represented as

$$\mathbf{\Theta} = \mathbf{\Phi}_{\#2}\mathbf{\Psi} = \mathbf{\Phi}_{M\times(\tilde{L}+1)M_t}\mathbf{W}^H\mathbf{W}\mathbf{V} \tag{4.42}$$

and

$$\tilde{\mathbf{\Theta}} = \mathbf{\Phi}_{M\times(L+\tilde{L})}\mathbf{\Psi} = \mathbf{\Phi}_{M\times(L+\tilde{L})}\mathbf{W}\mathbf{V} \tag{4.43}$$

where $\mathbf{V} = kron(\mathbf{I}_{\tilde{L}+1}, [\mathbf{v}(a_1), \ldots, \mathbf{v}(a_{N_a})])$ and $\mathbf{\Phi}_{i\times j}$ is an $i\times j$ Gaussian random matrix whose entries are of zero mean and variance $1/j$. For sufficiently large j, the column coherence of $\mathbf{\Theta}$ can be approximated as

$$\mu_{kk'}(\mathbf{\Theta}) = \frac{|\sum_i(\sum_m \Phi(m,i)\Phi^*(m,i))v_{kk'}(i)|}{\sqrt{\sum_i(\sum_m \Phi(m,i)\Phi^*(m,i))v_{kk}(i)\ \sum_i(\sum_m \Phi(m,i)\Phi^*(m,i))v_{k'k'}(i)}} \tag{4.44}$$

where $v_{kk'}(i)$ denotes the i-th diagonal element of the matrix $\mathbf{W}^H\mathbf{C}_{\lfloor\frac{2c_k}{cT_s}\rfloor}\mathbf{X}\mathbf{v}_m(a_k)\left(\mathbf{W}^H\mathbf{C}_{\lfloor\frac{2c_{k'}}{cT_s}\rfloor}\mathbf{X}\mathbf{v}_m(a_{k'})\right)^H$. Without loss of generality, we let the columns of $\mathbf{\Phi}$ be of unit norm. Then (4.44) can be

further written as

$$\mu_{kk'}(\boldsymbol{\Theta}) = \frac{|\sum_i v_{kk'}(i)|}{\sqrt{\sum_i v_{kk}(i) \sum_i v_{k'k'}(i)}}. \tag{4.45}$$

One can easily see from (4.45) that the coherence of $\boldsymbol{\Theta}$ is approximately equal to that of matrix $\mathbf{W}^H\mathbf{W}\mathbf{V}$. The same conclusion applies to $\tilde{\boldsymbol{\Theta}}$ as well, i.e., the coherence of $\tilde{\boldsymbol{\Theta}}$ is approximately equal to that of matrix $\mathbf{W}\mathbf{V}$. Since $\mathbf{W}^H\mathbf{W}$ is more ill-conditioned than $\mathbf{W}$, the conditional number of $\mathbf{W}^H\mathbf{W}\mathbf{V}$ is greater than that of $\mathbf{W}^H\mathbf{W}$. Therefore, utilizing $\boldsymbol{\Phi}_{\#2}$ increases the maximum CSM as compared to the Gaussian random measurement matrix with high probability. However, for the well conditioned $\mathbf{W}$, the increase of maximum CSM caused by $\boldsymbol{\Phi}_{\#2}$ can be neglected.

4.2.3 $\boldsymbol{\Phi}_{\#1}$ v.s. $\boldsymbol{\Phi}_{\#2}$

We have proposed two measurement matrices based on different performance metric. The advantages and disadvantages of $\boldsymbol{\Phi}_{\#1}$ and $\boldsymbol{\Phi}_{\#2}$ are summarized as follows.

- *Complexity*

  Solving $\boldsymbol{\Phi}_{\#1}$ involves a complex optimization problem and depends on a particular basis matrix, while $\boldsymbol{\Phi}_{\#2}$ only requires the knowledge of all the possible discretized time delays. Therefore, the construction of $\boldsymbol{\Phi}_{\#1}$ requires much more computations than does $\boldsymbol{\Phi}_{\#2}$.

- *Performance*

  $\boldsymbol{\Phi}_{\#1}$ aims at decreasing the coherence of the sensing matrix and enhancing SIR simultaneously. The tradeoff between CSM and SIR results in $\boldsymbol{\Phi}_{\#1}$ yielding lower SIR than $\boldsymbol{\Phi}_{\#2}$. Therefore, $\boldsymbol{\Phi}_{\#1}$ is expected to perform better than $\boldsymbol{\Phi}_{\#2}$ in the case of low interferences, while it should perform worse in the presence of strong interferences.

4.3 Simulation Results

In this section, we show the performance of CS-based MIMO radar when using the proposed measurement matrices $\mathbf{\Phi}_{\#1}$ and $\mathbf{\Phi}_{\#2}$, respectively. We consider a MIMO radar system with transmit and receive nodes uniformly located on a disk of radius 10m. The carrier frequency is $f = 5GHz$. The received signal is corrupted by zero-mean Gaussian noise. The signal-to-noise ratio (SNR) is defined as the inverse of the power of thermal noise at a receive node. A jammer is located at angle 7^o and transmits an unknown Gaussian random waveform. The targets are assumed to fall on the grid points.

4.3.1 The proposed measurement matrix $\mathbf{\Phi}_{\#2}$

SIR improvement

$M = 30$ compressed measurements are forwarded to the fusion center by each receive node. The maximum possible delay is $\tilde{L} = 100$. Figure 4.1 compares the numerical and theoretical SIR produced using the rectangular-pulse, Hadamard waveforms and randomly generated QPSK waveforms for the case of $M_t = 30$ transmit nodes and $N_r = 1$ receive node. The SIR performance, shown in Fig. 4.1, is the average of 1000 independent and random runs. The theoretical SIR of these three sequences are calculated based on (4.34), (4.36) and (4.35). The power of thermal noise is fixed to 1 and the power of the jammer varies from -20dB to 60dB. Applying the proposed measurement $\mathbf{\Phi}_{\#2}$ at the receivers, the rectangular pulse and Hadamard waveforms produce a significant SIR gain over the Gaussian random measurement matrix (GRMM), while the random QPSK sequence achieves almost no gain. Furthermore, the numerical SIR performance follows the theoretical SIR for all three sequences. Figure 4.2 demonstrates the SIR performance averaging over 500 independent and random runs for different values of the maximum time delay $\tilde{L}$. We consider a case in which only one target exists and the jammer power is 225. One can see

that a decrease in $\tilde{L}$ can significantly improve SIR yielded by QPSK waveforms when $\tilde{L}$ is less than 10. In contrast, Hadamard waveforms and rectangular pulse produce almost the same SIR for different values of $\tilde{L}$. This indicates that the prior information of possible delays enables SIR improvement for QPSK waveforms rather than the other two types of waveforms.

The CSM

Figure. 4.3 shows the histograms of the condition number and the maximum CSM using $\mathbf{\Phi}_{\#2}$ for Hadamard waveforms and the GRMM produced in 100 random and independent runs. We consider the case of $M = 30$, $M_t = N_r = 10$ and the grid step of the discretized angle-range space is $[0.5^{o}, 15m]$. One can see that the numerical results fit the observations in Section 4.2.2, i.e., $\mathbf{\Phi}_{\#2}$ increases the maximum CSM as compared to the GRMM with high probability. In Fig. 4.4 we use histograms to compare the CSM corresponding to adjacent columns over 100 independent and random runs. Although $\mathbf{\Phi}_{\#2}$ incorporates information on the waveforms, the distribution of the column correlation does not change significantly as compared to that of the conventional matrix. Among the three types of waveforms, the rectangular pulse gives rise to the worst CSM distribution, indicating that the performance of the proposed CS approach would be significantly degraded if rectangular pulses are transmitted. This is because the high autocorrelation of the rectangular pulse results in high CSM independent of the measurement matrix used.

In Table 1, we compare the CSM and the SIR based on $\mathbf{\Phi}_{\#2}$ using rectangular pulse, Hadamard waveforms and randomly generated QPSK waveforms. One can see that Hadamard waveforms can enhance SIR and preserve low coherence of the sensing matrix simultaneously.

Table 4.1: The comparison of SIR and CSM

	Rectangular pulse	Hadamard	QPSK
SIR	best	second best	worst
Coherence	worst	second best	best

4.3.2 The proposed measurement matrix $\mathbf{\Phi}_{\#1}$

We consider a scenario in which $M_t = Nr = 4$ and three stationary targets exist. The azimuth angle and range of three targets are randomly generated in 100 runs within $[0^o, 1^o]$ and $[1000m, 1090m]$, respectively. The data of one pulse is utilized and thus only the angle-range estimates can be obtained. The spacing of adjacent angle-range grid points is $[0.2^o, 15m]$. $\mathbf{\Phi_{\#1}}$ is obtained from (4.9) based on the special structure of (4.12). $\mathbf{\Phi}$ in (4.12) is replaced with $\mathbf{\Phi_{\#2}}$. We consider different values of the tradeoff coefficient $\tilde{\lambda}$ in (4.9). Transmit nodes send Hadamard waveforms of length $L = 128$. Only $M = 20$ measurements per pulse are collected and forwarded to the fusion center by each node for CS-based MIMO radar while 100 measurements feed MIMO radar based on the MFM.

Figure. 4.5 shows the distribution of CSM for the GRMM, $\mathbf{\Phi_{\#1}}$ and $\mathbf{\Phi_{\#2}}$ in 100 random and independent runs. One can see that the GRMM and $\mathbf{\Phi_{\#2}}$ lead to the similar coherence distribution. $\mathbf{\Phi_{\#1}}$ slightly reduces the maximum CSM and significantly increases the number of column pairs with low coherence as compared to the other two measurement matrices. $\mathbf{\Phi_{\#1}}$ solved from (4.9) using $\tilde{\lambda} = 0.6$ and $\tilde{\lambda} = 1.5$ produce the similar coherence distribution. Fig. 4.6 shows the SIR performance of CS-based MIMO radar using the GRMM, $\mathbf{\Phi_{\#1}}$ and $\mathbf{\Phi_{\#2}}$ for difference values of noise power in absence of jammer. One can see from Fig. 4.6 that $\mathbf{\Phi_{\#2}}$ outperforms the other two measurement matrices in terms of SIR. $\mathbf{\Phi_{\#1}}$ obtained from (4.9) using $\tilde{\lambda} = 0.6$ yields slightly better SIR than GRMM. As expected, increasing $\tilde{\lambda}$ from 0.6 to 1.5 moderately improves SIR.

Figure 4.7 and Fig. 4.8 compare the ROC performance of CS-based MIMO radar using

the three aforementioned measurement matrices and MIMO radar based on the MFM, for different combinations of SNR and jammer-signal power. The probability of detection (PD) here denotes the percentage of cases in which all the targets are detected. The percentage of cases in which false targets are detected is denoted by the probability of false alarm (PFA). It is demonstrated in Fig. 4.7 and Fig. 4.8 that $\mathbf{\Phi}_{\#1}$ and $\mathbf{\Phi}_{\#2}$ with the Hadamard waveforms can improve detection accuracy as compared to the GRMM in the case of mild and strong interference, respectively. Since an increase in the tradeoff coefficient $\tilde{\lambda}$ can enhance SIR, $\mathbf{\Phi}_{\#1}$ solved from (4.9) using $\tilde{\lambda} = 1.5$ can perform better in the case of strong interference than using $\tilde{\lambda} = 0.6$. Note that the three measurement matrices give rise to similar performance for $SNR = 10dB$ and $\beta = 0$. This is because the interference is sufficiently small so that all the measurement matrices perform well. Again, one can see that the MFM is inferior to the CS approach even with far more measurements than the CS approach.

It has been seen from Fig. 4.7 and Fig. 4.8 that the tradeoff coefficient $\tilde{\lambda}$ affects the performance of CS-based MIMO radar using $\mathbf{\Phi}_{\#1}$. In order to further investigate the effect of $\tilde{\lambda}$, the curves of probability of detection accuracy are shown in Fig. 4.9 for $\tilde{\lambda} = 0.6, 1, 1.5, 2$ v.s. different thresholds of hard detection. The probability of detection accuracy here denotes the percentage of cases in which all the targets are detected and no false estimation as well. By taking all the four combinations of SNR and jammer-signal power into account, $\tilde{\lambda} = 1.5$ excels the other three values of tradeoff coefficient. For a particular case, the optimal tradeoff coefficient depends on multiple factors, i.e., the basis matrix and the interferences. The manner in which SIR and the CSM affect the support recovery of a sparse signal still remains to be clarified. Therefore, it is impossible to theoretically determine the optimal tradeoff coefficient.

4.4 Conclusions

We have proposed two measurement matrices in order to improve target detection performance of CS-based MIMO radar for the case in which the targets may be located across several range bins. The first one $\mathbf{\Phi}_{\#1}$ aims at enhancing SIR and reducing the CSM at the same time. It is obtained by solving a convex optimization problem. This measurement matrix requires heavy computational load as compared to the conventional measurement matrix, and also needs to adapt to a particular basis matrix. The computational burden of solving $\mathbf{\Phi}_{\#1}$ can be alleviated through reducing the number of variables involved in the optimization problem. The second proposed measurement matrix $\mathbf{\Phi}_{\#2}$ targets improving SIR only. It is constructed based on the transmit waveforms and also accounts for all possible discretized delays of target returns within the given time window. $\mathbf{\Phi}_{\#2}$ is dependent of the range grid only and requires much lower complexity than $\mathbf{\Phi}_{\#1}$. It is shown that $\mathbf{\Phi}_{\#2}$ based on reduced bandwidth transmit waveforms can improves SIR, but on the other hand, using waveforms that are too narrowband increases the CSM, thus invalidating conditions for the application of the CS approach. Therefore, the waveforms must be chosen carefully to guarantee the desired performance using the second measurement matrix. Numerical results show that $\mathbf{\Phi}_{\#1}$ and $\mathbf{\Phi}_{\#2}$ with the proper waveforms (e.g.,Hadamard waveforms) can improve detection accuracy as compared to the Gaussian random measurement matrix in the case of small and strong interference, respectively.

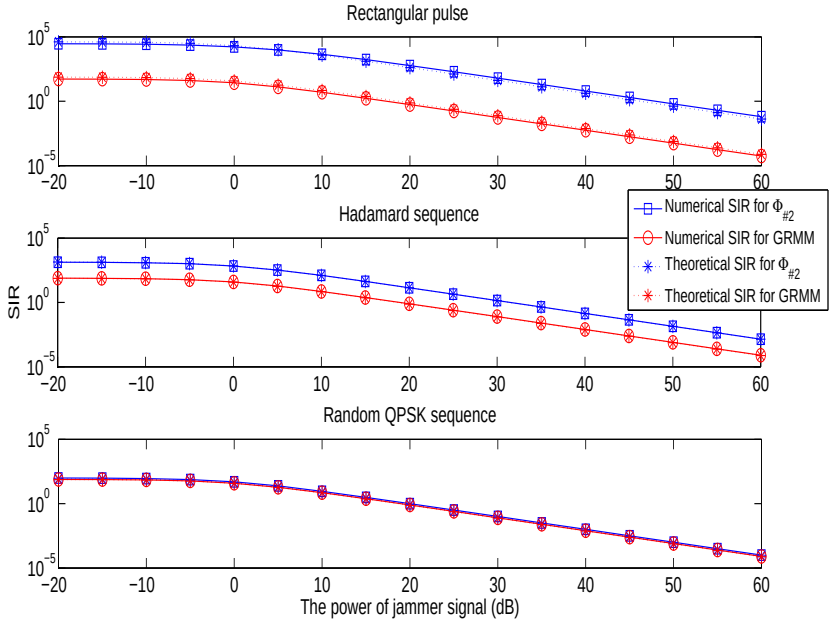

Figure 4.1: SIR produced by the GRMM and $\mathbf{\Phi}_{\#2}$ for different transmit waveforms ($M = M_t = 30$ and $N_r = 1$).

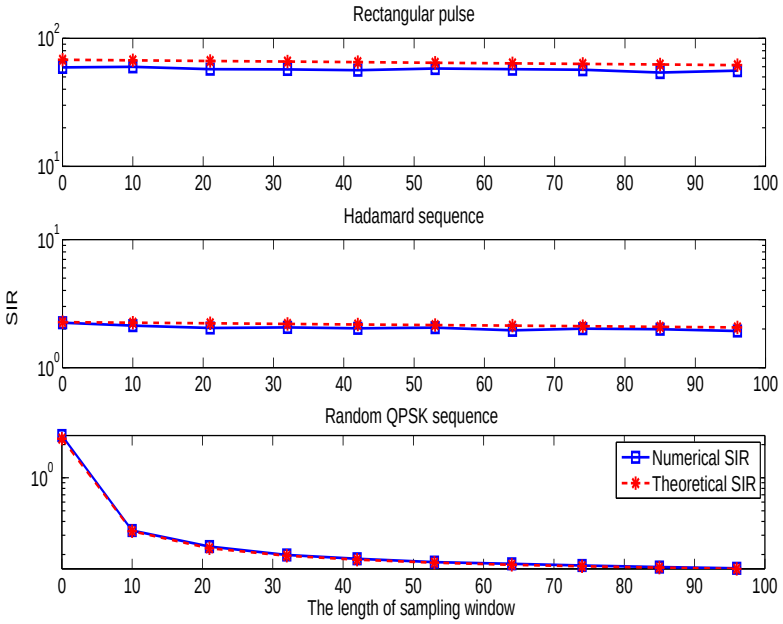

Figure 4.2: SIR produced by $\mathbf{\Phi}_{\#2}$ for different values of $\tilde{L}$ ($M = M_t = 30$ and $N_r = 1$).

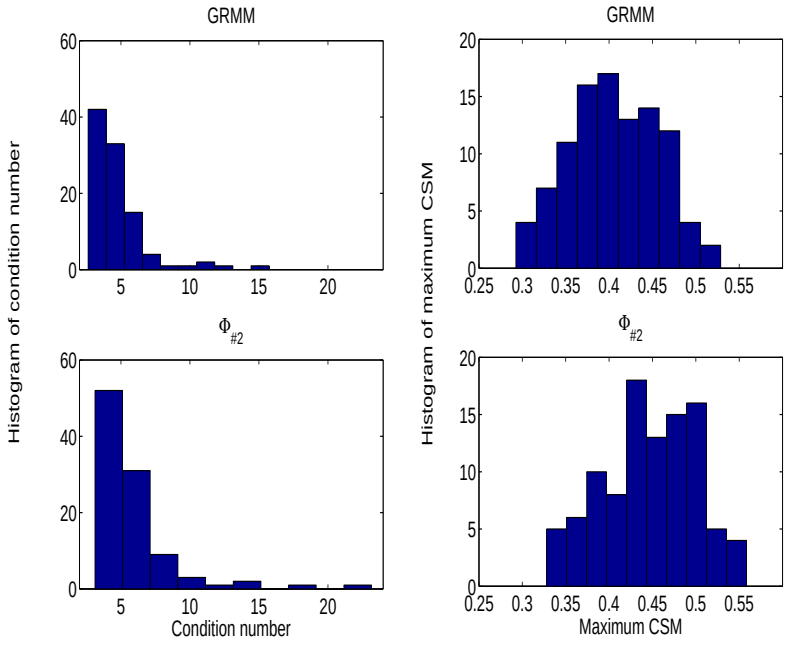

Figure 4.3: Conditional number and the maximum coherence of the sensing matrix based on $\mathbf{\Phi}_{\#2}$ ($M = 30$ and $N_r = M_t = 10$).

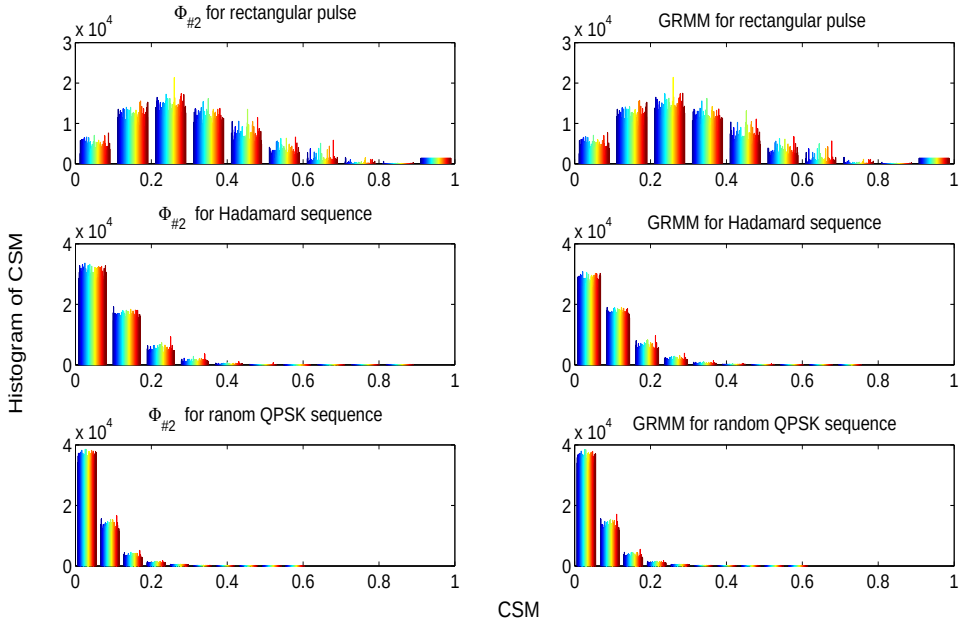

Figure 4.4: Coherence of adjacent columns of the sensing matrix based on $\mathbf{\Phi}_{\#2}$ for different transmit sequences ($M = 30$ and $M_t = N_r = 10$).

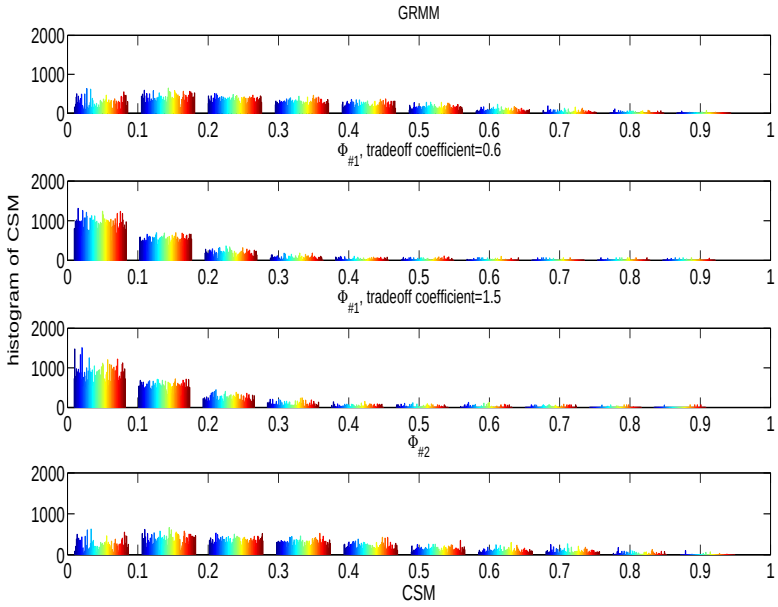

Figure 4.5: Coherence distribution of cross columns of the sensing matrix using $\mathbf{\Phi}_{\#1}$, $\mathbf{\Phi}_{\#2}$ and the GRMM ($M_t = N_r = 4$).

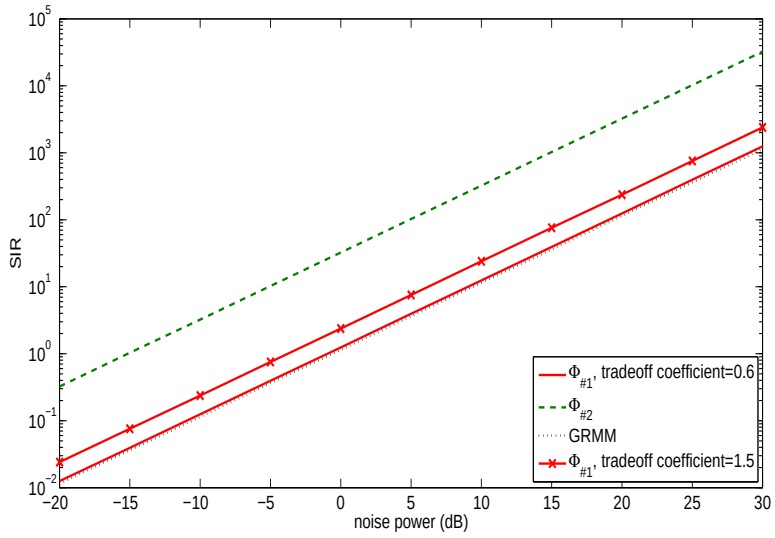

Figure 4.6: SIR for CS-based MIMO radar using $\mathbf{\Phi}_{\#1}$, $\mathbf{\Phi}_{\#2}$ and GRMM for different values of noise power ($M_t = N_r = 4$).

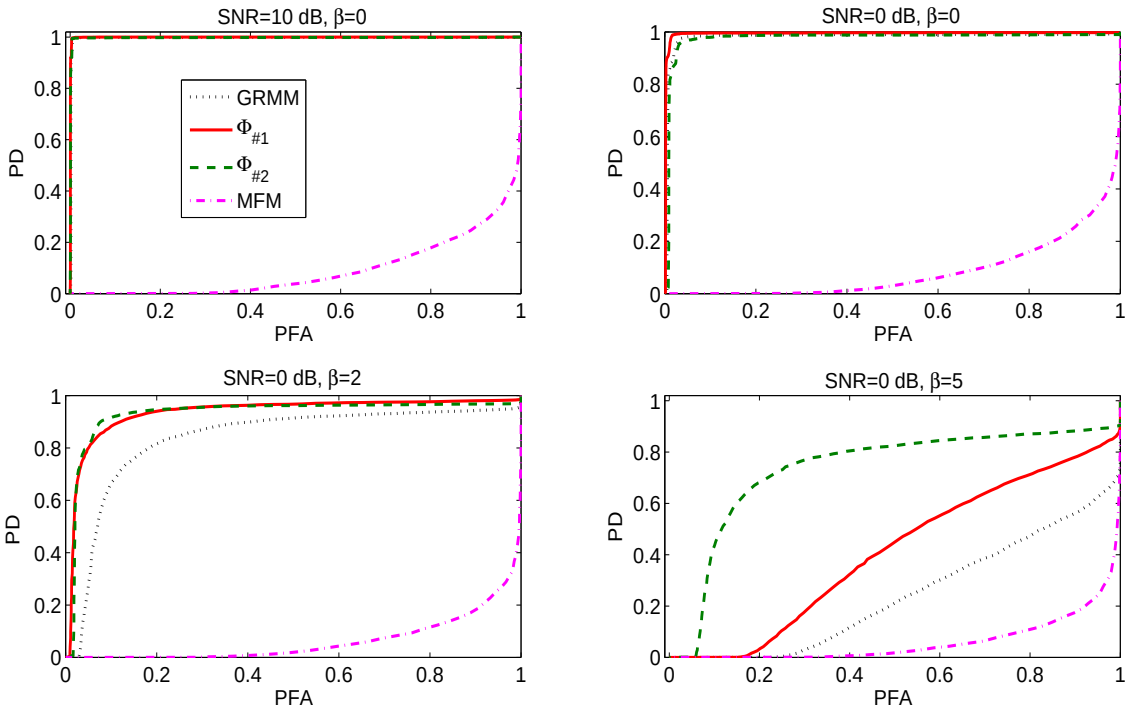

Figure 4.7: ROC curves for CS-based MIMO radar using $\mathbf{\Phi}_{\#1}$, $\mathbf{\Phi}_{\#2}$ and the GRMM, and for MIMO radar using the MFM ($M_t = N_r = 4$ and $\tilde{\lambda} = 0.6$).

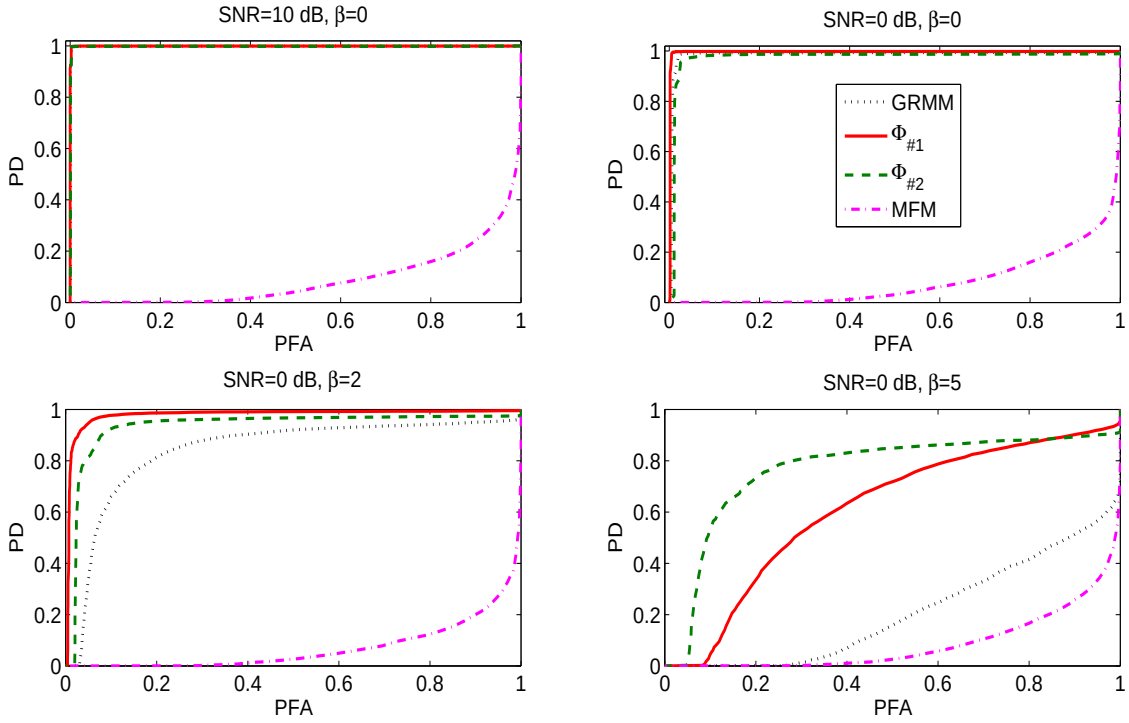

Figure 4.8: ROC curves for CS-based MIMO radar using $\mathbf{\Phi}_{\#1}$, $\mathbf{\Phi}_{\#2}$ and the GRMM, and for MIMO radar using the MFM ($M_t = N_r = 4$ and $\tilde{\lambda} = 1.5$).

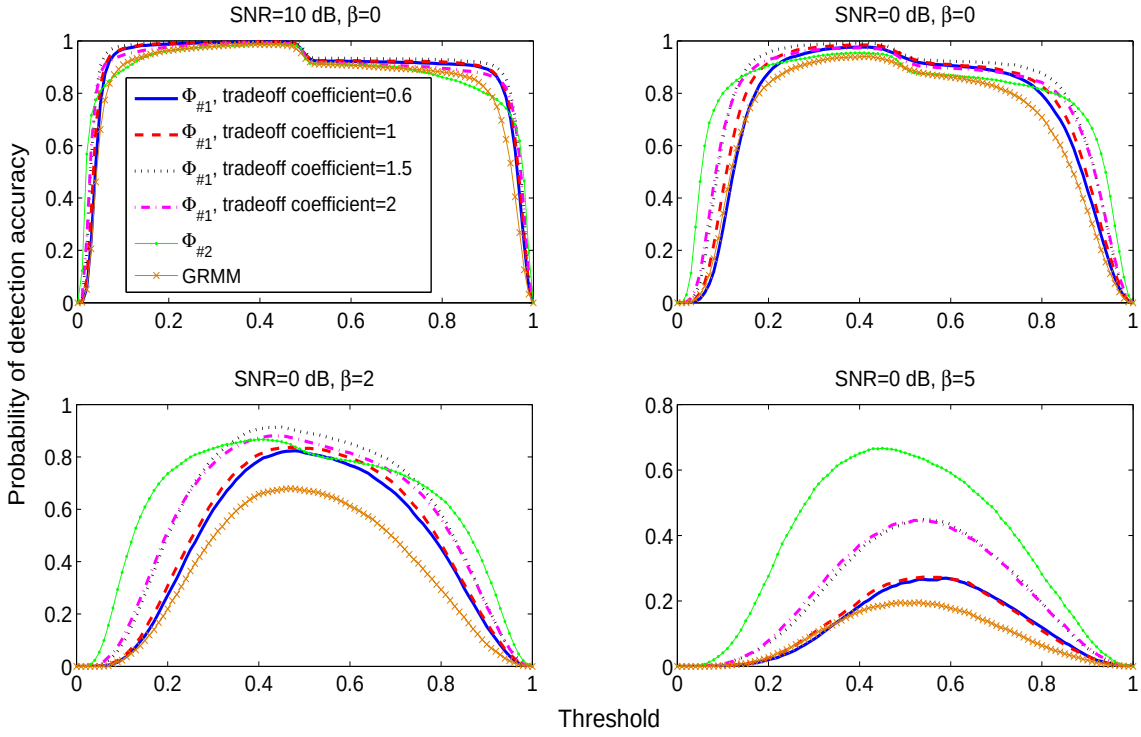

Figure 4.9: The probability of detection accuracy for CS-based MIMO radar using $\boldsymbol{\Phi}_{\#1}$, $\boldsymbol{\Phi}_{\#2}$ and the GRMM for different values of $\tilde{\lambda}$ ($M_t = N_r = 4$).

5. Summary and Suggested Future Research

5.1 Summary

In this dissertation, we have proposed a CS-based MIMO radar system that is implemented by a small-scale wireless network. Network nodes serve as transmitters or receivers. Each receive node applies compressive sampling to the received signal to obtain a small number of samples, which the node subsequently forwards to a fusion center. At the fusion center, the information on angle, Doppler and range is extracted.

First, we have presented an DOA-Doppler estimation approach for the case in which the targets are located in a small range bin and the sampling is synchronized with the first target return. Assuming that the targets are sparsely located in the angle-Doppler space, the fusion center formulates an ℓ_1-optimization problem, the solution of which yields target angle and Doppler information. For the stationary case, the performance of the proposed approach was compared to that of conventional approaches that have been proposed in the context of MIMO radar, i.e., Capon, APES, GLRT or MUSIC. For a mild jammer, the proposed method has been shown to be at least as good as the Capon, APES, GLRT and MUSIC techniques while using a significantly smaller number of samples. In the case of strong thermal noise and strong jammer, the proposed method performs slightly worse than the GLRT method. In that case, its performance is still acceptable, especially if one takes into account the fact that it uses significantly fewer samples than GLRT. For the case of moving targets, the proposed approach was compared to the MFM, and was shown to perform better in both single and multiple receive nodes cases.

In the second part of this dissertation we have considered a more general case that does not confine the targets to be within the same range cell, nor does it requires sampling synchronization. Unlike the case considered above for DOA-Doppler estimation, this general

case allows for range estimation. We presented a CSSF MIMO radar system that applies SF to CS-based MIMO radar. The technique of SF can significantly improve range resolution. We have shown that CSSF MIMO radar has the potential to achieve better resolution than MFSF MIMO radar, and that more pulses are required by RSFR than by LSFR to achieve the desired performance with all other parameters being the same. The angle-Doppler-range estimation requires discretization of the angle-Doppler-range space into a large number of grid points, which would increase the complexity of the CS approach. We have presented a CSSF MIMO radar scheme that by decoupling angle-range estimation and Doppler estimation achieves significant complexity reduction. The proposed technique applies to slowly moving targets and relies on initial rough angle-range estimates. Assuming that the initial estimates do not miss any targets, the proposed low complexity scheme maintains the high resolution of the CS approach.

Finally, We have proposed two measurement matrices in order to improve target detection performance of CS-based MIMO radar for the case in which the targets may be located across several range bins. The first one $\mathbf{\Phi}_{\#1}$ aims at enhancing SIR and reducing the CSM at the same time. It is obtained by solving a convex optimization problem. This measurement matrix requires heavy computational load as compared to the conventional measurement matrix, and also needs to adapt to a particular basis matrix. The complexity of solving $\mathbf{\Phi}_{\#1}$ can be reduced through minishing the number of variables involved in the optimization problem. The second proposed measurement matrix $\mathbf{\Phi}_{\#2}$ targets improving SIR only. It is constructed based on the transmit waveforms and also accounts for all possible discretized delays of target returns within the given time window. $\mathbf{\Phi}_{\#2}$ is dependent of the range grid only and requires much lower complexity than $\mathbf{\Phi}_{\#1}$. It is shown that $\mathbf{\Phi}_{\#2}$ based on reduced bandwidth transmit waveforms can improves SIR, but on the other hand, using waveforms that are too narrowband increases the coherence of the sensing matrix, thus invalidating conditions for the application of the CS approach. Therefore, the waveforms must be cho-

sen carefully to guarantee the desired performance using the second measurement matrix. Numerical results show that $\mathbf{\Phi}_{\#1}$ and $\mathbf{\Phi}_{\#2}$ with the proper waveforms (e.g.,Hadamard codes) can improve detection accuracy as compared to the Gaussian random measurement matrix in the case of small and strong interference, respectively.

5.2 Suggested Future Research

5.2.1 Node selection

We have considered a small scale network that acts as a MIMO radar system. Each node is equipped with one antenna, and the nodes are distributed at random on a disk of a certain radius. It should be worth investigating selecting TX and RX nodes to achieve a certain goal. There are two subtopics related to node selection:

- Select the minimum number of nodes to achieve desired performance given node locations;
- Find node locations to optimize performance of target detection given the number of nodes.

5.2.2 Target tracking

We have discussed target detection for CS-based MIMO radar in this dissertation. Based on the initial information on targets, we can keep tracking targets by using the latest data. In [68] and [69], the authors considered the problem of recursively reconstructing sparse signals in which the sparsity pattern changes slowly with time. They proposed CS schemes that make use of the signal support estimate in the previous instant and the new observations to update the support estimates. Support here refers to the location of the non-zero elements in the signal sparse representation The schemes of [68] and [69] were shown to lead to higher quality reconstructed image than using CS without any support informa-

tion for single-pixel camera imaging and static/dynamic MRI. Applying a similar approach to target tracking for CS-based MIMO radar is an interesting future research topic for the case of slowly moving targets.

Bibliography

[1] M.I. Skolnik, *Introduction to radar systems*, Boston: McGraw-Hill, 2001.

[2] B.R. Mahafza and A.Z. Elsherbeni, *MATLAB simulations for radar systems design*, Chapman and Hall/CRC, 2004.

[3] M.A. Richards, *Fundamentals of radar signal processing*, NY: McGraw-Hill, 2005.

[4] M.I. Skolnik, *Radar handbook*, New York: McGraw-Hill, 1990.

[5] W.D. Wirth, *Radar techniques using array antennas*, London: Institution of Electrical Engineers, 2001.

[6] D. Tse and P. Viswanath, *Fundamentals of wireless communication.*, Cambridge: Cambridge Univ Press, UK, 2005.

[7] E. Fishler, A. Haimovich, R. Blum, D. Chizhik, L. Cimini and R. Valenzuela, " MIMO radar: An idea whose time has come," in *Proc. IEEE Radar Conf.*, Philadelphia, PA, pp. 71-78, Apr. 2004.

[8] E. Fishler, A. Haimovich, R. Blum, L. Cimini, D. Chizhik and R. Valenzuela, "Performance of MIMO radar systems: advantages of angular diversity," in *Proc. 38th Asilomar Conf. Signals, Syst. Comput.*, Pacific Grove, CA, pp. 305-309, Nov. 2004.

[9] A.M. Haimovich, R.S. Blum and L.J. Cimini, "MIMO radar with widely separated antennas," *IEEE Signal Processing Magazine*, vol. 25, no. 1, pp. 116-129, Jan. 2008.

[10] E. Fishler, A.M. Haimovich, R. Blum, L. Cimini, D. Chizhik, and R. Valenzuela, "Spatial diversity in radars-models and detection performance," *IEEE Trans. Signal Process.*, vol. 54, no. 3, pp. 823-838, Mar. 2006.

[11] N.H. Lehmann, A.M. Haimovich, R.S. Blum, and L.J. Cimini, "High resolution capabilities of MIMO radar," in *Proc. 40th Asilomar Conf. Signals, Systems and Computers*, Pacific Grove, CA, pp. 25-30, Nov. 2006.

[12] P. Stoica and J. Li , "MIMO radar with colocated antennas," *IEEE Signal Processing Magazine*, vol. 24, no.5, pp. 106-114, Sep. 2007.

[13] J. Li, P. Stoica, L. Xu and W. Roberts, "On parameter identifiability of MIMO radar," *IEEE Signal Process. Lett.*, vol. 14, no. 12, pp. 968-971, Dec. 2007.

[14] L. Xu, J. Li and P. Stoica, " Radar imaging via adaptive MIMO techniques," in *Proc. European Signal Process. Conf.*, Florence, Italy, Sep. 2006.

[15] P. Stoica, J. Li and Y. Xie, "On probing signal design for MIMO radar," *IEEE Trans. Signal Process.*, vol. 55, no.8, pp. 4151-4161, Aug. 2007.

[16] T. Aittomaki and V. Koivunen, "Signal covariance matrix optimization for transmit beamforming in MIMO radars," in *Proc. 38th Asilomar Conf. Signals, Syst. Comput.*, Pacific Grove, CA, pp. 182-186, Nov. 2007

[17] D.R. Fuhrmann and G. San Antonio, "Transmit beamforming for MIMO radar systems using signal cross-correlation," *IEEE Trans. Aerospace and Electronic Systems*, vol. 44, no.1, pp. 171-186, January 2008.

[18] D.V. Donoho, "Compressed sensing," *IEEE Trans. Information Theory*, vol. 52, no. 4, pp. 1289-1306, April 2006.

[19] E.J. Candes, "Compressive sampling," *Proceedings of the International Congress of Mathematicians*, Madrid, Spain, 2006.

[20] E.J. Candes and M. B. Wakin, "An introduction to compressive sampling [A sensing/sampling paradigm that goes against the common knowledge in data acquisition]," *IEEE Signal Processing Magazine*, vol. 25, no. 2, pp. 21-30 , Mar. 2008.

[21] J. Romberg, "Imaging via compressive sampling [Introduction to compressive sampling and recovery via convex programming]," *IEEE Signal Process. Mag.*, vol. 25, no. 2, pp. 14-20, Mar. 2008.

[22] W. Bajwa, J. Haupt, A. Sayeed and R. Nowak, "Compressive wireless sensing," in *Proc. IEEE Inform. Process. in Sensor Networks*, Nashville, TN, pp. 134-142, Apr. 2006.

[23] J. L.Paredes, G. R. Arce, Z. Wang, "Ultra-wideband compressed sensing: channel estimation," *IEEE Journal of Selected Topics in Signal Processing*, vol.1, no. 3, pp. 383-395, Oct. 2007.

[24] J.A. Tropp and A.C. Gilbert, "Signal recovery from random measurement via orthogonal matching pursuit," *IEEE Trans. Informa. Theory*, vol. 53, no. 12, pp. 4655-4666, Dec. 2007.

[25] D. Needell and R. Vershynin, " Signal recovery from incomplete and inaccurate measurements via regularized orthogonal matching pursuit," *IEEE Journal of Selected Topics in Signal Process.*, vol. 4, no. 2, pp. 310-316, Apr. 2010.

[26] D. Needell and R. Vershynin, "Uniform uncertainty principle and signal recovery via regularized orthogonal matching pursuit," *Found. Comput. Math.*, vol. 9, no. 3, pp. 317-334, Apr. 2009.

[27] D. Needell and R. Vershynin, " COSAMP: Iterative signal recovery from incomplete and inaccurate samples," *Applied and Computational Harmonic Analysis*, vol. 26, no. 3, pp. 301-321, Apr. 2008.

[28] J.A. Tropp, "Just relax: convex programming methods for identifying sparse signals in noise," *IEEE Trans. Informa. Theory*, vol. 52, no. 3, pp. 1030-1051, Mar. 2006.

[29] E.J. Candes and J. Romberg, "ℓ_1-MAGIC: Recovery of sparse signals via convex programing," http://www.acm.caltech.edu/l1magic/, October 2008.

[30] S. Winter, H. Sawada and S. Makino "On real and complex valued ℓ_1-norm minimization for overcomplete blind source seperation," in *Proc. IEEE Workshop on Applications of Signal Process. to Audio and Acoustics*, New Paltz, NY, pp. 86-89, Oct. 2005.

[31] E.J. Candes, J. Romberg, and T. Tao, "Robust uncertainty principles: Exact signal reconstruction from highly incomplete frequency information," *IEEE Trans. Inform. Theory*, vol. 52, no. 2, pp. 489-509, Feb. 2006.

[32] E.J. Candes and T. Tao, "Near optimal signal recovery from random projections: universal encoding strategies?," *IEEE Trans. Inform. Theory*, vol. 52, no. 12, pp. 5406-5425, Dec. 2006.

[33] E.J. Candes and T. Tao, "Decoding by linear programming," *IEEE Trans. Inform. Theory*, vol. 51, no. 12, pp. 4203-4215, Dec. 2005.

[34] R. Baraniuk and P. Steeghs, "Compressive radar imaging," *Proc. Radar Conference*, pp. 128-133, April, 2007.

[35] A. C. Gurbuz, J. H. McClellan and W.R. Scott, "Compressive sensing for GPR imaging," *Proc. 41th Asilomar Conf. Signals, Syst. Comput*, pp. 2223-2227, Pacific Grove, CA, Nov. 2007.

[36] M. Herman and T. Strohmer, "Compressed rensing radar," in *Proc. IEEE Int'l Conf. Acoust. Speech Signal Process*, Las Vegas, NV, pp. 2617-2620, Mar. - Apr. 2008.

[37] A. C. Gurbuz, J. H. McClellan, V. Cevher, "A compressive beamforming method," in *Proc. IEEE Int'l Conf. Acoust. Speech Signal Process*, Las Vegas, NV, pp. 2617-2620, Mar. - Apr. 2008.

[38] H. Shu and Q. Liang, "Data fusion in a multi-target radar sensor network," in *Proc IEEE Radio and Wireless Symposium 2010,*, Long Beach, CA, pp. 129-132, Jan. 2007.

[39] Nadav Levanon and Eli Mozeson, *Radar Signals*, Hoboken, NJ: J. Wiley, 2004.

[40] A. P. Petropulu, Y. Yu and H. V. Poor, "Distributed MIMO radar using compressive sampling," *Proc. 42nd Asilomar Conf. Signals, Syst. Comput*, Pacific Grove, CA, pp. 203-207, Nov. 2008.

[41] C. Y. Chen and P. P. Vaidyanathan, "Compressed sensing in MIMO radar," *Proc. 42nd Asilomar Conf. Signals, Syst. Comput*, Pacific Grove, CA, pp. 41-44, Nov. 2008.

[42] H. Krim and M. Viberg, "Two decades of array signal processing research: The parametric approach," *IEEE Signal Processing Magazine*, vol. 13, no. 4, pp. 67-94, Jul. 1996.

[43] E. Candes and T. Tao, "The Dantzig selector: Statistical estimation when *p* is much larger than *n*," *Ann. Statist.*, vol. 35, no. 6, pp. 2313-2351, Dec. 2007.

[44] G. Tang and A. Nehorai, "Performance Analysis for Sparse Support recovery," IEEE Trans. Information Theory, vol. 56, no. 3, pp. 1383-1399, Mar. 2009.

[45] J.A. Tropp, "Greed is good: Algorithmic results for sparse approximation," IEEE Trans. Information Theory, vol. 50, no. 10, pp. 2231-2242, Oct. 2004.

[46] J.A. Tropp, "Just relax: Convex programming methods for identifying sparse signals," IEEE Trans. Information Theory, vol. 55, no. 2, pp. 917-918, Feb. 2009.

[47] M. A. Herman and T. Strohmer, "High-resolution radar via compressed sensing," in *IEEE Trans. Signal Process.*, vol. 57, no. 9, pp. 2275-2284, June. 2009.

[48] M. Grant and S. Boyd, CVX: Matlab software for disciplined convex programming, version 1.21, http://cvxr.com/cvx, Sep. 2010.

[49] M. Grant and S. Boyd, Graph implementations for nonsmooth convex programs, *Recent Advances in Learning and Control (a tribute to M. Vidyasagar)*, V. Blondel, S. Boyd, and H. Kimura, editors, pages 95-110, *Lecture Notes in Control and Information Sciences*, Springer, 2008, http://stanford.edu/~boyd/graph_dcp.html.

[50] H. Ochiai, P. Mitran, H. V. Poor and V. Tarokh, "Collaborative beamforming for distributed wireless ad hoc sensor networks," *IEEE Trans. Signal Process.*, vol. 53, no. 11, pp. 4110-4124, Nov. 2005.

[51] G. R. Curry, *Radar system performance modeling*, Boston: Artech House, 2005.

[52] A. Dogandzic and A. Nehorai, "Cramer-Rao bounds for estimating range, velocity, and direction with an active array," *IEEE Trans. Signal Process.*, vol. 49, no. 6, pp. 1122-1137, Jun. 2001.

[53] Y. Yu, A.P. Petropulu and H.V. Poor, "MIMO radar using compressive sampling," *IEEE Journal of Selected Topics in Signal Process.*, vol. 4, no. 1, pp. 146-163, Feb. 2010.

[54] T. Strohmer and B. Friedlander, "Compressed sensing for MIMO radar - algorithms and performance," in *Proc. 43rd Asilomar Conf. Signals, Syst. Comput.*, Pacific Grove, CA, pp. 464-468, Nov. 2009.

[55] G.S. Gill, "High-resolution step frequency radar," in *Ultra-Wideband Radar Technology*, Boca Raton, Florida: CRC, 2001.

[56] G.S. Gill, "Step frequency waveform design and processing for detection of moving targets in clutter," in *Proc. IEEE International Radar Conference*, Alexandria, VA, pp. 573-578, 1995.

[57] K. Lizuka, A.P. Freundofer, K.H. Wu, H. Mori, H. Ogura and V.K Nguyen, "Step-frequency radar," in *Journal of Applied Physics*, vol. 56, no. 9, pp. 2572-2583, Nov. 1984.

[58] A.C. Gurbuz, J.H. McClellan and W.R. Scott, "A compressive sensing data acquisition and imaging method for stepped frequency GPRs," *IEEE Trans. Signal Process.*, vol. 57, no. 7, pp. 2640-2650, Jul. 2009.

[59] Y-S. Yoon and M.G. Amin, "Imaging of behind the wall targets using wideband beamforming with compressive sensing," in *Proc. IEEE Workshop on Statistical Signal Process. (SSP2009)*, Cardiff, Wales (UK), pp. 93-96, Aug. 2009.

[60] S. Shah, Y. Yu and A.P. Petropulu, "Step-frequency radar with compressive sampling (SFR-CS)," in *Proc. IEEE Int'l Conf. Acoust. Speech Signal Process.*, Dallas, TX, pp. 1686-1689, Mar. 2010.

[61] C.J. Miosso, R.V. Borries, M. Argaez, L. Velazquez, C. Quintero and C.M. Potes, "Compressive sensing reconstruction with prior information by iteratively reweighted least-squares," *IEEE Trans. Signal Process.*, vol. 57, no. 6, pp. 2424-2431, Jun. 2009.

[62] N. Vaswani and W. Lu, "Modified-CS: modifying compressive sensing for problems with partially known support," in *Proc. IEEE International Symposium on Information Theory*, Seoul, Korea, pp. 488-492, Jun.-Jul. 2009.

[63] Y. Yu, A.P. Petropulu and H.V. Poor, "Reduced complexity angle-Doppler-range estimation for MIMO radar that employs compressive sensing," in *IEEE Proc. 43rd Asilomar Conf. Signals, Syst. Comput.*, Pacific Grove, CA, pp. 1196-1200, Nov. 2009.

[64] Y. Yu, A.P. Petropulu and H.V. Poor, "Range estimation for MIMO step-frequency radar with compressive sensing," in *Proc. 4th International Symposium on Communications, Control and Signal Process.*, Limassol, Cyprus, pp. 1-5, Mar. 2010.

[65] C. Chen and P.P. Vaidyanathan, "MIMO radar ambiguity properties and optimization using frequency-hopping waveforms," *IEEE Trans. Signal Process.*, vol. 56, no. 12, pp. 5926-5936, Dec.

[66] X. Song, S. Zhou and P. Willett, "The role of the ambiguity function in compressed sensing radar," in *Proc. IEEE Int'l Conf. Acoust. Speech Signal Process*, Dallas, TX, pp. 2758-2761, Mar. 2010.

[67] S.R.J. Axelsson, "Analysis of random step frequency radar and comparison with experiments," *IEEE Trans. Geoscience and Remote Sensing*, vol. 45, no. 4, pp. 890-904, Apr. 2007.

[68] N. Vaswani and W. Lu, "Modified-CS: modifying compressive sensing for problems with partially known support," to appear in *IEEE Trans. Signal Process*.

[69] N. Vaswani, "LS-CS-residual (LS-CS): compressive sensing on least squares residual," to appear in *IEEE Trans. Signal Process*.

Appendix A. Abbreviations

- AF: Ambiguity Function
- AOA: Angle of Arrival
- APES: Amplitude and Phase Estimation
- BP: Basis Pursuit
- CDF: Cumulative Density Function
- CS: Compressive Sensing/Sampling
- CSM: Coherence of The Sensing Matrix
- CWR: Continuous-wave Radar
- GLRT: Generalized Likelihood Ratio Test
- IDFT: Inverse Discrete Fourier Transform
- i.i.d.: Independent and Identically Distributed
- LP: Linear Program
- LSF: Linear Step Frequency
- LSFR: Linear-Step-Frequency Radar
- MF: Matched Filter
- MFM: Matched Filtering Method
- MIMO: Multiple-Input Multiple-Output

- MISO: Multiple-Input Single Output
- MP: Matching Pursuit
- MUSIC: Multiple Signal Classification
- PJR: Peak-to-Jammer Ratio
- PR: Pulse Radar
- PRR: Peak-to-Ripple Ratio
- QPSK: Quadrature Phase-Shift Keying
- RCS: Radar Cross Section
- RLSF: Random Step Frequency
- RSFR: Radom-Step-Frequency Radar
- SCSM: Sum of Coherence of The Sensing Matrix
- SF: Step Frequency
- SIMO: Single-Input Multiple-Output
- SIR: Signal-to-Interference Ratio
- SISO: Single-Input Single-Output
- SJR: Signal-to-Jam Ratio
- SNR: Signal-to-Noise Ratio
- SOCP: Second Order Cone Program
- UUP: Uniform Uncertainty Principle

Vita

General Yao Yu was born in Xian, China, in 1982.

Education

Drexel University, Philadelphia, PA, USA
Ph.D. in Electrical Engineering, December 2010 (GPA: 4.0/4.0)

City University of Hong Kong, Hong Kong SAR China
Mphil. in Electronic Engineering, August 2004 (GPA: 4.2/4.3)

Xidian University, Xian, China
B.S. in Telecommunication Engineering, July 2005 (GPA: 90/100)

Awards

⋆ IEEE MILCOM 2010 Student Travel Grant, 2010
⋆ Drexel University George Hill Jr. Endowed Fellowship, 2009
⋆ Drexel University Conference Travel Subsidy Award, 2009
⋆ Excellent Graduate Student of Xidian University, 2005
⋆ The First Grade Scholarship of Xidian University, 2004
⋆ Excellent Student of Xidian University, 2004
⋆ "Post and Telecommunication Institute" Scholarship, 2004
⋆ The First Grade Scholarship of Xidian University, 2003
⋆ Excellent Student of Xidian University, 2003
⋆ "Da Tang Telecommunication" Scholarship, 2002
⋆ The Special Grade Scholarship of Xidian University, 2002
⋆ Excellent Student of Xidian University, 2002

Publications

[1] **Y. Yu**, A.P. Petropulu and H.V. Poor, "MIMO radar using compressive sampling," *IEEE Journal of Selected Topics in Signal Process.*, vol. 4, no. 1, pp. 146-163, Feb. 2010.
[2] **Y. Yu**, Sarod Yatawatta, and Athina P. Petropulu, " A precoded OFDMA system with user cooperation," *EURASIP Journal on Wireless Communications and Networking*, vol. 2010, Article ID 843745, 12 pages, 2010. doi:10.1155/2010/843745.
[3] **Y. Yu**, A.P. Petropulu and H.V. Poor, "CSSF MIMO Radar: Low-complexity compressive sensing based MIMO radar that uses step frequency," submitted to *IEEE Trans. Aerospace and Electronic Systs.*.
[4] **Y. Yu**, A.P. Petropulu and H.V. Poor, " The measurement matrix design for compressive sensing based MIMO Radar," under preparation.
⋆ *Also 9 conference papers*.

Activities

⋆ **Reviewer** for *IEEE Trans. Signal Process., IEEE letters Signal Process., EURASIP Journal on Advances in Signal Process., Signal Process.* (A publication of the EURASIP), *IET Radar, Sonar and Navigation, Journal of Electromagnetic Waves and Applications, IEEE International Conference on Acoustics Speech and Signal Process.*, and *European Signal Process. Conference*.
⋆ **Student Member** of IEEE
⋆ **TPC member** of Wireless Communications and Networking Symposium of Chinacom 2011